



TECHNISCHE UNIVERSITÄT
CHEMNITZ

**Exploiting Substituent Effects to Control the
Mechanochromic Response of Spiropyran-
containing Copolymers**

Von der Fakultät für Naturwissenschaften der Technischen Universität
Chemnitz genehmigte Dissertation zur Erlangung des akademischen Grades

doctor rerum naturalium
(Dr. rer. nat.)

vorgelegt von

M. Sc. Fabian Kempe

geboren am 24.02.1990 in Dresden

eingereicht am 31.08.2020

Gutachter: Prof. Dr. Michael Sommer

Prof. Dr. Stefan Spange

Tag der Verteidigung: 17.03.2021

<https://nbn-resolving.org/urn:nbn:de:bsz:ch1-qucosa2-747251>

Abstract

Mechanochromic polymers respond to external force by changing their color. This can be achieved by the incorporation of a molecular switch such as spiropyran (SP) into polymers. SPs can be isomerized by mechanical force from their colorless form into colored merocyanines. Main-chain copolymerization of spiropyrans allows investigation of their mechanochromic behavior and potential use as force sensors. So far, several covalent polymer matrices have been used to investigate the mechanochromic response of SPs, among them poly(ϵ -caprolactone) (PCL). Less investigated is how the mechanochromic response can be fine-tuned by substituent effects. First, PCL with differently substituted spiropyrans at the chain's midpoint were used in order to investigate the effect of different substituents and their regiochemistry on the isomerization behavior of SPs under mechanical stress. A low activation barrier was observed for NO₂-substitution of “*ortho*”-spiropyrans compared to no substitution (R = H).

In order to investigate phenyl-substituted “*para,para*” spiropyrans, a newly developed kinked polyarylene was employed as covalent matrix material. This new polyarylene (PmmpP) has a *meta,meta,para* connection in its backbone and exhibits excellent mechanical properties. Its high strength allows the isomerization of this molecular switch with a large activation barrier. The phenyl-substituted “*para,para*” spiropyran showed transient mechanochromism and was switched 25 times in force-and-release cycles. The synthesis of PmmpP was carried out by a Suzuki polycondensation in three steps from commercial starting materials.

To further capitalize on the simplicity and properties of PmmpP, a two-step synthesis of a semifluorinated kinked polyarylene was demonstrated by direct arylation polycondensation with tetrafluorobenzene (F4). This partially fluorinated PmmpF4 was synthesized with a variety of side-chains. Resulting polymers exhibited a large range of glass transition temperatures, allowing for the production of tailor-made smart materials.

Keywords: spiropyran, polycaprolactone, polyarylene, cross-coupling, Suzuki reaction, direct arylation, fluoropolymer

Outline

This dissertation consists of an introduction, three publications and a summary. The publications are presented in chapter 2, 3 and 4. The contents of chapter 2 are currently prepared for publication. Chapter 3 was published in 2017 and chapter 4 is currently under review.

The contents of the publication chapters are as follows:

Chapter 2: Substituent-controlled energetics and barriers of mechanochromic spiropyran-functionalized poly(ϵ -caprolactone). F. Kempe, L. Metzler, O. Brügger, H. Buchheit, M. Walter, M Sommer, *in preparation*.

I carried out film preparation, tensile testing coupled with light absorption measurements and wrote the first draft. L. Metzler (equally contributed) was responsible for spiropyran design and synthesis as well as the first draft of the supporting information. H. Buchheit was responsible for all polymerizations. O. Brügger and M. Walter were responsible for DFT calculations. M. Sommer designed and supervised the work. All authors were involved in revising the manuscript.

Chapter 3: A Simply Synthesized, Tough Polyarylene with Transient Mechanochromic Response. F. Kempe, O. Brügger, H. Buchheit, S. N. Momm, F. Riehle, S. Hameury, M. Walter and M. Sommer, *Angew. Chem. Int. Ed.* **2018**, *57*, 997-1000.

<https://doi.org/10.1002/anie.201709142>

I designed and synthesized monomers and polymers, carried out characterizations (NMR, SEC, tensile testing / video) and wrote the first draft. O. Brügger and M. Walter were responsible for DFT calculations. H. Buchheit and F. Riehle optimized polymerization conditions. S. N. Momm optimized monomer synthesis, polymer purification and film preparation. S. Hameury prepared the catalyst. M. Sommer designed and supervised the work. All authors were involved in revising the manuscript.

Chapter 4: Semifluorinated, kinked polyarylenes via direct arylation polycondensation. F. Kempe, F. Riehle, H. Komber, R. Matsidik, M. Walter and M. Sommer, *Polym. Chem.* **2020, *11*, 6928-6934.**

<https://doi.org/10.1039/D0PY00973C>

I designed the monomer synthesis and wrote the first draft. F. Riehle synthesized polymers. H. Komber carried out NMR analysis including end-group characterization. M. Walter was responsible for DFT analysis. M. Sommer designed and supervised the work. All authors were involved in revising the manuscript.

Table of Contents

List of Figures	9
List of Schemes	13
List of Tables	14
Abbreviations	15
Chapter 1 Introduction	19
1. Smart materials.....	19
2. Spiropyran as molecular switch	20
2.1. General spiropyran properties	20
2.2. Spiropyrans as mechanical switches	22
3. C-C cross coupling reactions in material science	25
3.1. Suzuki polycondensation	25
3.2. Direct arylation polycondensation.....	28
4. High-performance polyarylenes.....	32
5. References.....	36
Chapter 2 Substituent-controlled Energetics and Barriers of Mechanochromic Spiropyran-functionalized Poly(ϵ - caprolactone)	41
1. Abstract.....	42
2. Introduction	42
3. Results and Discussion.....	43
4. Conclusion.....	48
5. Acknowledgements	48
6. Experimental Methods.....	49
6.1. General information.....	49
6.2. Overview of the initiator synthesis	50
6.3. Visible light absorption and stress-strain experiments.....	67
7. References.....	68
Chapter 3 Simply Synthesized, Tough Polyarylene with Transient Mechanochromic Response	71
1. Abstract.....	72
2. Introduction	72
3. Results and discussion	73
4. Conclusion.....	79
5. Acknowledgements	79

6. Experimental Methods.....	80
6.1. General information.....	80
6.2. Retrosynthetic Analysis.....	81
6.3. Preparation of monomers and catalyst.....	84
6.4. Polymers <i>PmmpP</i> P1-P5.....	89
6.5. Soxhlet fractionation: Solvent screening	96
6.6. Screening of monomer ratio	96
6.7. <i>SP/PmmpP</i> copolymer	97
6.8. Stress-strain experiment	101
6.9. Video Analysis	102
6.10. Differential scanning calorimetry.....	103
6.11. UV/VIS spectroscopy.....	105
6.12. Thermogravimetry.....	105
6.13. Theoretical methods.....	106
7. References.....	109

Chapter 4 Semifluorinated, kinked polyarylenes via direct arylation polycondensation 112

1. Abstract.....	113
2. Introduction	113
3. Results and Discussion	115
3.1. Synthesis	115
3.2. Thermal properties	117
3.3. Density functional theory calculations.....	120
4. Conclusion	123
5. Acknowledgements.....	124
6. Experimental Methods.....	125
6.1. General methods	125
6.2. Preparation of monomers	126
6.3. Preparation of polymers and SEC curves	132
6.4. NMR spectra of monomers.....	135
6.5. NMR spectra of polymers	141
6.6. Theoretical methods.....	147
7. References.....	149

Chapter 5 Conclusion 152

1. Summary Chapter 2	152
2. Summary Chapter 3	153
3. Summary Chapter 4	154

Declaration of self-reliance	156
Curriculum Vitae.....	157
Awards.....	157
Publications, posters and talks.....	158
Acknowledgements	159

List of Figures

Figure 1-1:	Stacking order of H (left) and J aggregates. +/- signs denote dipole moments.	22
Figure 1-2:	Common boron reagents for Suzuki cross coupling reactions.	26
Figure 1-3:	Possible mechanisms for Suzuki cross coupling reactions. ^[69,75,76] Top: "Oxo-Palladium" cycle with the base directly attached to the transition metal. Bottom: "Boronate" cycle with external activation of the boronic acid ester by the base. Ligands omitted for clarity.	27
Figure 1-4:	BDEs of direct arylation coupling partners (kcal/mol): thiophene, furan, pyridine, benzene, fluorobenzene, 1,3-difluorobenzene, 1,3,5-trifluorobenzene, tetrafluorobenzene (1,2,4,5-, 1,2,3,5-). ^[78] Only the proton with the lowest BDE is highlighted.	28
Figure 1-5:	Possible mechanisms of direct arylation reactions. Top: Concerted metalation deprotonation mechanism with a six-membered cyclic transition state. Bottom: External base cycle with intermolecular deprotonation during C-H bond activation. Ligands omitted for clarity. ^[79]	29
Figure 1-6:	Structure of tris(<i>o</i> -anisyl)phosphine.	31
Figure 1-7:	Direct arylation polymerization reported by the Ozawa group. ^[97] ...	32
Figure 1-8:	Novel high-performance polymer called SUPERBIO.	33
Figure 1-9:	Structure of a PC (Makrolon®) and the <i>PmpP</i> by the Schlüter group. ^[105]	34
Figure 1-10:	Polyarylene <i>PmpP</i> prepared by the Schlüter group. ^[105]	34
Figure 1-11:	"Shaving" approach by the Schlüter group in order to access unsubstituted and high molecular weight <i>PmpPs</i> . ^[109]	35
Figure 2-1:	a) Schematic experimental setup for in-situ VIS spectroscopy during stress-strain of films. After the yield point polycaprolactone becomes sufficiently translucent for visible light (450 – 800 nm). b) In-situ visible light absorption after the yield point during stress-strain experiment. Only the <i>ortho</i> -SP/ <i>p</i> -NO ₂ (purple) immediately isomerizes after the yield point. Values plotted correspond to absorption at 585 nm relative to 700 nm (= baseline). Bold line is floating average.	45
Figure 2-2:	Barriers for forward and backward reactions in the different SP derivatives investigated. Solid lines are electronic energies including vibrational energy contributions (the step-like features are numeric artifacts). The main contributions to the barrier are indicated. For color code see Scheme 2-2.....	47
Figure 2-3:	Overview of the SP initiator synthesis.	50
Figure 2-4:	SEC analysis of polymers in THF at 1 ml / min.....	66
Figure 3-1:	Tensile experiment of <i>PmmpP</i> containing 2 mol-% <i>p,p</i> -SPBr ₂ . a) Structures of SP (top) and MC (bottom) in the <i>PmmpP</i> matrix. b) Pictures of repeated strained and released samples. Pictures were	

	adjusted for brightness and contrast. c) Intensity of green color in the mid-section of the specimen during repeated force build-up and release. The time scale corresponds to the change in force as shown in Figure 3-5.....	76
Figure 3-2:	a), b) Chemical structures of SP derivatives modelled with arrows indicating pulling directions. The definitions of the pulling distance d , the bond distance b and the dihedral angle β between olefinic protons are indicated. c) Gibbs energy barriers in dependence of the external force corresponding to the polyarylene and nitro-substituted spiropyran. d) Force needed for coloration F in dependence of the loading rate α for the two SP derivatives.....	78
Figure 3-3:	Reversed functional groups are challenging due to the low melting point of 7 . Therefore this route was not explored any further.	82
Figure 3-4:	SEC of crude and purified polymer <i>PmmpP</i> P1 . Purification was carried out by Soxhlet extraction in cyclohexane. For purification with other solvents, see Figure 3-6.	83
Figure 3-5:	Stress-strain experiments on purified polymers P1 - P5 (10 mm/min). Specimen cut from rigid thin film (DIN 53504 type 3) after solvent-cast from dichloromethane.	95
Figure 3-6:	Soxhlet extraction of Polymer S1 for 16 h. iHex: Isohexane, Et ₂ O: diethyl ether, CH: cyclohexane, EE: ethyl acetate, EtOH: ethanol, ACN: acetonitrile, iPrOH: Isopropanol, TBME: <i>tert</i> -butyl methyl ether, MeOH: methanol.....	96
Figure 3-7:	Force-strain graph of SP/ <i>PmmpP</i> copolymer isomerization experiment.....	101
Figure 3-8:	Force-time graph of SP/ <i>PmmpP</i> copolymer isomerization experiment.....	101
Figure 3-9:	Picture from video indicating area of color analysis (white box)....	102
Figure 3-10:	Video analysis for three separate color channels.	102
Figure-3-11:	DSC of <i>PmmpP</i> P1 , 10 K / min, 2. heating.....	103
Figure 3-12:	DSC of <i>PmmpP</i> P2 , 10 K / min, 2. heating.	103
Figure 3-13:	DSC <i>PmmpP</i> P3 , 10 K / min, 2. heating.	104
Figure 3-14:	DSC of <i>PmmpP</i> P4 , 10 K / min, 2. heating.	104
Figure 3-15:	Transmission of P3 (film). Normalized to maximum transmission.	105
Figure 3-16:	Thermogravimetric analysis of P1 . 10 K / min. Blue: Air atmosphere; Red: Nitrogen atmosphere.	105
Figure 3-17:	Energetics for two different external forces.	107
Figure 3-18:	Discoloration process at zero force starting from 100% colored MC form (solid and dashed lines) and the resulting half times. The probability of MC converges for large time values against the	

	equilibrium value which is the Boltzmann factor associated to the energy difference between MC and SP at zero force.	108
Figure 4-1:	^1H (a) and ^{13}C (b) NMR spectra of <i>PmmpF4</i> (entry 2) in CDCl_3 with assignments.....	117
Figure 4-2:	Glass transition temperature of <i>PmmpF4</i> with <i>6n</i> as a function of molecular weight (a) and for varying side chains including entry 5 (b). Conditions: 2 nd heating, 10 K/min, N_2	118
Figure 4-3:	a,b) Possible chain chain interactions of <i>PmmpF4</i> and c) model compounds used for DFT calculations.....	120
Figure 4-4:	a) Scheme of binding energies between the model fragments of <i>PmmpF4</i> , for chemical structures see Figure 4-3c. b) Selected lowest energy structures. c) Binding energies in vdW-DF2 and PBE in the TS09 relaxed structure.....	122
Figure 4-5:	SEC eluograms of entries 1 – 5.....	133
Figure 4-6:	SEC eluograms of entries 6 – 11 compared to entry 2.....	133
Figure 4-7:	SEC eluograms of entries 2 and 2a, which was derived from entry 2 by soxhlet extraction with ethyl acetate.....	134
Figure 4-8:	^1H (a) and ^{13}C NMR spectrum (b) of 5,5'-dibromobiphenyl-2,2'-diol in $\text{DMSO}-d_6$	135
Figure 4-9:	^1H (a) and ^{13}C NMR spectrum (b) of 5,5'-dibromo-2,2'-bis(isopropoxy)biphenyl in CDCl_3	136
Figure 4-10:	^1H (a) and ^{13}C NMR spectrum (b) of 5,5'-dibromo-2,2'-bis(sec-butoxy)biphenyl in CDCl_3	137
Figure 4-11:	^1H (a) and ^{13}C NMR spectrum (b) of 5,5'-dibromo-2,2'-bis(cyclopentoxy)biphenyl in CDCl_3	138
Figure 4-12:	^1H (a) and ^{13}C NMR spectrum (b) of 5,5'-dibromo-2,2'-bis(octyloxy)biphenyl in CDCl_3	139
Figure 4-13:	^1H (a) and ^{13}C NMR spectrum (b) 5,5'-dibromo-2,2'-bis(2-ethylhexyloxy)biphenyl in CDCl_3	140
Figure 4-14:	^1H (a) and ^{19}F NMR spectrum (b) of entry 8 (3i) ($\text{C}_2\text{D}_2\text{Cl}_4$; 120 °C).141	
Figure 4-15:	^1H (a) and ^{19}F NMR spectrum (b) of entry 7 (4s) ($\text{C}_2\text{D}_2\text{Cl}_4$; 120 °C).	142
Figure 4-16:	^1H (a) and ^{19}F NMR spectrum (b) of entry 9 (5c) ($\text{C}_2\text{D}_2\text{Cl}_4$; 120 °C).	143
Figure 4-17:	^1H (a), ^{13}C (b) and ^{19}F NMR spectrum (c) of entry 2 (6n) (a,c: $\text{C}_2\text{D}_2\text{Cl}_4$; 120 °C and b: CDCl_3 , 30°C).	144
Figure 4-18:	^1H (a) and ^{19}F NMR spectrum (b) of entry 11 (8n) ($\text{C}_2\text{D}_2\text{Cl}_4$; 120 °C).....	145
Figure 4-19:	^1H (a) and ^{19}F NMR spectrum (b) of entry 6 (EH) ($\text{C}_2\text{D}_2\text{Cl}_4$; 120 °C).	146
Figure 4-20:	Development of the energetic distance ΔE between the best and the second best structure with number of structures tried for	

$C_{15}H_{14}$ (solid), $C_{16}H_{18}$ (dashed) and $C_{14}H_{14}O_2$ (dotted) in interaction with the color-coded smaller molecules. The dotted horizontal line indicates 4 kJ/mol. The structures involving $C_6H_2F_4$ show slower convergence than C_6H_6 or C_6F_6 147

Figure 4-21:	Lowest energy structures found. C: grey, O: red, H: white, F: green.	148
Figure 5-1:	Bifunctional SP as initiator in the ROP of ϵ -caprolactone.	152
Figure 5-2:	Structures of the 4 spiropyran-PCL copolymers synthesized in this investigation.	152
Figure 5-3:	a) Schematic experimental setup for in-situ VIS spectroscopy during stress-strain of films. After the yield point polycaprolactone becomes sufficiently translucent for visible light (450 – 800 nm). b) In situ visible light absorption after the yield point.	153
Figure 5-4:	Structure of the newly developed <i>PmmpP</i>	154
Figure 5-5:	Tensile experiment of <i>PmmpP</i> containing 2 mol-% <i>p,p</i> -SPBr ₂ . a) Structures of SP (top) and MC (bottom) in the <i>PmmpP</i> matrix. b) Pictures of repeated strained and released samples. Pictures were adjusted for brightness and contrast. c) Intensity of green color in the mid-section of the specimen during repeated force build-up and release.	154
Figure 5-6:	Synthesis of kinked, semifluorinated <i>PmmpF4</i> via DAP.	155

List of Schemes

Scheme 1-1: Geminal difluorocyclopropanes are mechanoresponsive under ultrasound. This leads to conrotatory bond scission (left). This is opposite to disrotatory thermal activation (right). ^[14]	19
Scheme 1-2: Diarylbibenzofuranone (DABBF) as mechanochromic force sensor in elastomeric polyurethane (PU). The radicals are blue coloured and stable for hours. ^[15]	19
Scheme 1-3: Examples of molecular switches. Azobenzene (top) and spiropyran.....	20
Scheme 1-4: SP → MC isomerization. C and T denote bond configurations <i>cis</i> / <i>s-cis</i> and <i>trans</i> / <i>s-trans</i> of double and single bonds α , β and γ (see top of figure). Of the two most stable MCs the mesomeric structure is also pictured.	21
Scheme 1-5: Spiropyran as initiator for the copolymerization of methyl acrylate. The SP copolymer was mechanochromic under tensile strain. ^[42]	23
Scheme 1-6: Olefin-substituted SP cross linker used in elastomeric PDMS. ^[41]	23
Scheme 1-7: Alternating SP copolymer synthesized by Suzuki coupling. This polymer was used for an anisotropic mechanochromic material by pre-alignment from electrospinning. ^[46]	24
Scheme 2-1: Synthesis of bifunctional SP initiators for the ring opening polymerization of ϵ -caprolactone. Reaction conditions: i) formaldehyde (aq., 37%), conc. HCl ii) H ₂ O iii) 1-(2-hydroxyethyl)-2,3,3-trimethylindoliniumiodide, ethanol, piperidine iv) acetic acid, HNO ₃ , v) NaOH (aq), vi) ϵ -caprolactone, Sn(oct) ₂ , 140 °C.....	44
Scheme 2-2: SP copolymers synthesized in this work to probe the influence of regio- („ <i>ortho</i> “ - vs. „ <i>para</i> “) as well as electronic (H or NO ₂) effects on the force-induced SP → MC reaction. The copolymer was poly(ϵ -caprolactone) (see Scheme 2-1).....	45
Scheme 3-1: Top: Retrosynthetic analysis of <i>PmmpP</i> compared to previous work. ^[3] Bromination of 2,2'-biphenol leads to a “double <i>meta</i> -” linkage in the backbone. Bottom: Synthesis of <i>PmmpP</i> . * = non-commercial Pd ₂ dba ₃	74
Scheme 3-2: Transition between spiropyran (SP) and CTC-merocyanine (MC) over the intermediate form (IN).....	106
Scheme 4-1: Synthesis of kinked, semifluorinated <i>PmmpF4</i> via DAP.	116

List of Tables

Table 2-1:	Molecular weights of SP copolymers as measured by SEC in THF (1 mL / min, 40 °C).	44
Table 3-1:	Mechanical and molecular weight data.	95
Table 3-2:	Molecular weight data for screening of monomer ratio.....	96
Table 4-1:	Optimization of reaction conditions for <i>n</i> -hexyl side chain.....	119
Table 4-2:	Glass transition temperatures of polyarylenes with different side chains.....	119

Abbreviations

3i	<i>isopropyl</i>
4s	<i>sec-butyl</i>
5c	<i>cyclopentyl</i>
6n	<i>n-hexyl</i>
8n	<i>n-octyl</i>
9-BBN	<i>9-Borabicyclo(3.3.1)nonane</i>
ACN	<i>acetonitrile</i>
aq	<i>aqueous</i>
Ar	<i>aryl</i>
BDE	<i>bond dissociation energy</i>
BE	<i>binding energy</i>
Bpin	<i>pinacolatoboron</i>
br	<i>broad</i>
C configuration	<i>cis configuration / s-cis conformation</i>
ca	<i>circa</i>
CAS	<i>Chemical Abstract Service registry number</i>
CB	<i>chlorobenzene</i>
CCSD(T)	<i>coupled cluster single-double-triple</i>
CH	<i>cyclohexane</i>
CMD	<i>concerted metalation-deprotonation</i>
COGEF	<i>Constrained Geometries Simulate External Force</i>
conc	<i>concentrated</i>
Đ	<i>dispersity</i>
d (NMR)	<i>dublet</i>
D (unit)	<i>Debye</i>
DABBF	<i>Diarylbibenzofuranone</i>
DAP	<i>direct arylation polycondensation</i>
dba	<i>dibenzylideneacetone</i>
DCM	<i>dichloromethane</i>
DFT	<i>density functional theory</i>
DMF	<i>N,N-dimethylformamide</i>
DMSO	<i>Dimethyl sulfoxide</i>

DSC	<i>differential scanning calorimetry</i>
E	<i>Young's modulus</i>
EA	<i>elemental analysis</i>
EE	<i>ethyl acetate</i>
EH	<i>2-ethylhexyl</i>
eq	<i>equivalents</i>
Et ₂ O	<i>diethyl ether</i>
EtOH	<i>ethanol</i>
F ₄	<i>tetrafluorobenzene</i>
g	<i>gram</i>
G	<i>Gibbs free energy</i>
h	<i>Planck constant</i>
Hal	<i>halogen</i>
Hex	<i>hexyl</i>
iHex	<i>isohexane</i>
IN	<i>intermediate</i>
iPrOH	<i>isopropanol</i>
k _b	<i>Boltzmann constant</i>
m (NMR)	<i>multiplet</i>
MC	<i>Merocyanine</i>
Me	<i>methyl</i>
Me ₆ TREN	<i>Tris[2-(dimethylamino)ethyl]amine</i>
MeOH	<i>methanol</i>
min	<i>minute</i>
M _n	<i>number average molecular weight</i>
MP2	<i>Møller–Plesset perturbation, second order</i>
MS	<i>mass spectrometry</i>
M _w	<i>weight average molecular weight</i>
MW	<i>molecular weight</i>
NBS	<i>N-bromosuccinimide</i>
NEt ₃	<i>triethylamine</i>
NMR	<i>nuclear magnetic resonance</i>
OAc	<i>acetate</i>
Oct	<i>octyl</i>
OPiv	<i>pivalate</i>
p	<i>yield</i>

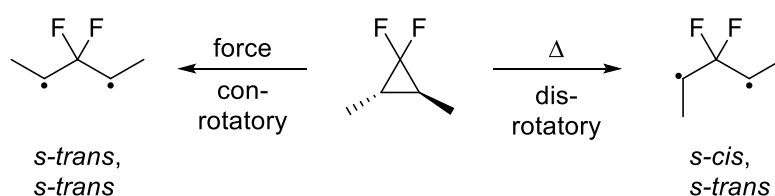
P3HT	<i>poly-3-hexylthiophene</i>
PBE	<i>Perdew, Burke and Ernzerhof</i>
PC	<i>polycarbonate</i>
PCL	<i>polycaprolactone</i>
PDMS	<i>polydimethylsiloxane</i>
PEEK	<i>polyether ether ketone</i>
PES	<i>polyethersulfone</i>
pF4	<i>1,2,4,5-tetrafluorobenzene</i>
PF8F4	<i>dioctylfluorene tetrafluorobenzene copolymer</i>
Ph	<i>phenyl</i>
PI	<i>polyimide</i>
pin	<i>pinacol</i>
PivOH	<i>pivalic acid</i>
pm	<i>picometre</i>
PMA	<i>poly(methyl acrylate)</i>
PmmpP	<i>Poly(meta-, meta-, para-phenylene)</i>
PmpP	<i>Poly(meta-, para-phenylene)</i>
PPE	<i>polyphenyl ether</i>
PpP	<i>poly-para-phenylenes</i>
PPS	<i>polyphenylene sulfide</i>
PU	<i>polyurethane</i>
q (NMR)	<i>quartet</i>
R _f	<i>retardation factor</i>
ROP	<i>ring opening polymerization</i>
s (NMR)	<i>singlet</i>
SEC	<i>size exclusion chromatography</i>
Sn(oct) ₂	<i>tin octanoate (tin(II) 2-ethylhexanoate)</i>
SP	<i>Spiropyran</i>
S-Phos	<i>2-Dicyclohexylphosphino-2',6'-dimethoxybiphenyl</i>
t (NMR)	<i>triplet</i>
T configuration	<i>trans configuration / s-trans conformation</i>
TBME	<i>tert-butyl methyl ether</i>
TfOH	<i>triflic acid</i>
T _g	<i>glass transition temperature</i>
THF	<i>tetrahydrofuran</i>
T _m	<i>melting temperature</i>

Tol	<i>toluene</i>
UV	<i>ultraviolet light</i>
VIS	<i>visible light</i>
vs	<i>versus</i>
X _n	<i>degree of polymerization</i>
ϵ	<i>strain</i>

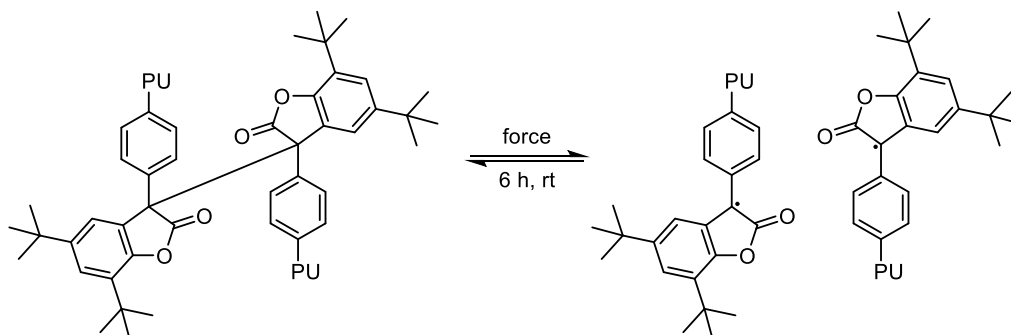
Chapter 1 Introduction

1. Smart materials

In material science, applications are described as “smart” if there is a specific response to an outside stimulus.^[1] These stimuli-responsive materials exhibit a basic input-output logic, making them “intelligent”.^[2-5] In mechanoresponsive materials the external stimulus is mechanical force, which facilitates unique chemical transformations.^[6] This may be applied in stress sensing, deformation studies and damage control.^[7] The diversity of mechanical properties makes polymers especially suitable for mechanoresponsiveness.^[8] These transformations may include selective cycloreversions, ring-opening reactions, conformational changes, deconstruction of aggregates and C-C bond breakage producing radicals.^[9] Specifically designed functional groups (mechanophores) may be placed in a polymer in order to undergo stress-induced transformations.^[10] The applied external force alters the potential energy landscape and the activation energy for bond dissociation is reduced.^[11] This may be accomplished by sonication (in solution, Scheme 1-1) or tensile experiments (Scheme 1-2).^[12-15]



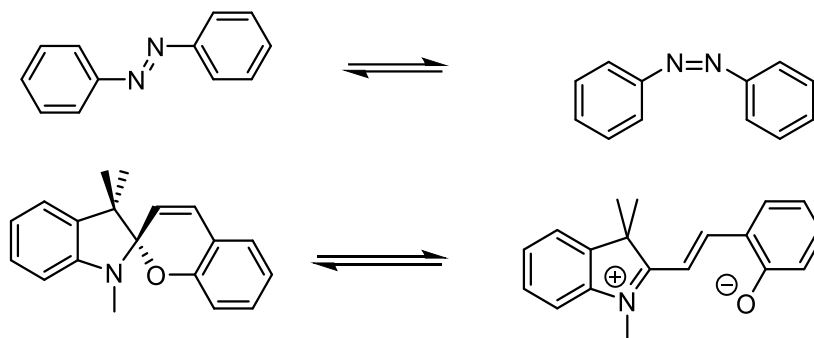
Scheme 1-1: Geminal difluorocyclopropanes are mechanoresponsive under ultrasound. This leads to conrotatory bond scission (left). This is opposite to disrotatory thermal activation (right).^[14]



Scheme 1-2: Diarylbibenzofuranone (DABBF) as mechanochromic force sensor in elastomeric polyurethane (PU). The radicals are blue coloured and stable for hours.^[15]

Mechanoresponsive polymers (as in Scheme 1-2) that absorb or emit color upon mechanical deformation are called mechanochromic.^[16] Other examples of

mechanochromic switches are azobenzenes and spiropyrans (Scheme 1-3). These molecular switches work by changes in their conjugation.^[17] Their change in conjugation alters their absorption, making a color change visible. This may happen either as a *cis/trans*-isomerization (as in azobenzenes^[18]) or an extension of the conjugation between parts of the molecule (as in spiropyrans^[19]).

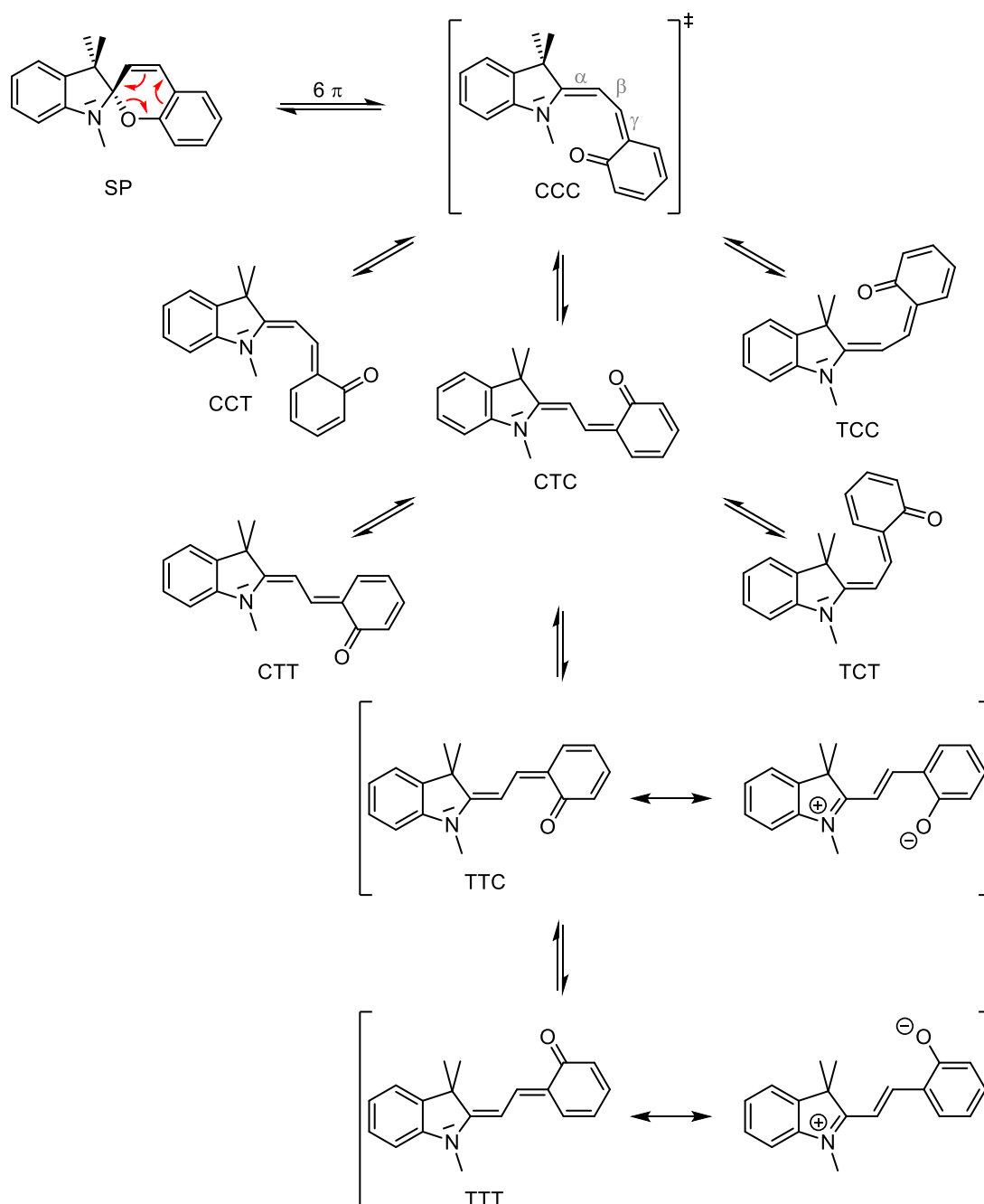


Scheme 1-3: Examples of molecular switches. Azobenzene (top) and spiropyran.

2. Spiropyran as molecular switch

2.1. General spiropyran properties

Spiropyrans (SP) are molecules that are named after the spiro carbon at their center, which connects an indolin half with a chromene half (Scheme 1-3, bottom).^[20] Both parts are therefore perpendicular to each other and not connected by their π -systems. SPs can isomerize from their colorless (leuko) form into the colored merocyanine (MC), a planar molecule with a C-C double bond connecting the two aromatic systems (Scheme 1-4).^[21] This equilibrium is influenced by several factors including pH, temperature, force, light and solvent polarity.^[22] The isomerization always occurs by cleavage of the C-O bond of the spiro-carbon. The ring opening reaction is an 1,6-electrocyclisation.^[23] MC can be depicted as either an uncharged or zwitterionic species, both of which are extreme representations of the true electronic state of the molecule.



Scheme 1-4: SP \rightarrow MC isomerization. C and T denote bond configurations *cis* / *s-cis* and *trans* / *s-trans* of double and single bonds α , β and γ (see top of figure). Of the two most stable MCs the mesomeric structure is also pictured.

The isomerization has been shown to generate *cis*-MC as an ephemeral species which itself rotates into one of the more stable *trans*-MC.^[24] There are several different isomers of *trans*-MC. They are denoted by the double bond configuration (starting from indoline) by CTC, CTT, TTC or TTT. All configurations including a C configuration in the middle were found to be unstable due to steric hindrance.^[25] The most stable conformation is TTC, which may be explained by hydrogen bonding stabilization which makes it more dominant than TTT.^[26]

The type of *trans*-MC is dependent on functional groups, stimuli and solvent/matrix.^[27] The SP → MC isomerization changes the light absorption from UV to visible absorption (typically 500 – 700 nm).^[28,29] The SP → MC isomerization also increases the dipole moment significantly. A NO₂-substituted SP was shown to have a dipole moment of ca. 5 D compared to ca. 20 D for MC.^[30] Additionally, the MC isomer is more acidic than SP due to better charge delocalization and has a larger affinity to metal ions.^[23,31] These drastically different properties also explain the diverse stimuli that can be used to trigger the SP → MC equilibrium.

The adjustment of SP and MC properties can be carried out by attachment of functional groups either on the indoline or chromene part.^[32] Hereby not only the properties but the isomerization behavior itself is changed by the change of energy levels of SP and MC relative to each other.^[33] Following the Bell-Evans-Polanyi principle, a lower MC energy level decreases the energy of the transition state.^[34] This lowers the activation energy and speeds up SP → MC isomerization.

MCs tend to aggregate both in solids and solution due to π - π stacking and dipole alignment.^[22,35] Aggregation can result in type H (antiparallel) or J (parallel, see Figure 1-1) with inverse impact on absorption.^[36] H aggregates show a hypsochromic shift while J aggregates cause a bathochromic shift compared to the single molecule. Curiously, both H and J aggregates have been observed concurrently in some instances.^[37]



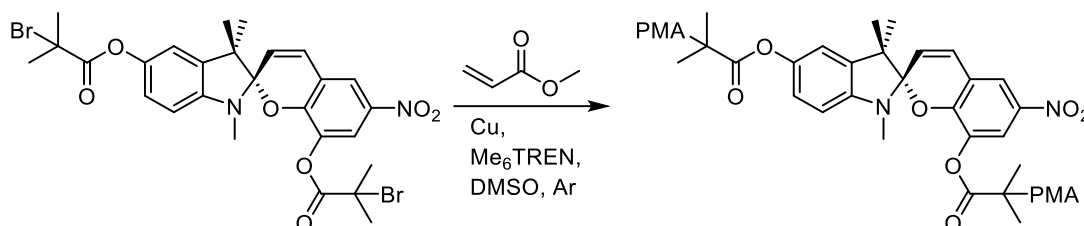
Figure 1-1: Stacking order of H (left) and J aggregates. +/- signs denote dipole moments.

Aggregation of MC stabilizes the open-ring isomer and slows down re-isomerization, hindering the use as a “smart” molecular switch.^[37] This can be mitigated by SP immobilization.^[38,39] In a solid, aggregation is hindered kinetically by reduced degrees of movement and thermodynamically by “dilution” of SP moieties. The immobilization of SPs in polymers will be discussed in detail in the following chapter.

2.2. Spiroyrans as mechanical switches

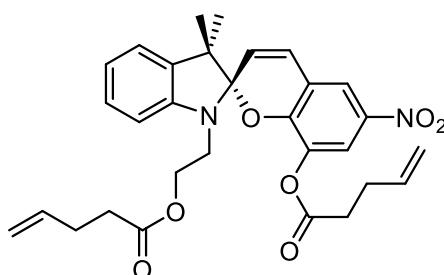
Spiroyrans can be isomerized by mechanical force which makes them good candidates as molecular force sensors.^[40] Mechanical isomerization is possible both

by positive and negative pressure (i.e. strain or compression experiments).^[41] Simple milling with a mortar will cause SP to give a color.^[22] More applicable is the immobilization of SP into a solid. Polymers are prime candidates for SP immobilization due to their variable chemistry, strength, polarity, elasticity and processability.^[40] Chain-end or side-chain SP copolymerization usually has only limited benefit due to poor stimuli response^[42,43] and is still limited to positive pressure.^[38]



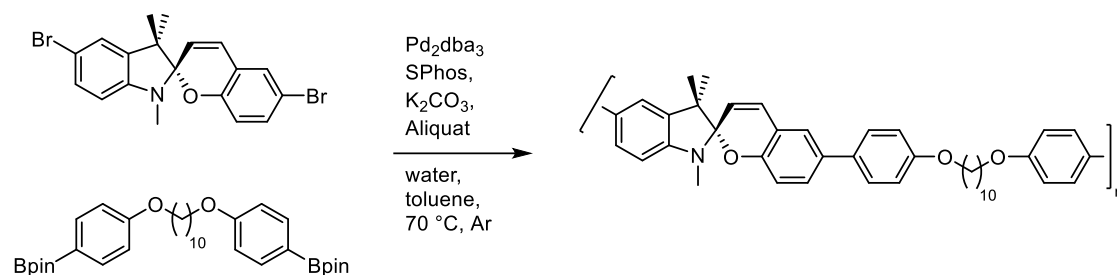
Scheme 1-5: Spiropyran as initiator for the copolymerization of methyl acrylate. The SP copolymer was mechanochromic under tensile strain.^[42]

Only appropriate covalent attachment or main-chain SP copolymerization allows for both reduced aggregation and efficient force transfer.^[44] It was demonstrated that SP has to be positioned to be close to the middle part of polymer chains, at least to some statistically significant degree. This was demonstrated by copolymerization of SP into poly(methyl acrylate) (PMA, Scheme 1-5).^[42] Elastomeric polydimethylsiloxane (PDMS) networks with olefin-substituted SPs as cross linker (Scheme 1-6) were used for repeatable switching by applying pressure (colored) and resetting with visible light (colorless).^[41,45]



Scheme 1-6: Olefin-substituted SP cross linker used in elastomeric PDMS.^[41]

Main-chain copolymers of SP can be processed with pre-alignment of chains by electrospinning, which gives an anisotropic mechanochromic response.^[46] This was achieved by using an alternating copolymer (Scheme 1-7) produced by Suzuki polycondensation.



Scheme 1-7: Alternating SP copolymer synthesized by Suzuki coupling. This polymer was used for an anisotropic mechanochromic material by pre-alignment from electrospinning.^[46]

Generally, the fixation of low molecular weight dyes prevents “leakage” from the material.^[22,47] Additionally, copolymers improve the solubility of SP in materials where SP would not dissolve independently.^[48] Copolymers of SP have shown improved fluorescence due to the reduced movement of SP which reduces quenching.^[49] Copolymers provide the ability to modify SP behavior not just by functional groups, but by the polymer itself as it forms a matrix around SP just like a solvent would. The polymer must have a sufficiently large free volume in order to allow rotation during SP → MC isomerization.^[24] Spectroscopic observations were simplified by SP immobilization as it stabilizes ephemeral species like *cis*-MC sufficiently long enough to be studied.^[50]

3. C-C cross coupling reactions in material science

C-C cross coupling reactions have emerged as a powerful tool in organic synthesis. They enable the synthesis of complex organic fragments under relatively mild conditions.^[51] C-C cross coupling reactions are typically carried out catalytically with nickel- or palladium-based metal complexes.^[52,53] Continuous development have broadened the versatility towards easily produced bromine and chlorine substrates as electrophiles.^[54]

In material science the use of C-C cross coupling reactions simplified modification of existing responsive building blocks.^[55] Furthermore, polymerization could be carried out by careful selection of conditions. A notable example is the chain growth Kumada polymerization leading to poly-3-hexylthiophene (P3HT).^[56] A dibrominated monomer precursors is metalated in situ by addition of a Grignard reagent. The metalation occurs once and not twice due to the high electron density of the metalated monomer. Despite the poor regioselectivity of the metalation, a regioregular polymerization occurs. This is achieved by the fact that the minor isomer is inactive to polymerization.^[57] For monomers without such unique characteristics, more general approaches are necessary. For instance, in Suzuki polycondensation and direct arylation polymerization, air-stable monomers can be employed.^[58] Those methods will be described in more detail in this section.

3.1. Suzuki polycondensation

The Suzuki cross coupling reaction is highly useful in material science due to the stability of the utilized reagents.^[59] Although instable reagents like alkyl boranes may be employed, it is equally possible to use boronic acid esters (see Figure 1-2). Cyclic and sterically hindered boronic acid esters like pinacol boranes are air-stable, may be purified by column chromatography and can be stored for years if bound to an arylene.^[60] Furthermore, air-stable potassium trifluoroborates may be employed, which hydrolyze during the reaction to the corresponding boronic acids.^[61,62] Potassium trifluoroborates can be synthesized under mild conditions (non-corrosive to glassware) from boronic acids and potassium fluoride by addition of tartaric acid.^[63]

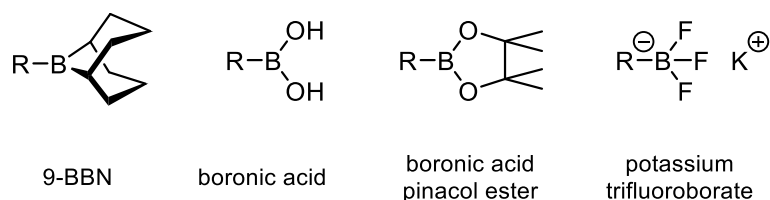


Figure 1-2: Common boron reagents for Suzuki cross coupling reactions.

High monomer stability was complemented by advancements in the catalyst system. Air-stable palladium precursors and phosphine ligands simplified the use of cross coupling reactions in material science.^[64–69] Only during the reaction itself an inert gas (nitrogen or argon) needs to be employed, but the balance can be used outside a glovebox beforehand. In some instances, air is tolerated even during the reaction.^[70] Another benefit of Suzuki cross couplings is the fact that it tolerates water. It was even hypothesized that the reaction may require trace amounts of water.^[71]

All Suzuki couplings are carried out under alkaline conditions regardless of the type of boron reagent.^[72] Independently of the choice of solvent or base, potassium is preferable as counter-ion over sodium or lithium for high catalytic activity.^[73,74] Two mechanisms are discussed in the literature for Suzuki couplings, which differ mainly in the role of the base (Figure 1-3).^[69,75]

In the “Oxo-Palladium” mechanism the cycle starts with oxidative addition of palladium(0) to the aryl halide (see Figure 1-3, top). Thereby the palladium is oxidized to palladium(II). The halide is exchanged by the base, which is fundamental in the next step. Here, transmetalation occurs by transfer of the organic coupling partner R from boron towards palladium. In a concerted fashion the base is transferred to the former boronic acid ester. The final product is now produced from the two ligands by reductive elimination of palladium, regenerating palladium(0). During the catalytic cycle the symmetry of the palladium complex changes from *cis* (after oxidative addition) to *trans* to *cis* (prior to reductive elimination).

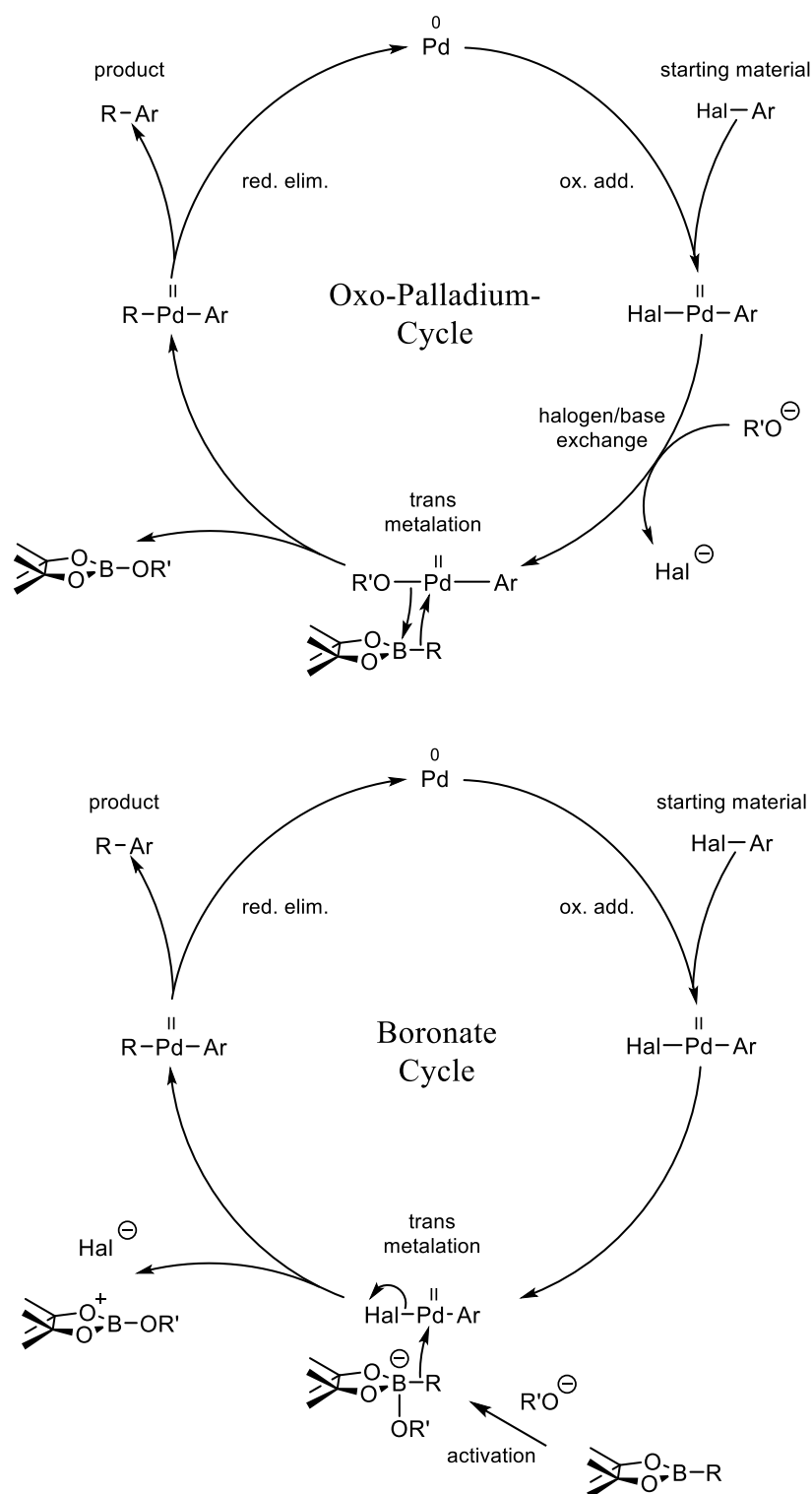


Figure 1-3: Possible mechanisms for Suzuki cross coupling reactions.^[69,75,76] Top: "Oxo-Palladium" cycle with the base directly attached to the transition metal. Bottom: "Boronate" cycle with external activation of the boronic acid ester by the base. Ligands omitted for clarity.

The "Boronate" mechanism works differently after the oxidative addition of palladium to the aryl halide (see Figure 1-3, bottom). Before transmetalation, the boronic acid ester is activated by nucleophilic attack of the base, generating a boronate anion. Therefore the electron density is considerably increased on the

otherwise electron-deficient boron atom. This increase in charge on boron destabilizes the organic substituent R and makes it more prone to transmetalation.

The Suzuki polycondensation follows the same principles as any other polycondensation reaction. Most importantly the Carother's equation applies. It states that the degree of polymerization (\bar{X}_n) is dependent on the yield (p) of the polymerization:[77]

$$\bar{X}_n = \frac{1}{1-p} \quad (1)$$

Hence, in order to reach high degrees of polymerization the monomer purity as well as stoichiometry of functional groups is of utmost importance.

3.2. Direct arylation polycondensation

Although direct arylation occurs on a C-H bond which involves a non-functionalised carbon in a classical context, reactivity varies widely between different types of aryles and heteroarenes, and is additionally influenced by neighboring functional groups. Calculated bond dissociation energies (BDEs) align very well with experimentally derived kinetic values.[78] Examples are given in Figure 1-4.

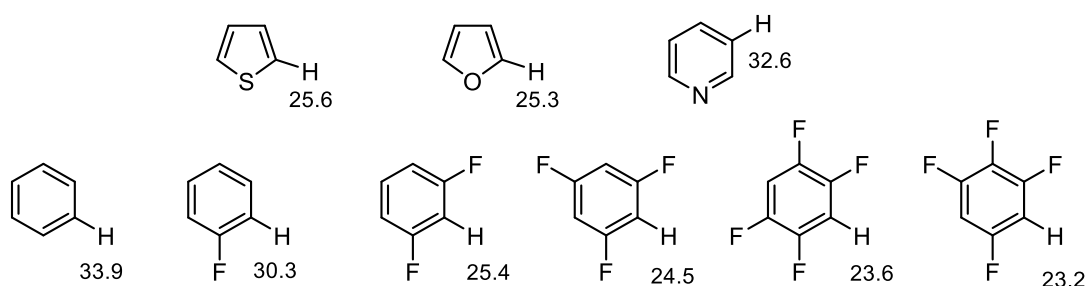


Figure 1-4: BDEs of direct arylation coupling partners (kcal/mol): thiophene, furan, pyridine, benzene, fluorobenzene, 1,3-difluorobenzene, 1,3,5-trifluorobenzene, tetrafluorobenzene (1,2,4,5-, 1,2,3,5-).[78] Only the proton with the lowest BDE is highlighted.

For this work the fluoroarenes are especially important. From the BDEs it is evident that a single fluorine atom is not sufficient in order to promote increased C-H activation compared to benzene. Only a second fluorine directly next to the C-H bond lowers the

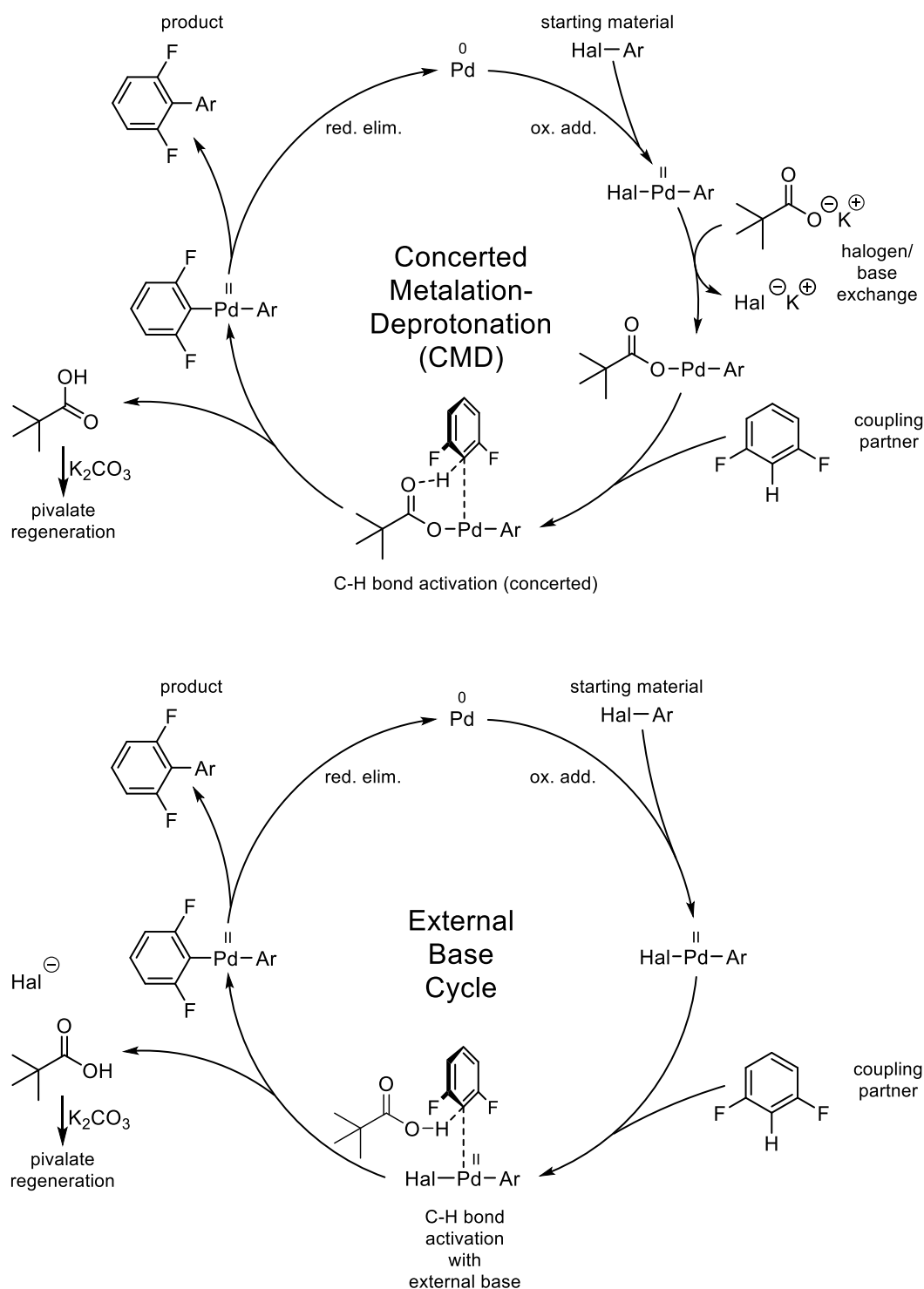


Figure 1-5: Possible mechanisms of direct arylation reactions. Top: Concerted metalation deprotonation mechanism with a six-membered cyclic transition state. Bottom: External base cycle with intermolecular deprotonation during C-H bond activation. Ligands omitted for clarity.^[79]

BDE significantly. The importance of proximity is evident from the tri- and tetrafluorobenzenes with a negligibly lower BDE than 1,3-difluorobenzene. This indicates that the influence of the fluorine atom occurs primarily along the σ system (single bonds) rather than the π system (double bonds), and is related to its high

electronegativity. Coupling reactions on “double *ortho*” positions (between two functional groups such as fluorine) are unusual compared to other cross coupling reactions, because steric hindrance would be expected to be much greater (energetically) than any electronic benefit. In the case of fluorine, steric effects are negligible due to the small van-der-Waals radius of fluorine, which is only 13 % greater than hydrogen (147 pm vs. 120 pm).^[80]

With regards to the base, *in situ* generation of potassium pivalate from K_2CO_3 and pivalic acid works significantly better than employing potassium pivalate (KOPiv) itself.^[79] Additionally, neither pivalic acid nor K_2CO_3 alone are effective.

Details of the mechanism for direct arylation reactions remain unknown and may vary from case to case. Two possible mechanisms have been proposed as shown in Figure 1-5.^[81]

The concerted metalation-deprotonation (CMD) begins by oxidative addition of Pd(0) to the aryl halide.^[81] After oxidative addition the halide is exchanged by the base (i.e. ^-OPiv or CO_3^{2-}). Furthermore, pre-coordination of the unfunctionalised arene to palladium leads towards C-H activation, analogous to the transmetalation step in Suzuki cross couplings.^[82] During the actual C-H activation a six-membered ring is formed between the carbon, proton, palladium and the base (with two oxygens and a carbon). The proton is transferred from the carbon towards the base in a concerted manner, while the carbon is transferred to the palladium.^[83] The two arenes on palladium now undergo reductive elimination and form the desired C-C aryl bond. The palladium is reduced to Pd (0), thereby closing the catalytic cycle.

In the “external base” cycle the halide stays on the palladium during the C-H bond activation step. The base never coordinates to palladium and is therefore only involved in intermolecular manner.^[79]

The symmetry of the metal center changes several times during the catalytic cycle. During oxidative addition, palladium forms a *cis* complex in regard to the aryl and halide ligands. The remaining coordination sites are typically occupied by one or more phosphine ligands. Afterwards the catalytic cycle continues only after isomerization to a *trans* complex. In this configuration C-H bond activation occurs. In order to produce the product by reductive elimination, the palladium complex has to isomerize once again into a *cis* configuration between both aryl ligands. This

cis-trans-cis cycle is well known from other cross coupling reactions with palladium or nickel.

Theoretically, the direct arylation catalytic cycle could also be described by a Pd(II)/Pd(IV) redox mechanism instead of Pd(0)/Pd(II). In the literature this is described as a high-valent palladium catalytic cycle, a term that includes Pd(I)/Pd(III).^[84–86] Organometallic Pd(IV) complexes have been synthesized in the presence of phosphine ligands.^[87] It has been theorized that reactions that follow a Pd(II)/Pd(IV) catalytic pathway should be stable to air and moisture.^[88] Hence, the air sensitivity of direct arylations would indicate a Pd(0)/Pd(II) mechanism. To date, the existence of Pd(IV) species during a catalytic direct arylation cross coupling reaction has not yet been proven on a spectroscopic basis. In contrast, there is strong evidence of high-valent palladium participation in catalytic reactions during trifluoromethylation and C-N bond formation, starting from C-H bonds. However, those reactions require the presence of strong oxidation reagents.^[89–91]

Although a large variety of catalyst, ligand and base combinations may be employed, protocols for direct arylation polymerization mainly rely on tris(*o*-anisyl)phosphine as a ligand (Figure 1-6).^[92] This is a monodentate phosphine that is air-stable and readily available from multiple suppliers. Tris(*o*-anisyl)phosphine allows direct arylation polycondensations of various C-H monomers with halides in several solvents like THF or toluene to be carried out effectively, while triphenylphosphine is commonly limited to polymerizations in DMF.^[93]

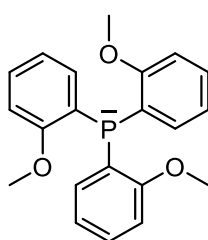


Figure 1-6: Structure of tris(*o*-anisyl)phosphine.

Direct arylations are atom economic (H as functional group on the coupling partner) and less toxic than other cross coupling reactions, especially when compared to Stille reactions.^[94] This is one of the most important advantages, especially as thiophene-based monomers are efficient C-H building blocks but are classically cross-coupled in their stannane form, the latter of which producing neurotoxic byproducts in stoichiometric amounts.^[81,95]

As a polycondensation method, direct arylation cross coupling reactions can be used with a variety of monomers. Previously, thiophene derivatives were used in order to synthesize a defect-free diketopyrrolopyrrol copolymer by direct arylation polycondensation (DAP).^[96] An especially impressive example is the defect-free copolymerization of dibromo dioctylfluorene and tetrafluorobenzene (Figure 1-7).^[97] Here a molecular weight of $M_n = 350\,000$ g/mol ($D = 2.8$) was reached in THF with $\text{Pd}_2\text{dba}_3 \cdot \text{CHCl}_3$ as palladium source.

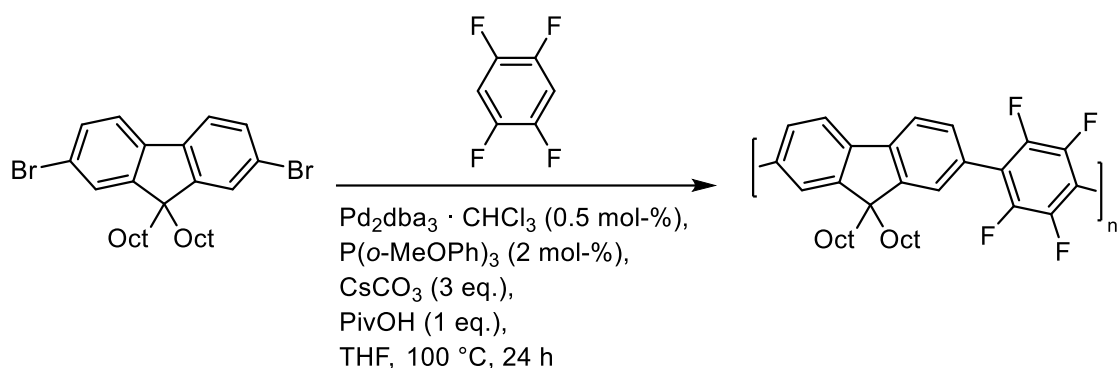


Figure 1-7: Direct arylation polymerization reported by the Ozawa group.^[97]

This thesis also employs direct arylation polymerization of tetrafluorobenzene as comonomer with a kinked biaryl monomer.

4. High-performance polyarylenes

High performance polymers are materials that exceed commodity polymers in regards of one or more properties such as high T_g , high T_m , chemical resistance, strength or optical transparency.^[98] The distinction between high performance and engineering polymers is less established, but is most commonly defined by temperature resistance.^[99] The difficulty of polymer classification becomes apparent with high performance fluoropolymers that have excellent chemical resistance, but low strength and limited wear resistance.^[100] Therefore the term “high performance polymer” will be used in a broad definition in this thesis. In some cases, molecular weight is a factor for exceptional properties. Ultra-high molecular weight polyethylene (UHMWPE, $M_w > 10^6$ g/mol) shows excellent toughness and abrasion resistance compared to its lower molecular weight analogues.^[101]

Further examples for semicrystalline high performance polymers are PEEK, PPS, PI, and polyaramides. Amorphous examples include PPE (polyphenyl ether, Noryl®), PC and PES.^[98,99]

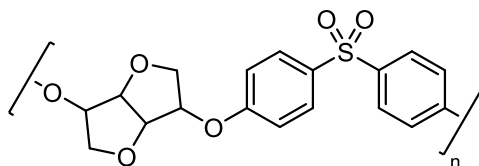


Figure 1-8: Novel high-performance polymer called SUPERBIO.

The field of high performance polymers is constantly evolving. A recent high T_g example is a material called SUPERBIO, a high strength polymer with a strain at break below 15 %.^[99]

It should be noted that most high performance polymers are at least partially aromatic. Polyarylenes are inherently stable materials due to their aromatic backbone. Despite this fact high-performance polyarylenes are rarely observed. For instance, poly*para*arylenes have poor solubility even at elevated temperatures during synthesis due to their low degrees of freedom: rotation is only possible as a whole aromatic subunit and not as a single methylene group as in aliphatic polymers. This inherent rigidity is also the reason for high T_g values of poly*para*arylenes, which makes them difficult to process.^[102] Solubility issues can be mitigated by attachment of aliphatic side-chains, which act as internal plasticizer.^[103] While aliphatic side-chains also lower T_g and improve processability, the mechanical properties of these poly*para*arylenes are insufficient for practical purposes.^[104]

In contrast, poly*meta*arylenes are expected to have better mechanical properties due to the kinked nature of their backbone. For a given molecular weight this should increase entanglement density and thereby improve mechanical properties such as maximum strain at break. However, medium molecular weight poly*meta*arylenes do not show a discernible benefit over their *para* derivatives. Only high molecular weight polyarylenes prepared by the Schlüter Group (Figure 1-9) displayed excellent strain at break values of 160 %.^[105] Therefore, high molecular weight polyarylenes can reach a strain similar to aromatic polycarbonates. The high molecular weight of the polyarylenes by the Schlüter group was achieved by both optimization of reaction conditions and fractionation of the resulting polymer by precipitation. The reaction was a Suzuki polycondensation of a *meta*-dibromide and a bis(boronic acid ester) (Figure 1-10).

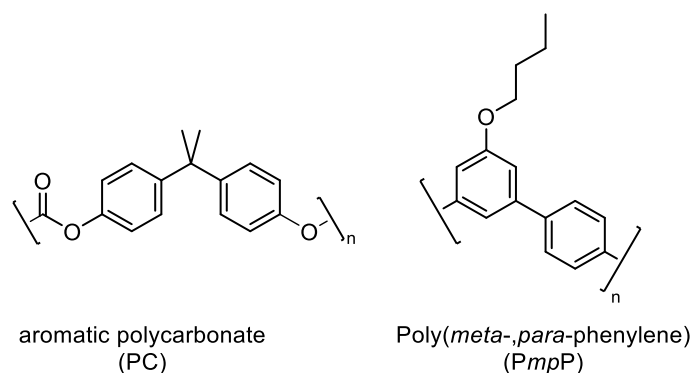


Figure 1-9: Structure of a PC (Makrolon®) and the PmpP by the Schlüter group.^[105]

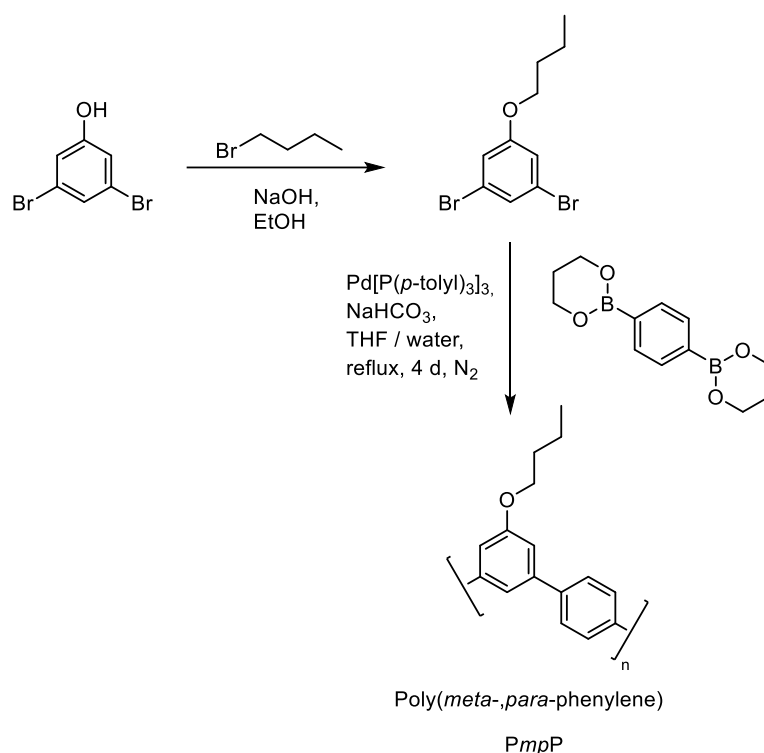


Figure 1-10: Polyarylene PmpP prepared by the Schlüter group.^[105]

It was later demonstrated by the Schlüter group that ring formation is a notable side reaction of the polycondensation reaction.^[106] Cyclic polymers lack any functional groups for further polycondensation and therefore are limited in molecular weight. The formation of cyclic polymers might be an explanation as to why the polycondensation reaction of polyarylenes is so sensitive to the reaction conditions. The fractionation of the PmpP by the Schlüter group was carried out by precipitation. Only the highest molecular weight fraction of $M_w = 255\,000$ g/mol showed good mechanical properties (second highest fraction: $M_w = 85\,000$ g/mol). Investigations of the chloro-derivative of the monomer limited the molecular weight to $M_w = 24\,000$ g/mol.^[107] Other variations of PmpP include a silyl-group as side

chain, which can be cleaved off after polymerization in order to investigate unsubstituted polyarylenes (Figure 1-11).^[108,109]

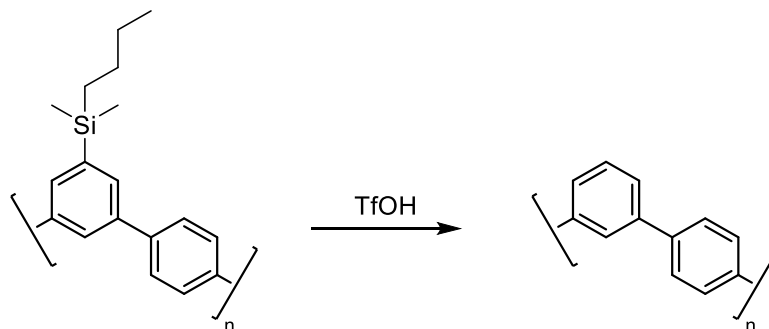


Figure 1-11: “Shaving” approach by the Schlüter group in order to access unsubstituted and high molecular weight *PmpPs*.^[109]

This “shaving” approach yielded unsubstituted *PmpPs* that are tough close to their T_g (180 °C), but brittle at room temperature.^[110] In contrast, the butoxy substituted *PmpP* was tough at room temperature (T_g 166 °C). This demonstrates that side chain functionalization is very effective for tuning the thermal and mechanical properties of kinked polyarylenes. Their synthesis will be discussed further in the discussion chapters.

5. References

- [1] I. Roy, M. N. Gupta, *Chemistry & Biology* **2003**, *10*, 1161–1171.
- [2] X.-J. Ju, R. Xie, L. Yang, L.-Y. Chu, *Expert Opin. Ther. Pat.* **2009**, *19*, 683–696.
- [3] T. Leydecker, M. Herder, E. Pavlica, G. Bratina, S. Hecht, E. Orgiu, P. Samori, *Nat. Nanotechnol.* **2016**, *11*, 769–775.
- [4] M. Chen, S. Deng, Y. Gu, J. Lin, M. J. MacLeod, J. A. Johnson, *J. Am. Chem. Soc.* **2017**, *139*, 2257–2266.
- [5] M. M. Caruso, D. A. Davis, Q. Shen, S. A. Odom, N. R. Sottos, S. R. White, J. S. Moore, *Chem. Rev.* **2009**, *109*, 5755–5798.
- [6] T. J. Kucharski, R. Boulatov, *J. Mater. Chem.* **2011**, *21*, 8237–8255.
- [7] O. Rifaie-Graham, E. A. Apebende, L. K. Bast, N. Bruns, *Adv. Mater.* **2018**, *30*, 1705483–1705529.
- [8] D. R. T. Roberts, S. J. Holder, *J. Mater. Chem.* **2011**, *21*, 8256–8268.
- [9] K. M. Wiggins, J. N. Brantley, C. W. Bielawski, *Chem. Soc. Rev.* **2013**, *42*, 7130–7147.
- [10] J. N. Brantley, K. M. Wiggins, C. W. Bielawski, *Polym. Int.* **2013**, *62*, 2–12.
- [11] W. Kauzmann, H. Eyring, *J. Am. Chem. Soc.* **1940**, *62*, 3113–3125.
- [12] M. Karman, E. Verde-Sesto, C. Weder, *ACS Macro Lett.* **2018**, *7*, 1028–1033.
- [13] G. O'Bryan, B. M. Wong, J. R. McElhanon, *ACS Appl. Mater. Interfaces* **2010**, *2*, 1594–600.
- [14] A. L. Black, J. M. Lenhardt, S. L. Craig, *J. Mater. Chem.* **2011**, *21*, 1655–1663.
- [15] K. Imato, T. Kanehara, S. Nojima, T. Ohishi, Y. Higaki, A. Takahara, H. Otsuka, *Chem. Commun.* **2016**, *52*, 10482–10485.
- [16] S. Jiang, L. Zhang, T. Xie, Y. Lin, H. Zhang, Y. Xu, W. Weng, L. Dai, *ACS Macro Lett.* **2013**, *2*, 705–709.
- [17] M. Kathan, S. Hecht, *Chem. Soc. Rev.* **2017**, *46*, 5536–5550.
- [18] S. K. Surampudi, H. R. Patel, G. Nagarjuna, D. Venkataraman, *Chem. Commun.* **2013**, *49*, 7519–7521.
- [19] C. K. Lee, D. A. Davis, S. R. White, J. S. Moore, N. R. Sottos, P. V. Braun, *J. Am. Chem. Soc.* **2010**, *132*, 16107–16111.
- [20] W. Qiu, P. A. Gurr, G. da Silva, G. G. Qiao, *Polym. Chem.* **2019**, *10*, 1650–1659.
- [21] A. V. Kulinich, A. A. Ishchenko, *Russ. Chem. Rev.* **2009**, *78*, 141.
- [22] R. Klajn, *Chem. Soc. Rev.* **2014**, *43*, 148–184.
- [23] B. S. Lukyanov, M. B. Lukyanova, *Chemistry of Heterocyclic Compounds* **2005**, *41*, 281–311.
- [24] N. Tamai, H. Miyasaka, *Chem. Rev.* **2000**, *100*, 1875–1890.
- [25] Y. Futami, M. L. S. Chin, S. Kudoh, M. Takayanagi, M. Nakata, *Chemical Physics Letters* **2003**, *370*, 460–468.
- [26] J. Hobley, V. Malatesta, W. Giroladini, W. Stringo, *Phys. Chem. Chem. Phys.* **2000**, *2*, 53–56.
- [27] C. J. Wohl, D. Kuciauskas, *J. Phys. Chem. B* **2005**, *109*, 22186–22191.
- [28] N. A. Murugan, S. Chakrabarti, H. Ågren, *J. Phys. Chem. B* **2011**, *115*, 4025–4032.

- [29] G. Berkovic, V. Krongauz, V. Weiss, *Chem. Rev.* **2000**, *100*, 1741–1754.
- [30] M. Bletz, U. Pfeifer-Fukumura, U. Kolb, W. Baumann, *J. Phys. Chem. A* **2002**, *106*, 2232–2236.
- [31] J.-W. Zhou, Y.-T. Li, X.-Q. Song, *Journal of Photochemistry and Photobiology A: Chemistry* **1995**, *87*, 37–42.
- [32] C. Beyer, H.-A. Wagenknecht, *The Journal of organic chemistry* **2010**, *75*, 2752–5.
- [33] T. Satoh, K. Sumaru, T. Takagi, K. Takai, T. Kanamori, *Phys. Chem. Chem. Phys.* **2011**, *13*, 7322–7329.
- [34] H. Mayr, A. R. Ofial, *Angew. Chem., Int. Ed.* **2006**, *45*, 1844–1854.
- [35] C. P. McCoy, L. Donnelly, D. S. Jones, S. P. Gorman, *Tetrahedron Lett.* **2007**, *48*, 657–661.
- [36] V. I. Minkin, *Chem. Rev.* **2004**, *104*, 2751–2776.
- [37] H. Tomioka, T. Itoh, *J. Chem. Soc., Chem. Commun.* **1991**, 532–533.
- [38] M. Irie, T. Iwayanagi, Y. Taniguchi, *Macromolecules* **1985**, *18*, 2418–2422.
- [39] A. Pucci, G. Ruggeri, *J. Mater. Chem.* **2011**, *21*, 8282–8291.
- [40] J. Li, C. Nagamani, J. S. Moore, *Acc. Chem. Res.* **2015**, *48*, 2181–2190.
- [41] G. R. Gossweiler, G. B. Hewage, G. Soriano, Q. Wang, G. W. Welshofer, X. Zhao, S. L. Craig, *ACS Macro Lett.* **2014**, *3*, 216–219.
- [42] D. a Davis, A. Hamilton, J. Yang, L. D. Cremer, D. Van Gough, S. L. Potisek, M. T. Ong, P. V. Braun, T. J. Martínez, S. R. White, J. S. Moore, N. R. Sottos, *Nature* **2009**, *459*, 68–72.
- [43] C. M. Kingsbury, P. A. May, D. A. Davis, S. R. White, J. S. Moore, N. R. Sottos, *J. Mater. Chem.* **2011**, *21*, 8381–8388.
- [44] S. L. Potisek, D. A. Davis, N. R. Sottos, S. R. White, J. S. Moore, *J. Am. Chem. Soc.* **2007**, *129*, 13808–13809.
- [45] H. Komber, S. Müllers, F. Lombeck, A. Held, M. Walter, M. Sommer, *Polym. Chem.* **2013**, *5*, 443–453.
- [46] M. Raisch, D. Genovese, N. Zaccheroni, S. B. Schmidt, M. L. Focarete, M. Sommer, C. Gualandi, *Adv. Mater.* **2018**, *30*, 1802813–1802813.
- [47] M. Plaschke, R. Czolk, H. J. Ache, *Analytica Chimica Acta* **1995**, *304*, 107–113.
- [48] J. Chen, P. Zhang, G. Fang, P. Yi, X. Yu, X. Li, F. Zeng, S. Wu, *J. Phys. Chem. B* **2011**, *115*, 3354–3362.
- [49] Y.-H. Chan, M. E. Gallina, X. Zhang, I.-C. Wu, Y. Jin, W. Sun, D. T. Chiu, *Anal. Chem.* **2012**, *84*, 9431–9438.
- [50] M. Irie, A. Menju, K. Hayashi, *Macromolecules* **1979**, *12*, 1176–1180.
- [51] G. C. Fortman, S. P. Nolan, *Chem. Soc. Rev.* **2011**, *40*, 5151–5169.
- [52] E. Negishi, A. O. King, N. Okukado, *J. Org. Chem.* **1977**, *42*, 1821–1823.
- [53] F.-S. Han, *Chem. Soc. Rev.* **2013**, *42*, 5270–5298.
- [54] C. E. I. Knappke, A. J. von Wangelin, *Chem. Soc. Rev.* **2011**, *40*, 4948–4962.
- [55] S. B. Schmidt, F. Kempe, O. Brüchner, M. Walter, M. Sommer, *Polym. Chem.* **2017**, *8*, 5407–5414.
- [56] A. Yokoyama, R. Miyakoshi, T. Yokozawa, *Macromolecules* **2004**, *37*, 1169–1171.

- [57] A. Kiriya, V. Senkovskyy, M. Sommer, *Macromol. Rapid Commun.* **2011**, *32*, 1503–1517.
- [58] P.-O. Morin, T. Bura, M. Leclerc, *Mater. Horiz.* **2015**, *3*, 11–20.
- [59] D. G. Hall, in *Boronic Acids* (Ed.: D.G. Hall), Wiley-VCH Verlag GmbH & Co. KGaA, **2005**, pp. 1–99.
- [60] A. J. J. Lennox, G. C. Lloyd-Jones, *Chem. Soc. Rev.* **2013**, *43*, 412–443.
- [61] G. A. Molander, C.-S. Yun, M. Ribagorda, B. Biolatto, *J. Org. Chem.* **2003**, *68*, 5534–5539.
- [62] G. A. Molander, N. Ellis, *Acc. Chem. Res.* **2007**, *40*, 275–286.
- [63] A. J. J. Lennox, G. C. Lloyd-Jones, *Angew. Chem. Int. Ed.* **2012**, *51*, 9385–9388.
- [64] C. Amatore, G. Broecker, A. Jutand, F. Khalil, *J. Am. Chem. Soc.* **1997**, *119*, 5176–5185.
- [65] N. G. Andersen, B. A. Keay, *Chem. Rev.* **2001**, *101*, 997–1030.
- [66] M. R. Netherton, G. C. Fu, *Org. Lett.* **2001**, *3*, 4295–4298.
- [67] T. E. Barder, S. D. Walker, J. R. Martinelli, S. L. Buchwald, *J. Am. Chem. Soc.* **2005**, *127*, 4685–4696.
- [68] M. R. Biscoe, B. P. Fors, S. L. Buchwald, *J. Am. Chem. Soc.* **2008**, *130*, 6686–6687.
- [69] R. Martin, S. L. Buchwald, *Acc. Chem. Res.* **2008**, *41*, 1461–1473.
- [70] A. N. Marziale, S. H. Faul, T. Reiner, S. Schneider, J. Eppinger, *Green Chem.* **2010**, *12*, 35–38.
- [71] C. Amatore, A. Jutand, G. Le Duc, *Chem. Eur. J.* **2011**, *17*, 2492–2503.
- [72] A. A. C. Braga, N. H. Morgon, G. Ujaque, F. Maseras, *J. Am. Chem. Soc.* **2005**, *127*, 9298–9307.
- [73] C. Amatore, A. Jutand, G. Le Duc, *Chem. Eur. J.* **2012**, *18*, 6616–6625.
- [74] C. Amatore, G. Le Duc, A. Jutand, *Chem. Eur. J.* **2013**, *19*, 10082–10093.
- [75] N. T. S. Phan, M. Van Der Sluys, C. W. Jones, *Adv. Synth. Catal.* **2006**, *348*, 609–679.
- [76] F. Kempe, Alkylierung von Spiropyranen Mittels Kumada- Und Suzuki-Kreuzkupplungen, Masterarbeit, Albert-Ludwigs-Universität Freiburg, **2015**.
- [77] S. Koltzenburg, M. Maskos, O. Nuyken, *Polymere: Synthese, Eigenschaften und Anwendungen*, Springer Spektrum, Berlin, **2014**.
- [78] S. I. Gorelsky, *Coordination Chemistry Reviews* **2013**, *257*, 153–164.
- [79] M. Lafrance, D. Lapointe, K. Fagnou, *Tetrahedron* **2008**, *64*, 6015–6020.
- [80] A. Bondi, *J. Phys. Chem.* **1964**, *68*, 441–451.
- [81] D. Alberico, M. E. Scott, M. Lautens, *Chem. Rev.* **2007**, *107*, 174–238.
- [82] S. I. Gorelsky, D. Lapointe, K. Fagnou, *J. Org. Chem.* **2012**, *77*, 658–668.
- [83] S. I. Gorelsky, D. Lapointe, K. Fagnou, *J. Am. Chem. Soc.* **2008**, *130*, 10848–10849.
- [84] A. J. Hickman, M. S. Sanford, *Nature* **2012**, *484*, 177–185.
- [85] D. C. Powers, E. Lee, A. Ariafard, M. S. Sanford, B. F. Yates, A. J. Canty, T. Ritter, *J. Am. Chem. Soc.* **2012**, *134*, 12002–12009.
- [86] D. C. Powers, T. Ritter, in *Higher Oxidation State Organopalladium and Platinum Chemistry* (Ed.: A.J. Canty), Springer, Berlin, Heidelberg, **2011**, pp. 129–156.
- [87] P. Sehnal, R. J. K. Taylor, I. J. S. Fairlamb, *Chem. Rev.* **2010**, *110*, 824–889.

- [88] L.-M. Xu, B.-J. Li, Z. Yang, Z.-J. Shi, *Chem. Soc. Rev.* **2010**, 39, 712–733.
- [89] M. Nappi, M. J. Gaunt, *Organometallics* **2019**, 38, 143–148.
- [90] X. Wang, L. Truesdale, J.-Q. Yu, *J. Am. Chem. Soc.* **2010**, 132, 3648–3649.
- [91] L.-S. Zhang, K. Chen, G. Chen, B.-J. Li, S. Luo, Q.-Y. Guo, J.-B. Wei, Z.-J. Shi, *Org. Lett.* **2013**, 15, 10–13.
- [92] M. Wakioka, F. Ozawa, *Asian Journal of Organic Chemistry* **2018**, 7, 1206–1216.
- [93] M. Wakioka, Y. Nakamura, M. Montgomery, F. Ozawa, *Organometallics* **2015**, 34, 198–205.
- [94] H. Bohra, M. Wang, *J. Mater. Chem. A* **2017**, 5, 11550–11571.
- [95] J.-R. Pouliot, F. Grenier, J. T. Blaskovits, S. Beaupré, M. Leclerc, *Chem. Rev.* **2016**, 116, 14225–14274.
- [96] S. Broll, F. Nübling, A. Luzio, D. Lentzas, H. Komber, M. Caironi, M. Sommer, *Macromolecules* **2015**, 48, 7481–7488.
- [97] M. Wakioka, Y. Kitano, F. Ozawa, *Macromolecules* **2013**, 46, 370–374.
- [98] M. Friedman, G. Walsh, *Polym. Eng. Sci.* **2002**, 42, 1756–1788.
- [99] S.-A. Park, H. Jeon, H. Kim, S.-H. Shin, S. Choy, D. S. Hwang, J. M. Koo, J. Jegal, S. Y. Hwang, J. Park, D. X. Oh, *Nat. Commun.* **2019**, 10, 2601.
- [100] H. Teng, *Appl. Sci.* **2012**, 2, 496–512.
- [101] M. Stürzel, F. Kempe, Y. Thomann, S. Mark, M. Enders, R. Mülhaupt, *Macromolecules* **2012**, 45, 6878–6887.
- [102] I. Yamaguchi, K. Goto, M. Sato, *Tetrahedron* **2009**, 65, 3645–3652.
- [103] S. Vanhee, R. Rulkens, U. Lehmann, C. Rosenauer, M. Schulze, W. Köhler, G. Wegner, *Macromolecules* **1996**, 29, 5136–5142.
- [104] J. Sakamoto, M. Rehahn, G. Wegner, A. D. Schlüter, *Macromol. Rapid Commun.* **2009**, 30, 653–687.
- [105] R. Kandre, K. Feldman, H. E. H. Meijer, P. Smith, A. D. Schlüter, *Angewandte Chemie International Edition* **2007**, 46, 4956–4959.
- [106] B. Hohl, L. Bertschi, X. Zhang, A. D. Schlüter, J. Sakamoto, *Macromolecules* **2012**, 45, 5418–5426.
- [107] R. Kandre, A. D. Schlüter, *Macromol. Rapid Commun.* **2008**, 29, 1661–1665.
- [108] S. Jakob, A. Moreno, X. Zhang, L. Bertschi, P. Smith, A. D. Schlüter, J. Sakamoto, *Macromolecules* **2010**, 43, 7916–7918.
- [109] B. Deffner, A. D. Schlüter, *Polym. Chem.* **2015**, 7833–7840.
- [110] B. Deffner, S. Jimaja, A. Kroeger, A. D. Schlüter, *Macromol. Chem. Phys.* **2017**, 218, 1600561–1600561.

Chapter 2 Substituent-controlled Energetics and Barriers of Mechanochromic Spiropyran-functionalized Poly(ϵ -caprolactone)

Fabian Kempe^{‡,1}, Lukas Metzler^{‡,3,5}, Oliver Brügger², Hannah Buchheit³,
Michael Walter^{2,4,6}, Michael Sommer^{*,1}

[‡] contributed equally

¹ Chemnitz University of Technology, Institute for Chemistry, Polymer Chemistry,
Straße der Nationen 62, 09111 Chemnitz, Germany

² Freiburg Center for Interactive Materials and Bioinspired Technologies (FIT),
Georges-Koehler-Allee 105, 79110 Freiburg, Germany

³ University of Freiburg, Institute for Macromolecular Chemistry, Stefan-Meier-Str. 31,
79104 Freiburg, Germany

⁴ Cluster of Excellence livMatS @ FIT – Freiburg Center for Interactive Materials and Bioinspired Technologies,
University of Freiburg, Georges-Köhler-Allee 105, 79110 Freiburg, Germany

⁵ University of Freiburg, Department of Microsystems Engineering (IMTEK),
Georges-Koehler-Allee 102, 79110 Freiburg, Germany

⁶ Fraunhofer IWM, MikroTribologie Centrum μ TC, Wöhlerstrasse 11, 79108 Freiburg, Germany

In preparation

1. Abstract

We demonstrate in a joint theoretical and experimental study that the onset of the mechanically-induced isomerization of spiropyran (SP) containing mechanochromic ϵ -polycaprolactone (ϵ -PCL) can be controlled both by the regiochemistry of chain attachment and the substitution pattern of SP. *In-situ* visible light absorption measurements of thin films during uniaxial strain experiments demonstrate varying activation barriers of the force-induced ring-opening reaction of SP covalently incorporated into tough, semicrystalline ϵ -PCL. SPs with ϵ -PCL in *ortho*-position isomerize earlier than *para* analogs. This notable difference in onset delay is in contrast with observations on soft materials by other research groups. NO₂-substituted SP mechanophores exhibited a lower activation barrier compared to H-substituted ones, an effect which is most prominent when the NO₂ substituent is attached to the *para* position. The herein reported results allow for a better understanding of polymeric force sensor design.

2. Introduction

Spiroyrans (SP) are classical candidates for mechanochromic materials with a wide range of possible stimuli such as ultraviolet light, pH and mechanical force.^[1] Therefore they are applicable as force sensors in order to indicate mechanical loads dynamically before irreversible stress cracking occurs.^[2–5] In order to rationally design stress sensors, structure-activity relationships need to be investigated.^[6–10] Ideally, SP derivatives with a series of different activation barriers should enable the visualization of specific force thresholds.^[11]

Existing literature is not sufficiently consistent in order to compare different SP derivatives with altered substitution pattern and regio-chemistry. Previous DFT calculations by us indicated a strong correlation between the substitution pattern of spiropyran and the molecular force needed for their ring-opening reaction.^[12] Similarly, large effects of regiochemistry of the polymeric anchor points on the coloration probability were shown for ϵ -PCL and PDMS.^[3,13–16] However, barrier heights and trajectories are scarcely considered and many details remain largely unknown.^[17]

Here we will demonstrate that SP isomerization behavior differs significantly in tough, semicrystalline ϵ -PCL compared to elastomeric PDMS.

We prepared a series of SP initiators with varying substitution (NO_2 or H) and chain attachment (“*ortho*” and “*para*”) as depicted in Scheme 2-2. Those spiropyrans were used as bifunctional initiators during ϵ -polycaprolactone synthesis as demonstrated previously.^[14] Thereby SP was placed in the middle of polycaprolactone chains for the majority of chains (see Experimental section for details). Those main-chain spiropyran copolymers are especially suited for mechanical activation compared to end-functionalized or side-chain copolymers.^[1]

PCL is a semicrystalline polymer which is tough if a sufficiently large molecular weight is reached.^[18,19] While turbid in the relaxed (unstrained) state, polycaprolactone becomes sufficiently translucent beyond the yield point while both width and thickness are reduced significantly. PCL has previously been used to study spiropyran in multiple studies.^[14,15,20]

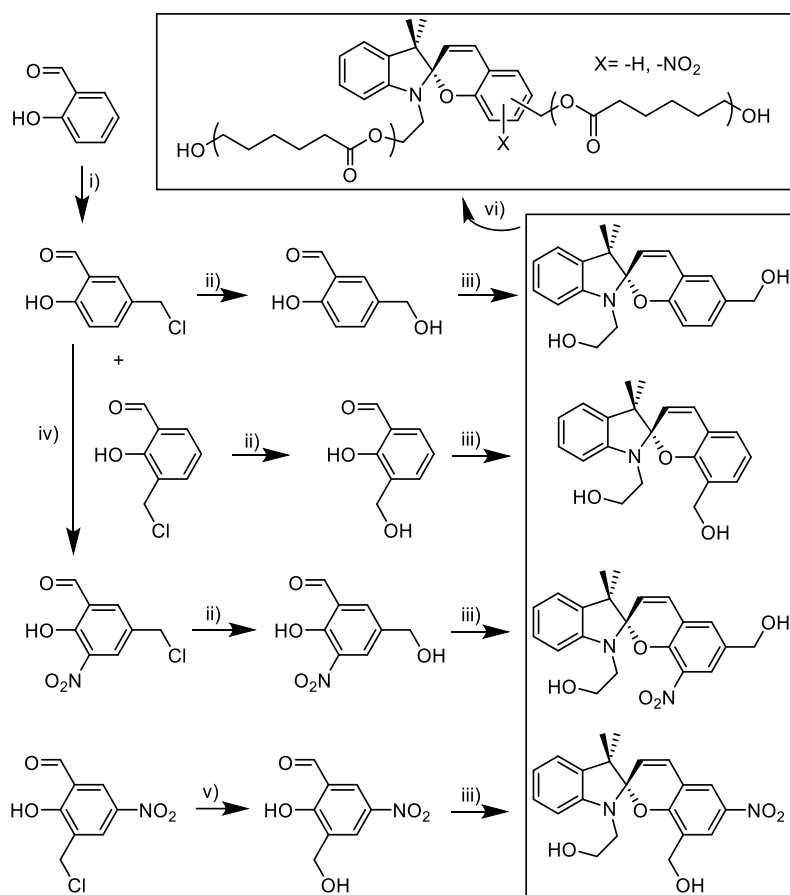
3. Results and Discussion

Four distinct SP copolymers were synthesized in this work (Scheme 2-1 and Scheme 2-2). Molecular weights were determined by SEC in THF (Table 2-1). Some of the bifunctional SP-initiators and their resulting functionalized poly(ϵ -caprolactone)s are literature-known.^[3,15] SP was incorporated into the chain either by an „*ortho*–“ or „*para*–“ connection. Generally, the *ortho*-SP would be expected to open more easily upon external force due to a better mechanical „lever“ present in an *ortho*-attached polymer chain. Hence, the majority of the literature used this kind of *ortho*-linkage.^[14,15] Most importantly, the same chemistry of chain attachment (methylene group) was used on all derivatives to ensure the same electronic effect of the polymer linkage upon the SP aromatic ring system. Furthermore each regioisomer was either left unsubstituted (-H as functional group) or substituted with a nitro group (- NO_2) in the position unused for linkage to the polymer chain.

SP copolymers were mixed in a 1 : 1 ratio with commercial ϵ -PCL for molecular weight equalization and an automated film coater was used in order to assure reproducibility. Films were prepared from the melt, which likely provides some extent of alignment beneficial for the stress-strain experiment.^[21]

Table 2-1: Molecular weights of SP copolymers as measured by SEC in THF (1 mL / min, 40 °C).

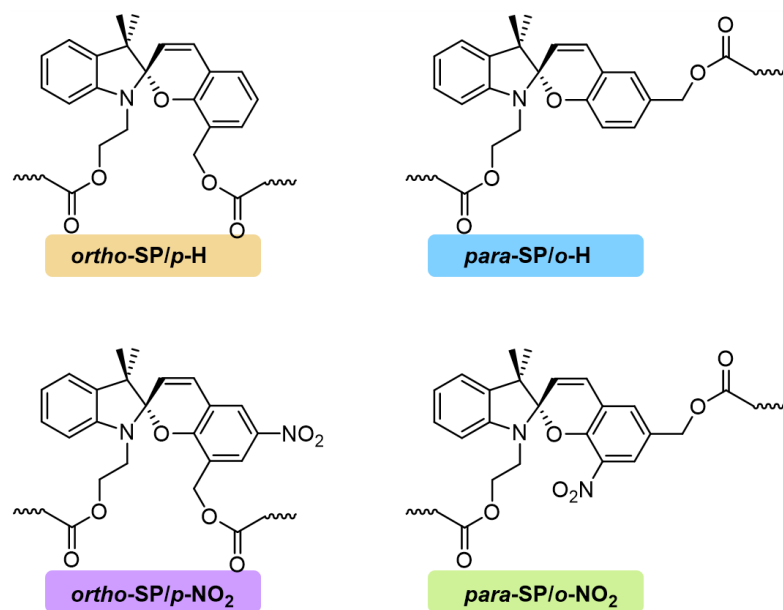
Sample	M_n / g/mol	\bar{D}
<i>ortho</i> -SP/ <i>p</i> -H	22 400	1.6
<i>para</i> -SP/ <i>o</i> -H	30 500	1.4
<i>ortho</i> -SP/ <i>p</i> -NO ₂	19 300	1.9
<i>para</i> -SP/ <i>o</i> -NO ₂	27 700	1.5



Scheme 2-1: Synthesis of bifunctional SP initiators for the ring opening polymerization of ϵ -caprolactone. Reaction conditions: i) formaldehyde (aq., 37%), conc. HCl ii) H₂O iii) 1-(2-hydroxyethyl)-2,3,3-trimethylindoliniumiodide, ethanol, piperidine iv) acetic acid, HNO₃, v) NaOH (aq), vi) ϵ -caprolactone, Sn(oct)₂, 140 °C.

The samples were punched from the film with a geometry which reliably allows yielding in the middle of the sample where the light absorption measurement takes place (Figure 2-1a).

We also prepared two analogous SP bifunctional initiators with methoxy-substituents and their corresponding ϵ -PCL polymers, but these materials turned reddish upon doctor blading from the melt, as a result of the energetically most favorable isomerization into the protonated merocyanine MCH⁺ form.^[12,22] Hence, these polymers were not further investigated here.



Scheme 2-2: SP copolymers synthesized in this work to probe the influence of regio- („*ortho*“ vs. „*para*“) as well as electronic (H or NO₂) effects on the force-induced SP → MC reaction. The copolymer was poly(ε-caprolactone) (see Scheme 2-1).

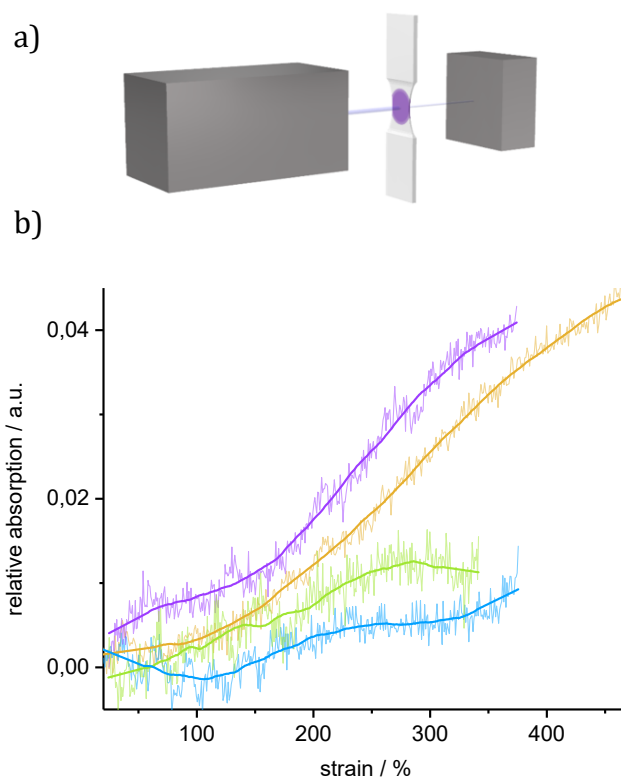


Figure 2-1: a) Schematic experimental setup for in-situ VIS spectroscopy during stress-strain of films. After the yield point polycaprolactone becomes sufficiently translucent for visible light (450 – 800 nm). b) In-situ visible light absorption after the yield point during stress-strain experiment. Only the *ortho*-SP/*p*-NO₂ (purple) immediately isomerizes after the yield point. Values plotted correspond to absorption at 585 nm relative to 700 nm (= baseline). Bold line is floating average.

Figure 2-1b shows the *in-situ* visible light absorption at 585 nm for all four SP polymers during the stress-strain experiments. Only values after the yield point are plotted because film thickness stabilized afterwards. Small variations in film thickness were corrected by normalizing the absorption to the signal at 700 nm, a region that is well outside the absorption range of all SP derivatives investigated. Precautions were taken to exclude other stimuli for SP \rightarrow MC isomerization during measurement. Light absorption measurements were carried out with a halogen lamp (450 – 800 nm) and in a closed cell with small windows in order to shield the sample from ambient light.

Immediately after the yield point only the absorption of *ortho*-SP/*p*-NO₂ (purple in the MC form) significantly increased beyond signal noise. The isomerization of all other SP polymers was delayed up until 100 % strain if signal noise is taken into consideration. At this point the absorption of *ortho*-SP/*p*-H (orange) started continually to increase, while both *para*-SP/*o*-NO₂ (green) and *para*-SP/*o*-H (blue) remained at a low level of absorption. At 340 % strain, which is the largest value reached by all SP polymers, the difference in absorption between the *ortho*-SPs and *para*-SPs is most pronounced. This confirms previous observations in literature that the regiochemistry of polymer linkage is an important factor and *ortho*-linkage generally provides a higher degree of SP isomerization.

The substituent effect of NO₂ vs. H is evident from the comparison of the *ortho*-SPs. The NO₂ derivative isomerizes immediately, while the onset of the corresponding H derivative is delayed until 100 % strain. A possible factor is the increase of the π -system by NO₂. This seems to stabilize the transition state for SP \rightarrow MC isomerization and thus lowers the barrier.

Force-dependent DFT analysis of free activation energies for the SP \rightarrow MC transition corroborate this assumption. Figure 2-2 shows activation barriers for the forward (SP \rightarrow MC, blue) and backward isomerization (MC \rightarrow SP). As would be expected for the forward SP \rightarrow MC transition, the activation barrier is lower if external force is applied. It should be noted that values derived from these calculations are overestimated due to the fact that calculations are carried out under assumption of isolated molecules in the gas phase. There are two relevant barriers in the ring-opening reaction of SP.^[17,23] Firstly, there is the barrier to break and reform the central C-O bond. Secondly, there is the barrier for β -rotation of the intermediate

MC-CCC to the final MC-CTC form.^[23] Bond rupture is induced from thermal fluctuations on the force-transformed energy surface^[24] that constantly split and reform the bond. It is thus a stochastic process, where the bond breaks with high probability if the forward-barrier towards MC is low and the backward-barrier towards bond reforming is high.

The barriers in *ortho*-derivatives diminish quickly at small external forces, where they are dominated by the barrier for C-O breaking in forward direction from SP \rightarrow MC. *ortho*-SP/*p*-NO₂ has a steeper negative slope compared to *ortho*-SP/*p*-H indicating a larger reduction of the activation barrier by external force. Equally important is the fact that the forward barrier in *ortho*-SP/*p*-NO₂ is deviating from the backward reaction early on at 0.1 nN. This makes bond rupture statistically more likely compared to *ortho*-SP/*p*-H due to the competition between bond breaking and reforming. During visible light absorption, the substituent effect in the *para*-SPs seems more pronounced compared to *ortho* if the floating average is considered.

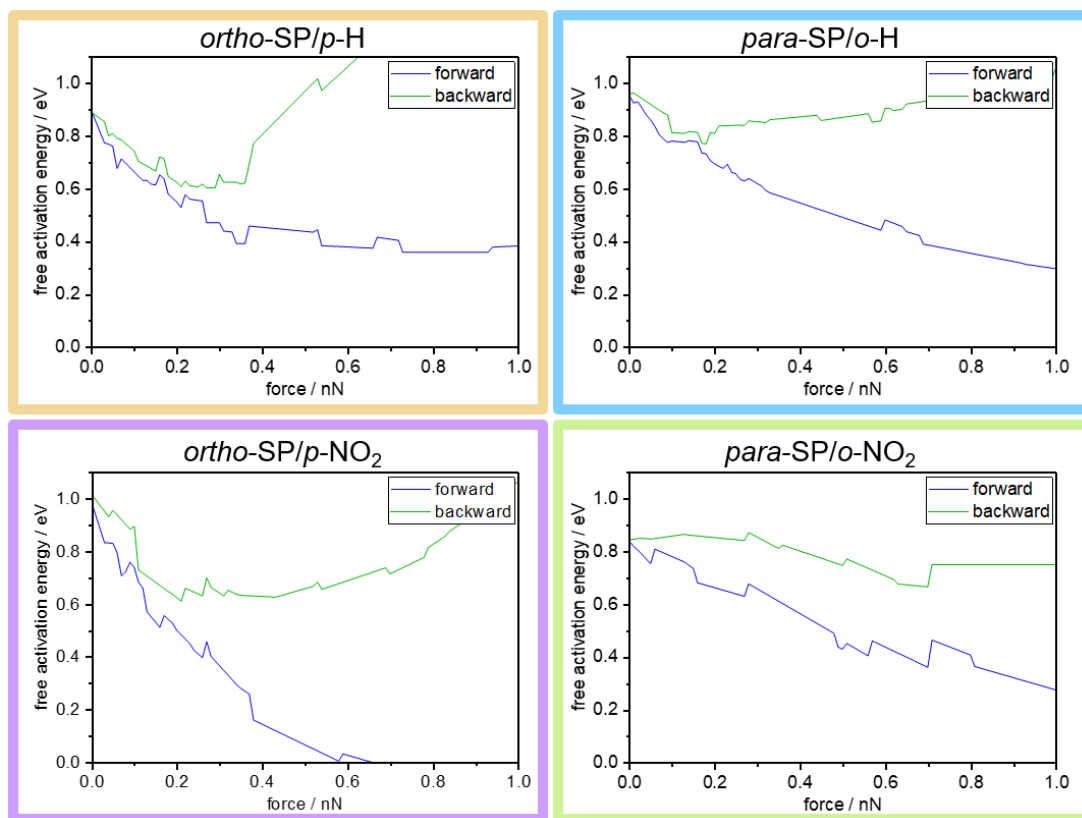


Figure 2-2: Barriers for forward and backward reactions in the different SP derivatives investigated. Solid lines are electronic energies including vibrational energy contributions (the step-like features are numeric artifacts). The main contributions to the barrier are indicated. For color code see Scheme 2-2.

However, a closer look at the underlying data (half-transparent line, Figure 2-1b) reveals that the signal-to-noise ratio is worse than in the case of *ortho*-SPs, as would be expected for smaller overall absorption values. Taking this noise into consideration, *para*-SP/*o*-NO₂ only deviates significantly from zero absorption after 180 % strain. Without NO₂ (*para*-SP/*o*-H) this deviation from zero is also delayed towards 180 % strain. Hence, there is no significant effect of NO₂-substitution in the *para*-SPs. Accordingly, force-dependent DFT analysis shows smaller slopes for the forward isomerization SP → MC of *para* compared to *ortho* (Figure 2-2).

Consequently, NO₂ increases overall absorption of SP, but only in the case of *ortho*-SPs it also removes the delay in mechanochromic response.

4. Conclusion

In summary, we have shown that regiochemistry and the substitution pattern of SP covalently incorporated into ϵ -PCL has a large influence on the onset of SP → MC isomerization, with ϵ -PCL attached in *ortho*-position to SP showing significantly faster isomerization compared to *para* in analogs. This in contrast to observations by other studies on elastomeric PDMS^[13] and highlights the dependence of SP isomerization behavior on the surrounding material. NO₂-substitution increases overall absorption of SP in agreement with literature. With respect to isomerization onset, NO₂ substitution had only a positive effect in *ortho*-SP, where the NO₂ group resides in the *para*-position. This was corroborated by force-dependent DFT calculations of the isomerization barrier of the SP → MC transition. The free activation energy of *ortho*-SPs was lowered the most by external force compared to *para*-, an effect even more pronounced with NO₂ substitution. The better understanding of substitution and regiochemistry effects of SP allows for more control in the design of tailor-made force sensor materials.

5. Acknowledgements

Funding from the DFG (SO 1213/7-1 and MW 1687/ 9) is acknowledged. O.B. and M.W. are grateful for computational resources from FZ-Jülich (HFR08) and from the bwForCluster NEMO in Freiburg. The authors acknowledge M. Hagios for SEC measurements.

6. Experimental Methods

6.1. General information

All **chemicals** were obtained from Sigma Aldrich and used without further treatment unless specified.

DSC measurements were acquired on a NETZSCH DSC 204 F1 Phoenix under a nitrogen atmosphere at a heating and cooling rate of 10 K / min.

NMR spectra were measured on a Bruker ARX 300 and a Bruker Avance III 500 machine. All spectra were recorded at 303 K in CDCl₃ as solvent and were referenced to the residual solvent peak ($\delta = 7.26$ ppm) and analysed using Bruker TOPSPIN 2.1 software package.

UV/VIS-spectroscopy was carried out with rigid thin films on the Flame-S UV-Vis-spectrometer from Ocean Optics, controlled by the OceanView 1.5.2 software.

SEC measurements were carried out on three SDV gel 5 μm columns and a pre-column, with pore sizes ranging from 10^3 to 10^5 Å (PSS), connected in series with a 254 nm UV-Detector detector and calibrated with polystyrene standards. THF was used as eluent at 30 °C at a flow rate of 1.0 mL / min.

6.2. Overview of the initiator synthesis

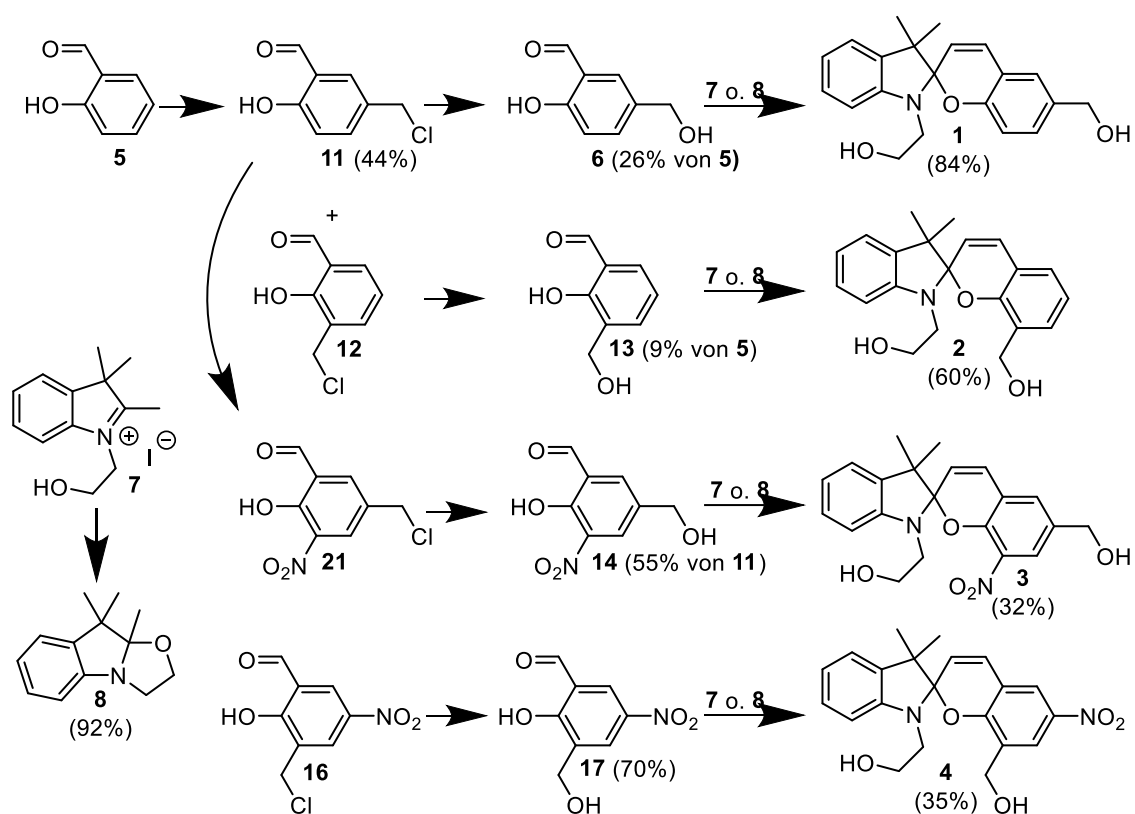
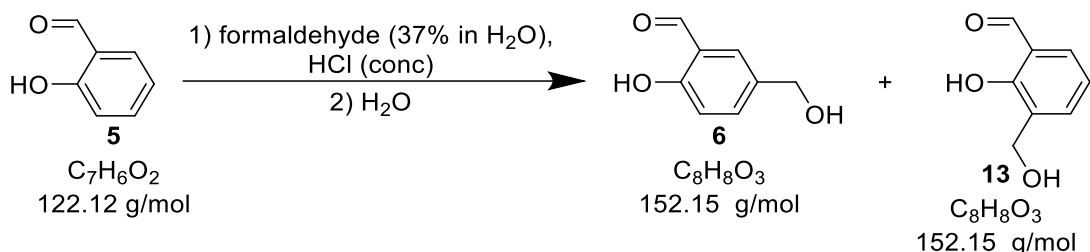


Figure 2-3: Overview of the SP initiator synthesis.

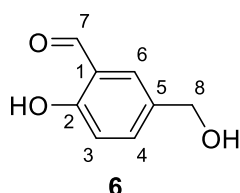
6.2.1. Synthesis of salicylaldehydes

6.2.1.1. 2-Hydroxy-5-hydroxymethylbenzaldehyde (and 2-hydroxy-3-hydroxymethylbenzaldehyde)

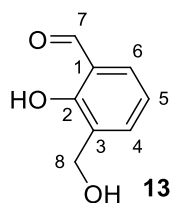


Salicylaldehyde (9.0 ml, 86 mmol) was added to a mixture of conc. HCl (42 mL) and aqueous formaldehyde solution [37% (stabilized with MeOH), 17.0 mL, 228 mmol, 2.65 eq]. The mixture was stirred for 25 min at 85 °C and stored at 4 °C overnight. The solid was filtered off, dissolved in boiling water (200 mL), heated under reflux for 30 min and stored overnight at 4 °C for crystallization. The colorless crystals were filtered off and recrystallized from CHCl₃. The product was obtained as colourless crystals (3.40 g, 22.3 mmol, 26 %).

2-Hydroxy-3-hydroxymethylbenzaldehyde is obtained as a side-product and has been isolated from the mother liquor.



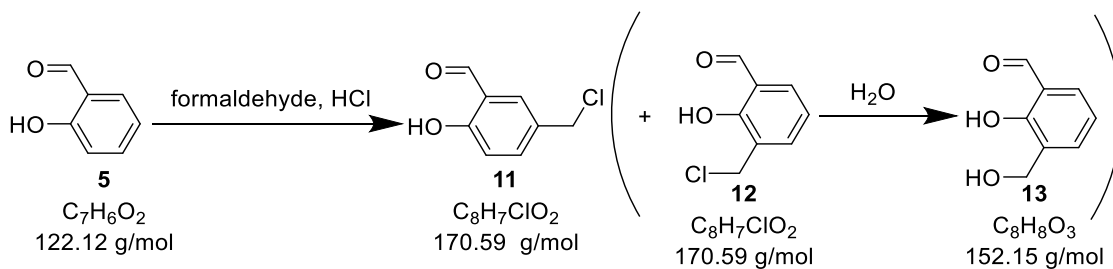
2-Hydroxy-5-hydroxymethylbenzaldehyde: ¹H-NMR (300 MHz, CDCl₃): δ = 1.73 (t, 8-OH, *J*_{8-OH, 8H} = 5.6 Hz), 4.68 (d, 8-H₂, *J*_{8, 8-OH} = 5.6 Hz), 7.0 (d, 3-H, *J*_{3,4} = 8.5 Hz), 7.53 (dd, 4-H, *J*_{4,3} = 8.5 Hz, *J*_{4,6} = 2.1 Hz), 7.59 (dd, 6-H, *J*_{6,4} = 2.1 Hz, *J*_{6,7} = 0.5 Hz), 9.90 (d, 7-H, *J*_{7,6} = 0.5 Hz), 10.99 (s, 2-OH) ppm.



2-Hydroxy-3-hydroxymethylbenzaldehyde: $^1\text{H-NMR}$ (300 MHz, CDCl_3): δ = 2.24 (t, 8-OH, $J_{8\text{-OH}, 8\text{H}}$ = 6.5 Hz), 4.77 (d, 8-H₂, $J_{8, 8\text{-OH}}$ = 6.5 Hz), 7.04 (dd, 5-H, $J_{5,4}$ = 7.7 Hz, $J_{5,6}$ = 7.5 Hz), 7.53 (dd, 4-H, $J_{4,5}$ = 7.7 Hz, $J_{4,6}$ = 1.8 Hz), 7.60 (ddd, 6-H, $J_{6,5}$ = 7.5 Hz, $J_{6,4}$ = 1.8 Hz, $J_{6,7}$ = 0.6 Hz), 9.90 (s, 2-OH), 11.38 (d, 7-H, $J_{7,6}$ = 0.6 Hz) ppm.

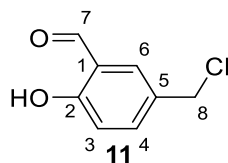
Related literature: United States Patent: 6355658 - Example 3^[25]

6.2.1.2. 5-Chloromethyl-2-hydroxybenzaldehyde

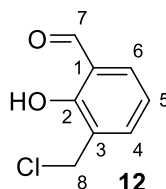


A mixture of conc. HCl (200 mL) and aqueous formaldehyde solution [37% (stabilized with MeOH), 14.4 mL, 193 mmol, 1.01 eq] was mixed with salicylaldehyde (20.0 mL, 23.4 g, 192 mmol) and stirred for 24 hours at room temperature. The resulting solid was filtered off and recrystallized from hexane after decanting the hot solution from the pink oil and storing it overnight at 4 °C. 5-Chloromethylsalicylaldehyde was obtained as colourless crystals (2.14 g, 70.5 mmol, 37 %).

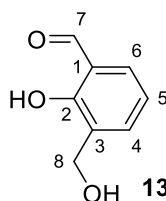
The mother liquor contains a mixture of 5-chloromethyl-2-hydroxybenzaldehyde and 3-chloromethyl-2-hydroxybenzaldehyde. The mixture was heated in water (150 mL) with reflux (2 h), decanted hot and extracted with dichloromethane (4 x 25 mL). By column chromatography [(first IH/EE 5/1; then more polar) R_f (2-hydroxy-3-hydroxymethylbenzaldehyde) = 0.5, R_f (2-hydroxy-5-hydroxymethylbenzaldehyde) = 0.3] 2-hydroxy-3-hydroxymethylbenzaldehyde (2.66 g, 17.5 mmol, 9 % from salicylaldehyde) was isolated.



5-chloromethyl-2-hydroxybenzaldehyde $^1\text{H-NMR}$ (300 MHz, CDCl_3): δ = 4.59 (s, 8-H₂), 7.00 (d, 3-H, $J_{3,4}$ = 8.5 Hz), 7.56 (dd, 4-H, $J_{4,3}$ = 8.5 Hz, $J_{4,6}$ = 2.4 Hz), 7.59 (dd, 6-H, $J_{6,4}$ = 2.4 Hz, $J_{6,7}$ = 0.5 Hz), 9.90 (d, 7-H, $J_{7,6}$ = 0.5 Hz), 11.06 (s, 2-OH) ppm.



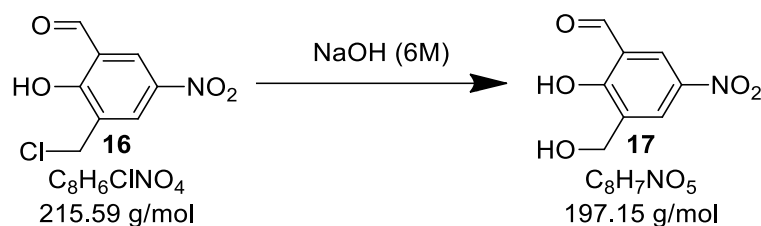
3-chloromethyl-2-hydroxybenzaldehyde $^1\text{H-NMR}$ (300 MHz, CDCl_3): δ = 4.70 (s, 8-H₂) 7.05 (dd, 5-H, $J_{5,4}$ = 7.6 Hz, $J_{5,6}$ = 7.6 Hz), 7.57 (dd, 4-H, $J_{4,5}$ = 7.6 Hz, $J_{4,6}$ = 1.8 Hz), 7.65 (ddd, 6-H, $J_{6,5}$ = 7.6 Hz, $J_{6,4}$ = 1.8 Hz, $J_{6,7}$ = 0.5 Hz), 9.92 (s, 2-OH), 11.45 (d, 7-H, $J_{7,6}$ = 0.5 Hz) ppm.



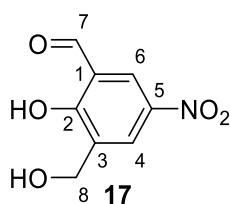
2-hydroxy-3-hydroxymethylbenzaldehyde: $^1\text{H-NMR}$ (300 MHz, CDCl_3): δ = 2.24 (t, 8-OH, $J_{8\text{-OH},8\text{H}}$ = 6.5 Hz), 4.77 (d, 8-H₂, $J_{8,8\text{-OH}}$ = 6.5 Hz), 7.04 (dd, 5-H, $J_{5,4}$ = 7.7 Hz, $J_{5,6}$ = 7.5 Hz), 7.53 (dd, 4-H, $J_{4,5}$ = 7.7 Hz, $J_{4,6}$ = 1.8 Hz), 7.60 (ddd, 6-H, $J_{6,5}$ = 7.5 Hz, $J_{6,4}$ = 1.8 Hz, $J_{6,7}$ = 0.6 Hz), 9.90 (s, 2-OH), 11.38 (d, 7-H, $J_{7,6}$ = 0.6 Hz) ppm.

Related literatur: Naik et al., 2008^[26]

6.2.1.3. 2-Hydroxy-3-hydroxymethyl-5-nitrobenzaldehyde

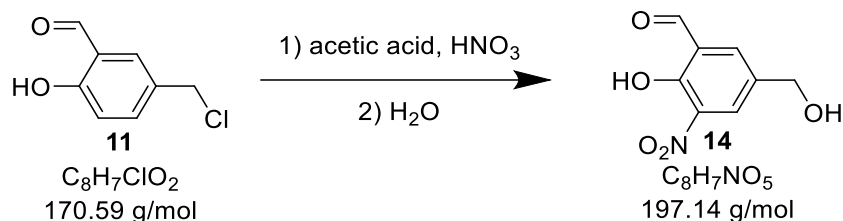


3-chloromethyl-2-hydroxy-5-nitrobenzaldehyde (1.02 g, 4.72 mmol) was dispersed in water under vigorous stirring and heated under reflux. After 15 min, aqueous NaOH solution (6 M, 0.77 mL, 4.62 mmol, 0.98 eq) was added within 10 min. After another 90 min under reflux, the mixture was hot filtered and stored at 4 °C overnight for crystallization. After filtration, the product (0.655 g, 3.32 mmol, 70%) was obtained in the form of yellowish needles.

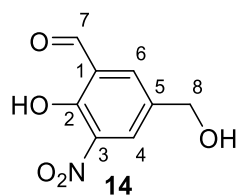


2-Hydroxy-3-hydroxymethyl-5-nitrobenzaldehyde $^1\text{H-NMR}$ (300 MHz, CDCl_3): δ = 2.16 (s, 8-OH), 4.85 (s, 8-H₂), 8.48 (d, 4-H, $J_{4,6}$ = 2.9 Hz) 8.55 (d, 6-H, $J_{6,4}$ = 2.8 Hz), 10.01 (s, 7-H), 11.86 (br s, 2-OH) ppm.

6.2.1.4. 2-Hydroxy-5-hydroxymethyl-3-nitrobenzaldehyde



To a solution of 5-chloromethyl-2-hydroxybenzaldehyde (2.01 g, 11.8 mmol) in glacial acetic acid (100 %, 23.5 mL), a mixture of fuming nitric acid (100 %, 0.52 mL, 12.5 mmol, 1.06 eq) and glacial acetic acid (100 %, 12.0 mL) was added within 30 min using a syringe pump. The mixture was stirred for 2 h at room temperature, poured on ice and filtered. The filter residue was heated for 1 h in refluxed water, filtered hot and stored overnight at 4 °C for crystallization. The mixture was then stirred at room temperature, poured on ice and filtered. After filtration, the product (1.34 g, 55 %) was obtained in the form of yellow crystals.

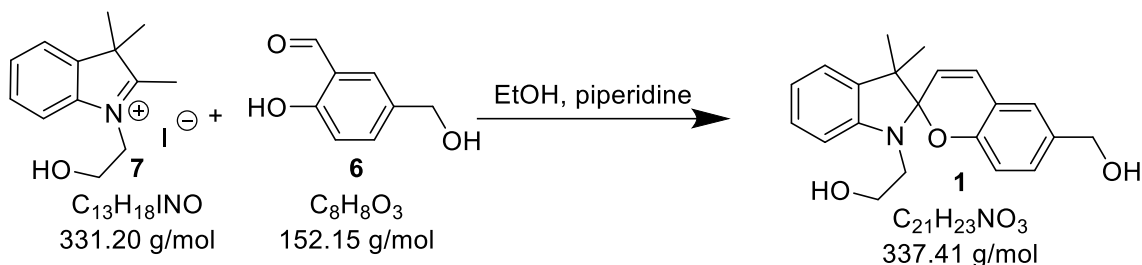


2-Hydroxy-5-hydroxymethyl-3-nitrobenzaldehyde $^1\text{H-NMR}$ (300 MHz, CDCl_3): δ = 1.91 (t, 8-OH, $J_{8\text{-OH},8}$ = 5.5 Hz), 4.76 (d, 8-H, $J_{8\text{-OH},8}$ = 5.5), 8.11 (d, 4-H, $J_{4,6}$ = 2.3 Hz), 8.39 (d, 6-H, $J_{6,4}$ = 2.3 Hz), 10.42 (s, 7-H), 11.37 (s, 2-OH) ppm.

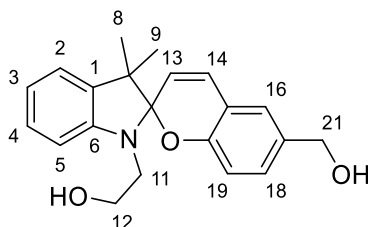
Related literature: Braude and Gal'bershtam, 1978^[27]

6.2.2. Synthesis of the bifunctional spiropyran initiators

6.2.2.1. Spiro[1-(2-hydroxyethyl)-3,3-dimethylindoline-2,2'-6'-hydroxymethylbenzopyran]



A solution of 1-(2-hydroxyethyl)-2,3,3-trimethylindoliniumiodide¹ (0.343 g, 1.04 mmol), 2-hydroxy-5-hydroxymethylbenzaldehyde (0.156 g, 1.03 mmol, 1.0 eq) and piperidine (0.15 mL, 1.5 mmol, 1.5 eq) in ethanol (6 mL) was heated under reflux for 5 h. The solvent was removed from the reaction mixture under reduced pressure, dissolved in ethyl acetate (10 mL) and washed with water (3 x 5 mL). The solvent was removed under reduced pressure. The product (0.292 g, 0.865 mmol, 84 %) was obtained as a greenish solid.



¹H-NMR (300 MHz, CDCl₃): δ = 7.17 (s, 8-H₃*), 1.31 (s, 9-H₃*), 2.78 - 3.37 und 3.45 - 3.55 (m, 11-H₂), 3.70 - 3.77 (m, 12-H), 4.56 (s, 21-H₂), 5.70 (d, 13-H, $J_{13,14}$ = 10.2 Hz), 6.63 (d, 5-H, $J_{5,4}$ = 7.8 Hz), 6.68 (d, 19-H, $J_{19,18}$ = 7.9 Hz), 6.83 (d, 13-H, $J_{14,13}$ = 10.2 Hz), 6.86 (ddd, 3-H, $J_{3,4}$ = 7.5 Hz, $J_{3,2}$ = 7.3 Hz, $J_{3,5}$ = 1.0 Hz), 7.06 (s, 16-H), 7.08 (dd, 2-H und 16-H J_{ortho} = 7.5, J_{meta} = 1.6), 7.16 (ddd, 4-H, $J_{4,3}$ = 7.7 Hz, $J_{4,5}$ = 7.6 Hz, $J_{4,1}$ = 1.3 Hz) ppm.

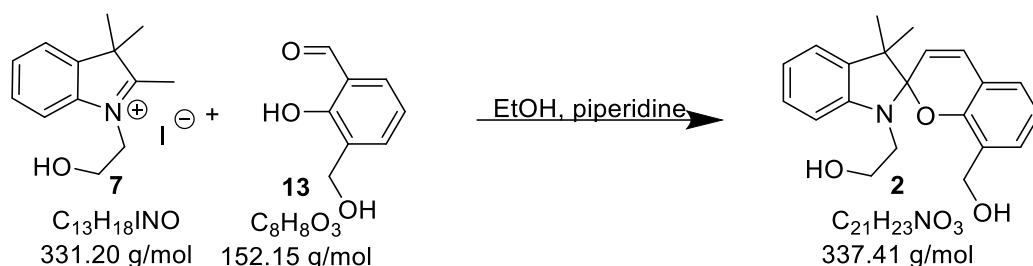
* Exchangeable assignment

¹ The synthesis of 1-(2-hydroxyethyl)-2,3,3-trimethylindoliniumiodide was analogous to Reddington et al. 2007^[28] and Raymo et al. 2001^[29].

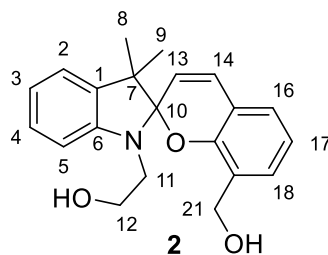
Mass spectroscopy:

[SP+Na]⁺	calculated: 360.15701 (C ₂₁ H ₂₃ NO ₃ Na) measured: 360.15714
[SP+H]⁺	calculated: 338.17507 (C ₂₁ H ₂₄ NO ₃) measured: 338.17526

6.2.2.2. Spiro[1-(2-hydroxyethyl)-3,3-dimethylindoline-2,2'-8'-hydroxymethylbenzopyran]



A solution of 1-(2-hydroxyethyl)-2,3,3-trimethylindoliniumiodide (1.229 g, 3.71 mmol), 2-hydroxy-3-hydroxymethylbenzaldehyde (0.565 g, 3.71 mmol, 1.00 eq) and piperidine (0.55 mL, 5.6 mmol, 1.5 eq) in ethanol (23 mL) was heated under reflux for 6 hours. After removing the solvent from the reaction mixture under reduced pressure, it was dissolved in ethyl acetate (25 mL) and washed with water (3 x 10 mL). The solvent was removed under reduced pressure and the crude product was purified by column chromatography (eluent: ethyl acetate, R_f = 0.77). The product fractions were concentrated under reduced pressure to a viscous oil and stored overnight at room temperature for crystallization. After washing the crystals with hexane, the product (0.444 g, 1.31 mmol, 35 %) was obtained as brown crystals.

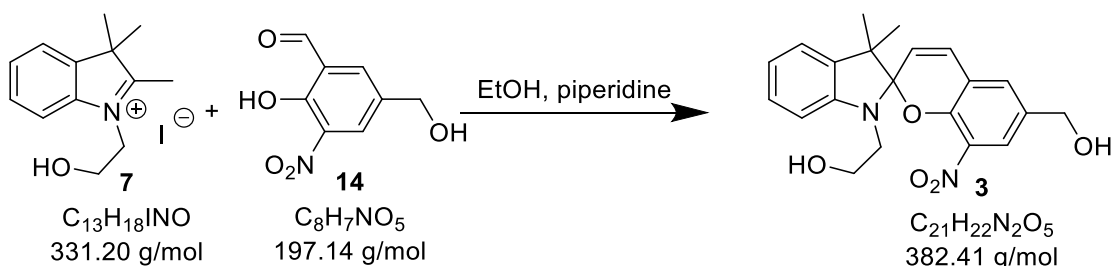


$^1\text{H-NMR}$ (300 MHz, CDCl_3): δ = 1.20 und 1.32 (s, 8- H_3 und 9- H_3), 3.22 – 3.31 und 3.43 – 3.53 (m, 11- H_2), 3.65 – 3.71 (m, 12- H), 4.33 und 4.55 (m, 21- H_2), 5.70 (d, 13- H , $J_{13,14}$ = 10.2 Hz), 6.60 (d, 5- H , $J_{5,4}$ = 7.9 Hz), 6.83 (dd, 17- H , 2 x J_{ortho} = 7.4 Hz), 6.84 (ddd, 3- H , J_{ortho} = 7.5 Hz, J_{ortho} = 7.3 Hz, $J_{3,5}$ = 1.0 Hz), 6.83 (d, 14- H , $J_{14,13}$ = 10.2 Hz), 7.02 (dd, 16- H , $J_{16,17}$ = 7.5 Hz, $J_{16,18}$ = 1.6 Hz), 7.07 (dd, 2- H und 16- H $J_{2,3}$ = 8.2, $J_{2,4}$ = 1.1), 7.11 (dd, 18- H , $J_{18,17}$ = 7.6 Hz, $J_{18,16}$ = 1.5 Hz), 7.14 (ddd, 4- H , 2 x J_{ortho} = 7.6 Hz, $J_{4,2}$ = 1.2 Hz) ppm.

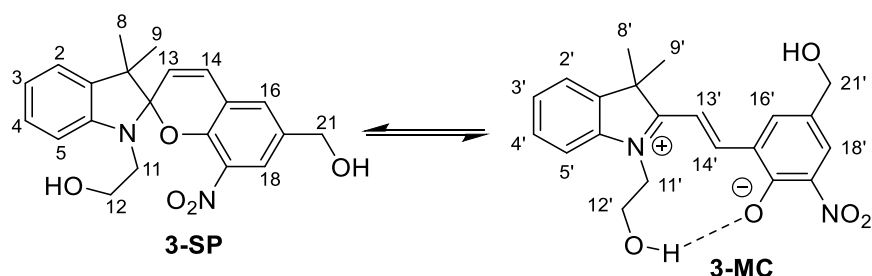
$^{13}\text{C-NMR}$ (126 MHz, CDCl_3): δ = 20.44 und 25.56 (8- C und 9- C), 45.88 (11- C), 51.84 (7- C), 60.71 (12- C), 60.97 (21- C), 104.80 (10- C), 106.57 (5- C), 118.46 (15- C), 119.18 (13- C), 119.38 (3- C), 120.22 (17- C), 121.77 (2- C), 126.46 (16- C), 126.84 (19- C), 127.63 (4- C), 129.29 (18- C), 129.37 (14- C), 136.12 (1- C), 146.93 (6- C), 151.32 (20- C) ppm.

Mass spectroscopy:	$[\text{SP}+\text{Na}]^+$	calculated: 360.15701 ($\text{C}_{21}\text{H}_{23}\text{NO}_3\text{Na}$)
		measured: 360.15686
	$[\text{SP}+\text{H}]^+$	calculated: 338.17507 ($\text{C}_{21}\text{H}_{24}\text{NO}_3$)
		measured: 338.17490

6.2.2.3. Spiro[1-(2-hydroxyethyl)-3,3-dimethylindoline-2,2'-6'-hydroxymethyl-8'-nitrobenzopyran]



A solution of 1-(2-hydroxyethyl)-2,3,3-trimethylindoliniumiodide (0.522 g, 1.58 mmol), 2-hydroxy-5-hydroxymethyl-3-nitrobenzaldehyde (0.320 g, 1.62 mmol, 1 eq) and piperidine (0.24 mL, 2.4 mmol, 1.5 eq) in ethanol (10 mL) was stirred under reflux for 5 h. The solvent was removed from the reaction mixture under reduced pressure, dissolved in ethyl acetate (15 mL) and washed with water (3 x 7 mL). The solvent was removed under reduced pressure and the crude product was purified by column chromatography (ethyl acetate, NEt_3 (2.5 %), R_f = 0.7). The product (32 %) was obtained as a violet solid.



In CDCl_3 a mixture of SP and MC (ratio 1:5) is observed. For clarity, the peaks of the two molecules are listed separately.

SP: $^1\text{H-NMR}$ (500 MHz, CDCl_3): δ = 1.20 und 1.33 (s, 8- H_3 und 9- H_3), 3.58 und 3.41 (m, 11- H_2), 3.80 (m, 12- H), 4.67 (s, 21- H_2), 5.87 (d, 13- H , $J_{13,14}$ = 10.5 Hz), 6.66 (d, 5- H , $J_{5,4}$ = 7.9 Hz), 6.88 (ddd, 3- H , 2 x J_{ortho} = 7.2 Hz, $J_{3,5}$ = 1.0 Hz), 6.92 (d, 14- H , $J_{14,13}$ = 10.4 Hz), 7.07 (dd, 2- H , $J_{2,3}$ = 7.2 Hz, $J_{2,4}$ = 1.1 Hz), 7.17 (ddd, 4- H , 2x J_{ortho} = 7.5 Hz, $J_{4,2}$ = 1.3 Hz), 7.33 (d, 16- H , $J_{16,18}$ = 2.1), 7.72 (d, 18- H , $J_{18,16}$ = 2.1) ppm.

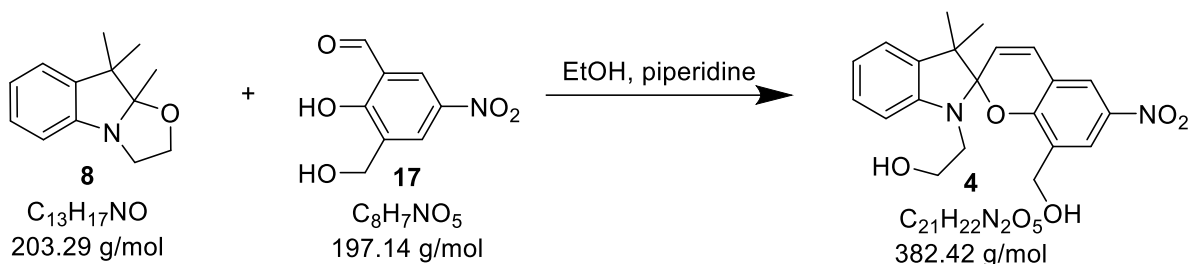
SP: ^{13}C -NMR (126 MHz, CDCl_3): δ = 20.33 und 25.91 (8-C und 9-C), 45.96 (11-C), 52.96 (7-C), 60.61 (12-C), 63.72 (21-C), 106.81 (5-C), 107.10 (10-C), 119.83 (3-C), 121.60 (2-C), 121.67 (15-C), 122.18 (13-C), 123.74 (18-C), 127.74 (4-C), 128.41 (14-C), 129.91 (16-C), 132.44 (17-C), 135.39 (1-C), 136.97 (19-C), 146.44 (6-C), 147.23 (20-C) ppm.

MC: ^1H -NMR (500 MHz, CDCl_3): δ = 1.21 und 1.49 (s, 8'-H₃ und 9'-H₃*), 3.50 und 3.73 (m, 11'-H₂), 3.67 und 3.84 (m, 12'-H), 4.73 (s, 21'-H₂), 6.49 (d, 13'-H, $J_{13',14'} = 16.1$ Hz), 6.84 (d, 5'-H, $J_{5',4'} = 7.9$ Hz), 6.98 (ddd, 3'-H, $2 \times J_{ortho} = 7.4$ Hz, $J_{3',5'} = 1.0$ Hz), 7.12 (dd, 2'-H, $J_{2',3'} = 7.3$ Hz, $J_{2',4'} = 1.2$ Hz), 7.20 (ddd, 4'-H, $2 \times J_{ortho} = 7.5$ Hz, $J_{4',2'} = 1.4$ Hz), 7.23 (d, 14'-H, $J_{14',13'} = 16.0$ Hz), 7.82 (d, 16'-H, $J_{16',18'} = 2.1$), 8.08 (d, 18'-H, $J_{18',16'} = 2.1$), 11.1 (br s, 19-OH) ppm.

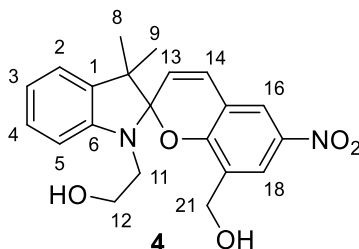
MC: ^{13}C -NMR (126 MHz, CDCl_3): δ = 20.46 und 28.49 (8'-C und 9'-C), 47.96 (7'-C), 50.24 (11'-C), 63.67 (12'-C), 63.82 (21'-C), 109.82 (10'-C), 112.05 (5'-C), 121.77 (3'-C), 122.09 (18'-C), 122.39 (2'-C), 124.99 (14'-C), 127.65 (4-C), 128.95 (15'-C), 130.26 (13'-C), 132.44 (17'-C), 133.47 (16'-C), 133.81 (19'-C), 139.59 (1'-C), 150.52 (6'-C), 152.28 (20-C) ppm.

Mass spectroscopy:	[SP+Na]⁺	calculated: 405.14209 ($\text{C}_{21}\text{H}_{22}\text{N}_2\text{O}_5\text{Na}$)
		measured: 405.14215
	[SP+H]⁺	calculated: 383.16015 ($\text{C}_{21}\text{H}_{23}\text{N}_2\text{O}_5$)
		measured: 383.16019

6.2.2.4. Spiro[1-(2-hydroxyethyl)-3,3-dimethylindoline-2,2'-8'-hydroxymethyl-6'-nitrobenzopyran]



A solution of 2,3,3-trimethylindolino[1,2-b]oxazoline (0.145 g, 0.713 mmol), 2-hydroxy-3-hydroxymethyl-5-nitrobenzaldehyde (0.139 g, 0.705 mmol) and piperidine (0.1 mL, 1.1 mmol) in ethanol (2.7 mL) was heated under reflux for 5 hours. The solvent was removed under reduced pressure. Subsequently, the reaction mixture was dissolved in ethyl acetate (10 mL) and washed with water (3 x 7 mL). After drying the organic phase over Na_2SO_4 and removing the solvent, the product was purified by column chromatography (ethyl acetate, NEt_3 (2.5 %)). The product (total: 0.096 g, 0.25 mmol, 35 %) was obtained as a violet solid².



¹H-NMR (300 MHz, CDCl_3): δ = 1.19 (s, 8- H_3^*), 1.28 (s, 9- H_3^*), 3.25 – 3.34 und 3.42 – 3.52 (m, 11- H_2), 3.68 – 3.73 (m, 12- H), 4.35 und 4.52 (m, 21- H_2), 5.86 (d, 13- H , $J_{13,14}$ = 10.3 Hz), 6.62 (d, 5- H , $J_{5,4}$ = 7.8 Hz), 6.86 (ddd, 3- H , 2 x J_{ortho} = 7.4 Hz, $J_{3,5}$ = 1.0 Hz), 6.91 (d, 14- H , $J_{14,13}$ = 10.4 Hz), 7.07 (dd, 2- H , $J_{2,3}$ = 7.2 Hz, $J_{2,4}$ = 1.0 Hz), 7.15 (ddd, 4- H , 2 x J_{ortho} = 7.6 Hz, $J_{4,2}$ = 1.3 Hz), 7.93 (d, 16- H , 2.8 Hz), 8.07 (d, 18- H , 2.8 Hz) ppm.

* exchangeable assignment

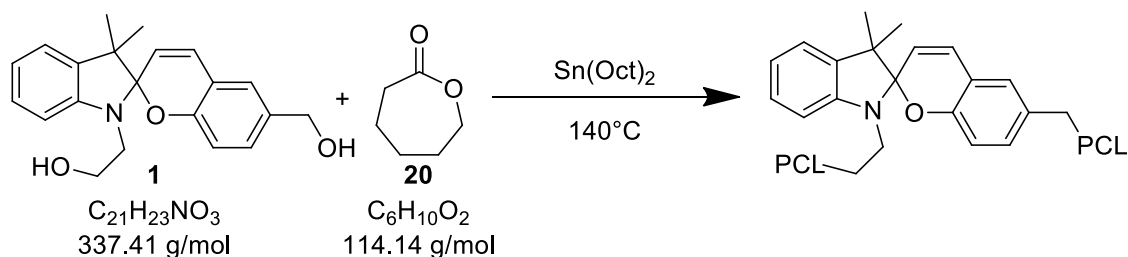
² When drying under vacuum, it should be noted that the viscous oil multiplies its volume by inflating into a solid foam.

Mass spectroscopy:

[SP+Na]⁺	calculated: 405.14209 (: C ₂₁ H ₂₂ N ₂ O ₅ Na)
	measured: 405.14206
[SP+H]⁺	calculated: 383.16015(C ₂₁ H ₂₃ N ₂ O ₅)
	measured: 383.16019

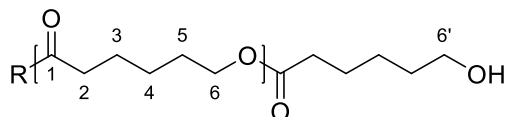
related literature: O'Bryan et al., 2010^[30]

6.2.3. Tin-mediated polymerization of ϵ -caprolactone



A predried KPG stirring apparatus with vacuum closure was equipped with a predried 50 mL three-necked flask. The initiator, here **1** (0.0261 g, 0.08 mmol, monomer/initiator = 350), tin(II)-2-ethylhexanoates (0.0110 g, 0.03 mmol, monomer/catalyst = 1000) and freshly distilled ϵ -caprolactone (3.0 mL, 27 mmol) were added to the flask under nitrogen countercurrent. The mixture was stirred at 140°C (150 rpm) for 90 min³. After allowing the mixture to cool down, it was dissolved in THF (2 x 8 mL) and precipitated in cold methanol.

The molecular weight can be controlled by the reaction time and the monomer/initiator ratio.



¹H-NMR (300 MHz, CDCl_3): δ = 1.37 (m, 4- H_2), 1.64 (m, 3- H_2 und 5- H_2), 2.29 (t, 2- H_2 , $J_{2,3}$ = 7.3 Hz), 3.63 (t, 6'- H_2 , $J_{6',5}$ = 6.5 Hz) 4.05 (t, 6- H_2 , $J_{6,5}$ = 6.7 Hz) ppm. In addition, the signals of the respective initiator are visible.

³ After a reaction time of about 60 min the reaction should be observed as the viscosity of the mixture increases strongly. At lower temperatures, different initiator/catalyst-ratios and/or monofunctional initiators, the reaction time can change considerably.

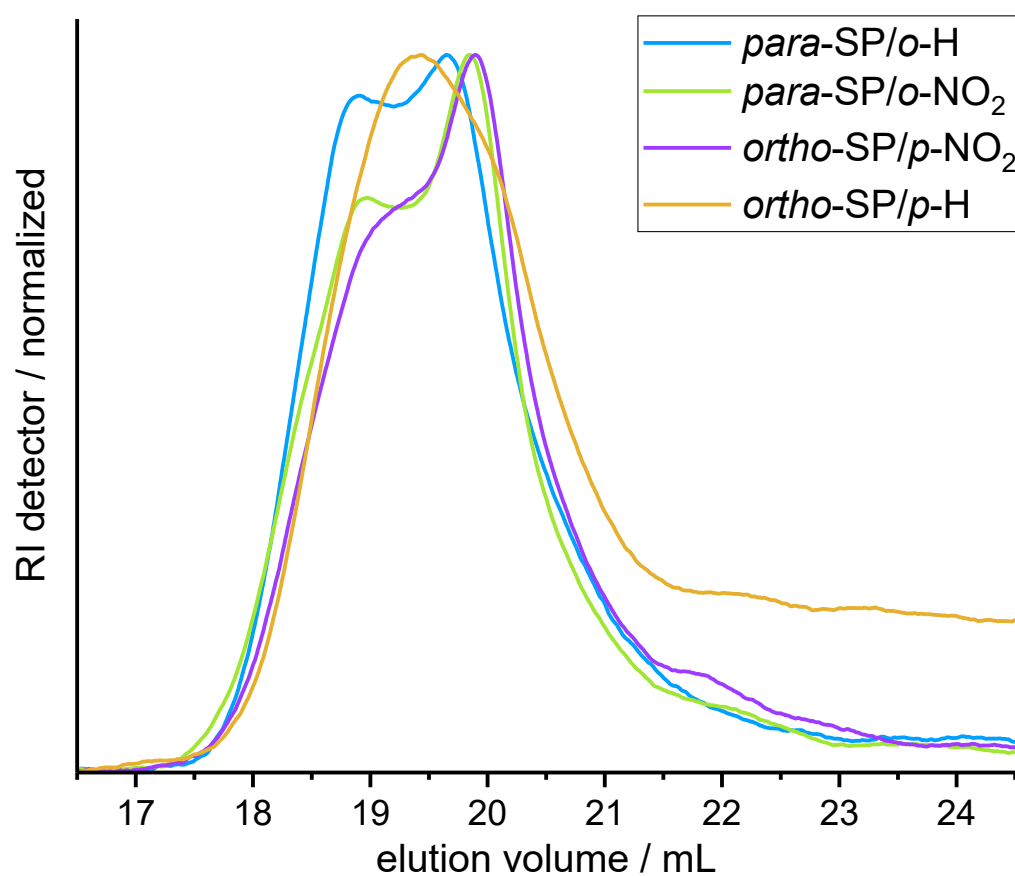


Figure 2-4: SEC analysis of polymers in THF at 1 ml / min.

6.3. Visible light absorption and stress-strain experiments

6.3.1. Preparation of mechanochromic films

The SP-containing sample (250 mg) was mixed with a 1:1 ratio with commercial PCL ($M_n = 80\,000$ g/mol) in DCM (p.a., 3 mL) and precipitated in methanol (techn., 300 mL). The precipitate was filtered off and dried under reduced pressure at 50 °C overnight.

The sample was melted on a glass plate at 75 °C and doctor bladed on an automated machine. Directly after the film was cooled down by placement of the hot glass plate on ice until the film was turbid. The film was removed from the glass plate carefully by applying slight slight sideward pressure on the edges of the film. Specimen for stress-strain experiments were punched from the film in the same orientation as the doctorblade was applied. Hereby the shape of the specimen was optimized for the thinnest part to be located in the middle. Therefore, the yielding would always take place where the absorption measurement was carried out.

6.3.2. Visible light absorption and stress-strain experiments

Stress-strain experiments were carried out at 10 mm/min with a TST-350 (Linkam Scientific Instruments Ltd.). An OceanView UV-VIS setup was used without the deuterium lamp in order to exclude UV light from the measurement. Optic fibers were kept in place by a custom-made mount directly above and below the stress strain chamber. The halogen lamp was pre-heated for 5 minutes. Calibration was carried out in the actual stress-strain setup. Measurements were taken in 1 s intervals. Each data point of 10 ms was smoothed (boxcar = 3) and averaged over 10 measurements (= 100 ms total).

7. References

- [1] R. Klajn, *Chem. Soc. Rev.* **2014**, *43*, 148–84.
- [2] M. Li, Q. Zhang, Y.-N. Zhou, S. Zhu, *Prog. Polym. Sci.* **2018**, *79*, 26–39.
- [3] G. I. Peterson, M. B. Larsen, M. A. Ganter, D. W. Storti, A. J. Boydston, *ACS Appl. Mater. Interfaces* **2015**, *7*, 577–583.
- [4] J. Li, C. Nagamani, J. S. Moore, *Acc. Chem. Res.* **2015**, *48*, 2181–2190.
- [5] N. Willis-Fox, E. Rognin, T. A. Aljohani, R. Daly, *Chem* **2018**, *4*, 2499–2537.
- [6] T. J. Kucharski, R. Boulatov, *J. Mater. Chem.* **2011**, *21*, 8237–8255.
- [7] C. Weder, *J. Mater. Chem.* **2011**, *21*, 8235–8236.
- [8] M. H. Barbee, T. Kouznetsova, S. L. Barrett, G. R. Gossweiler, Y. Lin, S. K. Rastogi, W. J. Brittain, S. L. Craig, *J. Am. Chem. Soc.* **2018**, *140*, 12746–12750.
- [9] M. M. Caruso, D. A. Davis, Q. Shen, S. A. Odom, N. R. Sottos, S. R. White, J. S. Moore, *Chem. Rev.* **2009**, *109*, 5755–5798.
- [10] A. L. Black, J. M. Lenhardt, S. L. Craig, *J. Mater. Chem.* **2011**, *21*, 1655–1663.
- [11] H. Zhang, Y. Chen, Y. Lin, X. Fang, Y. Xu, Y. Ruan, W. Weng, *Macromolecules* **2014**, *47*, 6783–6790.
- [12] O. Brüchner, T. Reichenbach, M. Sommer, M. Walter, *J. Phys. Chem. A* **2017**, *121*, 2683–2687.
- [13] Y. Lin, M. H. Barbee, C.-C. Chang, S. L. Craig, *J. Am. Chem. Soc.* **2018**, *140*, 15969–15975.
- [14] D. a Davis, A. Hamilton, J. Yang, L. D. Cremer, D. Van Gough, S. L. Potisek, M. T. Ong, P. V. Braun, T. J. Martínez, S. R. White, J. S. Moore, N. R. Sottos, *Nature* **2009**, *459*, 68–72.
- [15] G. O'Bryan, B. M. Wong, J. R. McElhanon, *ACS Appl. Mater. Interfaces* **2010**, *2*, 1594–600.
- [16] E. Izak-Nau, D. Campagna, C. Baumann, R. Göstl, *Polym. Chem.* **2020**, *11*, 2274–2299.
- [17] O. Brüchner, M. Walter, *Phys. Rev. Mater.* **2018**, *2*, 113603–113609.
- [18] F. Tuba, L. Olah, P. Nagy, *Express Polym. Lett.* **2014**, *8*, 869–879.
- [19] D. H. S. Ramkumar, M. Bhattacharya, *Polym. Eng. Sci.* **1998**, *38*, 1426–1435.
- [20] C. K. Lee, B. A. Beiermann, M. N. Silberstein, J. Wang, J. S. Moore, N. R. Sottos, P. V. Braun, *Macromolecules* **2013**, *46*, 3746–3752.
- [21] B. A. Beiermann, S. L. B. Kramer, P. A. May, J. S. Moore, S. R. White, N. R. Sottos, *Adv. Funct. Mater.* **2014**, *24*, 1529–1537.
- [22] H. Komber, S. Müllers, F. Lombeck, A. Held, M. Walter, M. Sommer, *Polym. Chem.* **2013**, *5*, 443–453.
- [23] F. Kempe, O. Brüchner, H. Buchheit, S. N. Momm, F. Riehle, S. Hameury, M. Walter, M. Sommer, *Angew. Chem. Int. Ed.* **2018**, *57*, 997–1000.
- [24] J. Ribas-Arino, D. Marx, *Chem. Rev.* **2012**, *112*, 5412–5487.
- [25] M. Reboud-Ravaux, L. Pochet, C. Doucet, B. Pirotte, N. Boggetto, J. Delarge, *Coumarin Derivatives, Methods of Preparation and Application as Medicines*, **2002**, US6355658 (B1).

- [26] P. U. Naik, G. J. McManus, M. J. Zaworotko, R. D. Singer, *Dalton Trans.* **2008**, 4834–4836.
- [27] E. V. Braude, M. A. Gal'bershtam, *Chem. Heterocycl. Compd.* **1978**, *14*, 153–156.
- [28] M. V. Reddington, *Bioconjug. Chem.* **2007**, *18*, 2178–2190.
- [29] F. M. Raymo, S. Giordani, *J. Am. Chem. Soc.* **2001**, *123*, 4651–4652.
- [30] G. O'Bryan, B. M. Wong, J. R. McElhanon, *ACS Appl. Mater. Interfaces* **2010**, *2*, 1594–600.

Chapter 3 Simply Synthesized, Tough Polyarylene with Transient Mechanochromic Response

Fabian Kempe,^[a,b] Oliver Brügner,^[a] Hannah Buchheit,^[c] Sarah N. Momm,^[c] Felix Riehle,^[c] Sophie Hameury,^[c,d] Michael Walter^[a] and Michael Sommer*^[a,b]

[a] Freiburg Center for Interactive Materials and Bioinspired Technologies (FIT),
Georges-Köhler-Allee 105, 79110 Freiburg, Germany

[b] Present address: Professur Polymerchemie, TU Chemnitz, Str. der Nationen 62, 09111 Chemnitz, Germany

[c] Institute for Macromolecular Chemistry, Albert-Ludwigs-Universität Freiburg,
Stefan-Meier-Str., 79104 Freiburg, Germany

[d] Present address: Laboratoire Hétérochimie Fondamentale et Appliquée, (UMR CNRS 5069),
Université de Toulouse, UPS, 118, route de Narbonne, Bât. 2R1, 31062 Toulouse, France

Reproduced from *Angew. Chem. Int. Ed.* **2018**, 57, 997–1000 with permission from
WILEY-VCH Verlag GmbH & Co. KGaA.

<https://doi.org/10.1002/anie.201709142>

1. Abstract

A simple, straightforward and high-yielding route to tough polyarylenes of type poly(*meta,meta,para*-phenylene) (*PmmpP*) is developed. *PmmpP* is already tough in its as-synthesized state at intermediate molar mass of $M_w \sim 60$ kg/mol and exhibits outstanding mechanical properties for further optimized molecular weight ($M_w = 96$ kg/mol, $E = 0.9$ GPa, $\varepsilon = 300$ %). Statistical copolymers with *para,para*-spiropyran (SP) are mechanochromic, whereby the tough behavior allows to investigate mechanochromism. Strained samples instantaneously lose color upon force release. DFT calculations show this phenomenon to be caused by i) the tough *PmmpP* matrix that allows build-up of sufficiently large forces to be transduced to SP, and ii) the relatively unstable corresponding merocyanine (MC) form arising from the aromatic comonomer. MC units covalently incorporated into *PmmpP* show a drastically reduced half life time of 3.1 s compared to 4.5 h obtained for SP derivatives with common 6-nitro substitution.

2. Introduction

Polyarylenes have intrigued material scientists since the invention of transition metal catalyzed cross coupling reactions.^[1,2] In 2007, Schlüter *et al.* introduced a high molecular weight (MW) Poly(*meta,para*-phenylene) *PmpP* by careful selection of catalyst, solvent mixture, concentration and temperature.^[3] In their pioneering work a crude polymer of $M_w = 83$ kg/mol was synthesized and the MW further increased to $M_w = 255$ kg/mol by fractionation. After fractionation, this material showed a toughness close to that of aromatic polycarbonates ($E = 1$ GPa, $\varepsilon = 122$ %). This was a remarkable feat both from a synthetic as well as a material science point of view, because polyarylenes are inherently more chemically stable than polycarbonates due to the exclusive presence of aryl-aryl bonds in the backbone. Subsequently, Schlüter *et al.* investigated various kinked polyarylenes, with some of them exhibiting toughness at high molecular weight after fractionation.^[3-7]

Our interest in tough polyarylenes stems from their potentially ideal use as stable, tough yet amorphous matrices for covalent incorporation of mechanochromic dyes such as spiropyrans (SPs).^[8-10] SPs isomerize to their colored merocyanine (MC) form under a number of external stimuli, including force, and can therefore be used

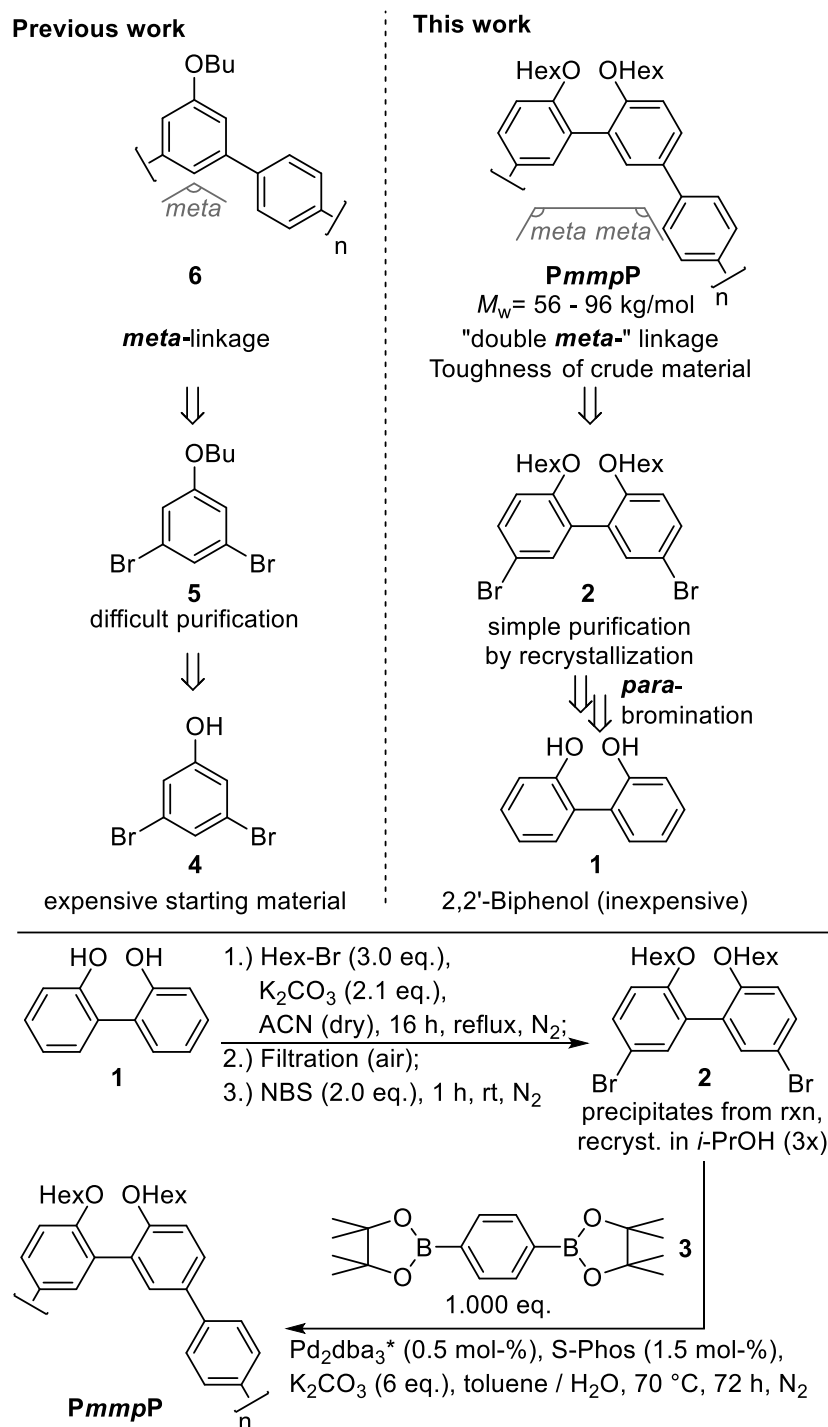
as mechanical force sensors.^[11–15] Compared to matrix polymers used so far in combination with covalently linked SPs, tough polyarylenes have several distinct advantages. Their toughness allows drawing samples and thus to transduce mechanical force to SP. Also, they are typically amorphous, hence mechanochromism can be investigated within an isotropic matrix not possible with semicrystalline polymers. Here we show that the nature and high strength of polyarylenes is of striking additional advantage in that high forces can be transduced to SP comonomers.

We found existing protocols for kinked polyarylene synthesis to be cumbersome, expensive and inefficient due to significant loss of polymer during fractionation.^[3,4,7] Moreover, existing polyarylenes show limited solubility and high glass transition temperatures (T_g) of up to 160 °C, which required processing at too high temperatures for thermolabile SP copolymers. The design of new, tough polyarylenes satisfying all mentioned criteria required straightforward synthesis of monomers starting from inexpensive compounds. Therefore, we designed a new kinked polyarylene, Poly(*meta,meta,para*-phenylene) *PmmpP*.

3. Results and discussion

Para-bromination of 2,2'-biphenol **1** results in the solid monomer **2**, which can be conveniently purified by recrystallization. Suzuki polycondensation (SPC) with **3** gives the kinked polyarylene *PmmpP* with a “double *meta*-” linkage in its backbone (Scheme 1). High weight average molecular weights $M_w \sim 56 - 96$ kg/mol were obtained with almost all molecular weights showing a yield point. Details regarding retrosynthetic analysis, molecular and mechanical characterization are given in the Supporting Information.

SPs have been covalently incorporated into various polymer architectures.^[11,14,16,17] Notably, almost all of these systems use 6-nitro-SP derivatives. The nitro group lowers the energy of the corresponding MC form and hence facilitates SP \rightarrow MC isomerization.^[18]



Scheme 3-1: Top: Retrosynthetic analysis of *PmmpP* compared to previous work.^[3] Bromination of 2,2'-biphenol leads to a "double *meta*-" linkage in the backbone. Bottom: Synthesis of *PmmpP*. * = non-commercial Pd₂dba₃.

The previously reported main-chain alternating *para,para*-SP copolymers did not show toughness and hence the mechanochromic behavior of the *para*-linked SP without the nitro-substituent could not be investigated using uniaxial positive strain.^[8-10] The mechanochromic response of *PmmpP* with 2 mol-% copolymerized *p,p*-SPBr₂ is shown in Figure 3-1 (*M_w* = 134 kg/mol, *D* = 5.5). For the first time, copolymers with *p,p*-SPBr₂ were mechanochromic under positive strain. Yet more

remarkable is the observation that samples immediately lost their color upon force release. Figure 3-1 shows that repeated switching was possible for 25 times. This is a marked difference compared to SP-based mechanochromic systems reported so far showing persistent colors.^[10,13,17]

We hypothesized the reason for the observed transient mechanochromic behavior of *PmmpP* with instantaneous loss of color upon force release is two-fold. Firstly, covalent incorporation of SP through *para*-linkages compared to commonly used *ortho*-linked SP mechanophores leads to a rather inefficient molecular lever and transduction of mechanical force to the weak C-O bond. The replacement of the commonly used nitro-group in 6-position by the phenyl ring of comonomer **3** further adds up to this effect, as the electronic effect of the phenyl ring destabilizes the MC form compared to the nitro group.^[18] In order to be able to observe mechanochromism regardless, the high strength of *PmmpP* of up to 50 MPa at yield is probably key (see Supporting Info). Secondly, once MC forms under the conditions of the stress-strain experiment, it is only stable under the applied force due to the discussed substitution pattern, but immediately isomerizes back to SP when the force is released. This behavior of a rather unstable MC form leads to the observed transient mechanochromic response.

To further corroborate this assumption and get more insight into the uncommon mechanochromic behavior of the SP copolymer, density functional theory (DFT) calculations were performed. Bond breaking under the action of an external force F_{ext} mostly is a stochastic process as it is initiated by thermal fluctuations.^[19-22] Only in case of extremely rapid pulling, thermal effects are overcome and the force corresponding to the maximal derivative of the potential gets visible. The force needed to break a bond thus depends on the loading rate $\alpha = dF_{\text{ext}}/dt$. We modeled two SP derivatives, one having the SP substitution pattern as in *PmmpP* and “*para,para*- pulling direction”, and one with the commonly used 6-nitro group (SP-NO₂) and “*para,ortho*- pulling direction”.^[23,24]

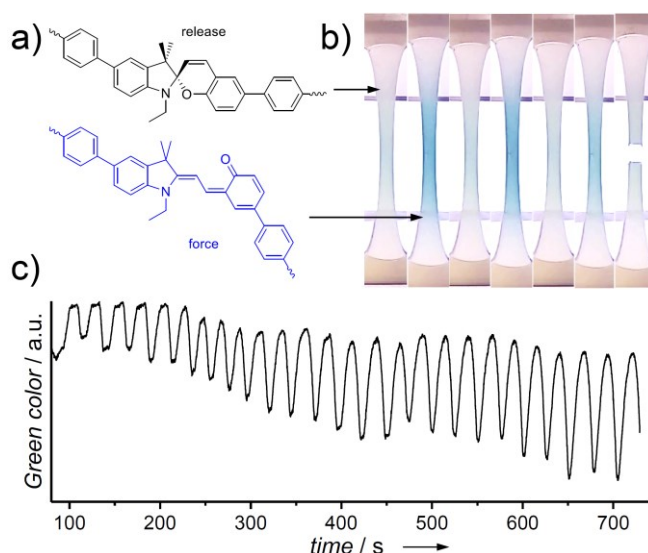


Figure 3-1: Tensile experiment of *PmmpP* containing 2 mol-% *p,p*-SPBr₂. a) Structures of SP (top) and MC (bottom) in the *PmmpP* matrix. b) Pictures of repeated strained and released samples. Pictures were adjusted for brightness and contrast. c) Intensity of green color in the mid-section of the specimen during repeated force build-up and release. The time scale corresponds to the change in force as shown in Figure 3-5.

The structures are depicted in Figure 3-2. Calculations were performed within the projector augmented wave method as implemented in the GPAW package.^[25,26] The exchange-correlation energy was approximated as devised by Perdew, Burke, and Ernzerhof.^[27] In order to obtain the force needed for the transition from SP to MC, we applied a two-dimensional Constrained Geometries Simulate External Force (COGEF) method, where the energy barriers in dependence of F_{ext} are determined (see experimental section for details).^[22,28]

We found two energy barriers with an instable intermediate state along the transition, which belong to the C-O cleavage (increasing of bond length b) and the *cis-trans* isomerization by rotation of the dihedral angle β (see Figure 3-2a,b). Figure 3-2c depicts the rate determining total energy barriers in forward $\Delta G_{f,\text{total}}(F_{\text{ext}})$ and backward $\Delta G_{b,\text{total}}(F_{\text{ext}})$ direction which are relative to the energies of the SP and MC forms, respectively. For small forces the barrier for β rotation is decisive, while for large forces it is C-O bond breaking. While this behavior is similar in both SP derivatives, the transition happens at much lower external force for SP-NO₂ compared to SP in *PmmpP*. Figure 3-2c also shows that the forward barrier for nitro is smaller than for polyarylene in a large force range. The transition rates k can be obtained from the barriers using the Eyring equation^[20,29]

$$k = \frac{k_B T}{h} \exp\left(-\frac{\Delta G}{k_B T}\right), \quad (2)$$

where k_B is the Boltzmann and h the Planck constant. From these the probabilities for the presence of each isomer at fixed force and temperature T can be determined through solving the corresponding coupled rate equations for the probabilities $P_S(F_{\text{ext}})$ with $S = \text{SP, IN, MC}$ (see supporting info for details).

Coloration happens as soon as the C-O bond breaks. Therefore the probability for the colored form is $P_c = 1 - P_{\text{SP}} = P_{\text{IN}} + P_{\text{MC}}$. The average force for coloration F is then obtained as

$$F = \int_0^{\infty} \frac{dP_c(F_{\text{ext}})}{dF_{\text{ext}}} F_{\text{ext}} dF_{\text{ext}} \quad (3)$$

By assuming a constant loading rate α , integral (3) can be evaluated and leads to $F(\alpha)$ as shown in Figure 3-2d. The rupture forces for SP in *PmmpP* are larger compared to SP-NO₂ within a wide range of loading rates except for very large values of $\alpha \geq 10^5$ nN/s. This is a result of the higher forward energy barrier for SP in *PmmpP* for low external forces that is decisive for small loading rates (Figure 3-2d). Only for very high loading rates external forces $F_{\text{ext}} \geq 0.7$ nN are reached and SP in *PmmpP* isomerizes faster than SP-NO₂. The sharp increase of the rupture force for SP-NO₂ and the deeper understanding of the force-dependent energy barriers obtained from the method of calculation are subject of future studies.

Here, we estimate the loading rate to be less than $\alpha = 1$ nN/s such that the rupture force for SP in *PmmpP* is larger by more than a factor of two. This explains why SP in *PmmpP* isomerizes at larger mechanical stress than the commonly used SP-NO₂. Figure 3-2c also shows that the backward barrier of SP-NO₂ is substantially higher than that of SP in *PmmpP*. As the SP isomer is energetically favored, discoloration happens spontaneously with a theoretical half time of 4.5 h for SP-NO₂, but only with 3.1 s for SP in *PmmpP*, which is in excellent agreement with the fast de-coloration observed in the experiment. Next to these unique electronic substituent effects, the high strength and elongation at break enabling transient mechanochromic response, the SP in *PmmpP* additionally benefits from the strong absorption of UV light of *PmmpP* (see supporting info), which may reduce photo-bleaching as a major drawback of SP-based materials considerably.^[30–32]

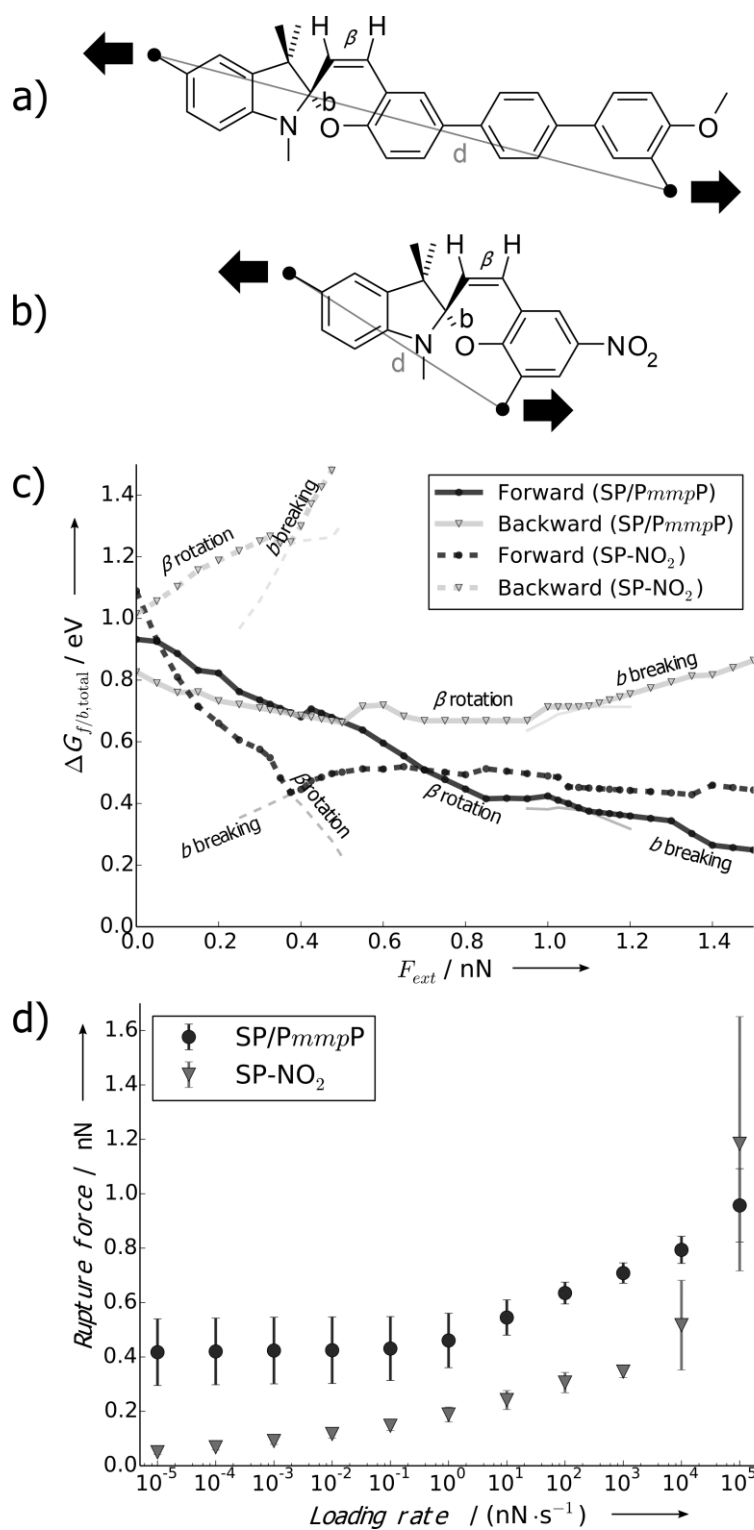


Figure 3-2: a), b) Chemical structures of SP derivatives modelled with arrows indicating pulling directions. The definitions of the pulling distance d , the bond distance b and the dihedral angle β between olefinic protons are indicated. c) Gibbs energy barriers in dependence of the external force corresponding to the polyarylene and nitro-substituted spiropyran. d) Force needed for coloration F in dependence of the loading rate α for the two SP derivatives.

4. Conclusion

In conclusion, we designed a simple and high-yielding synthetic route to polyarylenes of type *PmmpP* with *meta,meta,para* backbone that are tough without prior purification and at intermediate molecular weight. Our rational monomer design employs inexpensive and readily available 2,2'-biphenol as a starting material, from which solid monomers can be made in high purity by simple recrystallization in multigram scale. The availability of highly pure and solid monomers allowed for high molecular weight polycondensates to be made, which further improved mechanical properties to outstanding values. Copolymers of *PmmpP* with spiropyran are mechanochromic under positive uniaxial strain, but lose color instantaneously after force release. With this transient response enabling the direct visualization stress in polymeric materials without delay, engineering both the substitution pattern of covalently incorporated SP units as well as the polymer matrix allows to tailor-make smart materials for specific applications.

5. Acknowledgements

F. K., O. B., M. W. and M. S. acknowledge funding from the DFG (SO 1213/ 7-1, SO 1213/ 8-1, MW 1687/ 9). O. B. and M. W. are grateful for computational resources from FZ-Jülich (HFR08) and from the bwForCluster NEMO in Freiburg. F. K. acknowledges Mats Moskopp for help with video analysis.

6. Experimental Methods

6.1. General information

All **chemicals** were obtained from Sigma Aldrich and used without further treatment unless specified.

DSC measurements were acquired on a NETZSCH DSC 204 F1 Phoenix under a nitrogen atmosphere at a heating and cooling rate of 10 K / min.

NMR spectra were measured on a Bruker ARX 300 and a Bruker Avance III 500 machine. All spectra were recorded at 303 K in CDCl₃ as solvent and were referenced to the residual solvent peak ($\delta = 7.26$ ppm) and analysed using Bruker TOPSPIN 2.1 software package.

UV/VIS-spectroscopy was carried out with rigid thin films on the Flame-S UV-Vis-spectrometer from Ocean Optics, controlled by the OceanView 1.5.2 software.

SEC measurements were carried out on three SDV gel 5 μm columns and a pre-column, with pore sizes ranging from 10^3 to 10^5 Å (PSS), connected in series with a 254 nm UV-Detector detector and calibrated with polystyrene standards. THF was used as eluent at 30 °C at a flow rate of 1.0 mL / min.

6.2. Retrosynthetic Analysis

The development of polyarylenes has been fueled by potential applications as active materials for organic electronics. Poly-*para*-phenylenes (PpPs) as basic examples exhibit very limited solubility and precipitate early during synthesis.^[33] The introduction of side chains as internal solubilizers^[34] or plasticizers greatly increases solubility, simplifies processing and modifies their mechanical properties.^[35,36] Next to PpPs, several polyarylenes with *meta*- or even *ortho*-linkages were prepared for optical properties investigations and as ligands.^[37–40] Those kinked polyarylenes showed poor mechanical properties, presumably because of their low molecular weight (MW).

As shown by Schlüter *et al.*, kinked polyarylene backbones were essential to generate tough materials, but the respective *meta*-substituted arene monomers required expensive starting materials and are tedious to purify (Scheme 3-1, top left). Retrosynthetic analysis of existing polymer structures suggested that the use of *meta*-substitution patterns of arene monomers can be circumvented by a clever combination of *ortho*- and *para*-substituents. However, one major disadvantage of having both *ortho*- and *para*-substituents in a single arene is sterical hindrance during cross coupling polycondensation which is unlikely to allow high molecular weight materials to be made. In order to avoid single arene monomers with *ortho*- and *para*-substituents, we looked at diarenes that are already coupled in the *ortho*-, *ortho*-position with each other, leaving only the *para*-position to be coupled in the polymerization step. The obvious choice are *ortho,ortho*-biphenyl derivatives with 2,2'-biphenol being an inexpensive and widely available starting material, which itself may be produced from phenol by radical oxidative coupling on industrial scale.^[41]

We alkylated 2,2'-biphenol (**1**) with 1-hexyl bromide and brominated with NBS (Scheme 1).^[42,43] The resulting monomer 5,5'-dibromo-2,2'-bis(hexyloxy)-1,1'-biphenyl **2** with a *meta,meta* (*mm*) motif directly precipitated from solution and was isolated by filtration (purity ≥ 99.6 % after recrystallization). Notably, the melting point of 65 °C makes handling of **2** very convenient. **2** was synthesized on an 8 g scale (final, pure monomer). The *para*-comonomer 1,4-bis(boronic acid pinacol ester) benzene **3** (Ph(Bpin)₂) was prepared similar to existing protocols and obtained with a purity of ≥ 99.6 %.^[44] The inexpensive starting materials, affordable

reagents and simple purification makes this system easily scalable which is ideal for polycondensation. Note that we also considered the possibility of using monomers with reversed functional groups, i.e. Hexylbiphenol boronic acid pinacol ester and dibromobenzene (Figure 3-3). We found crystallization of the former (T_m ca. 5 °C) to be challenging and tedious which further suggests **2** as ideal monomer in terms of simple synthesis, purification and handling.

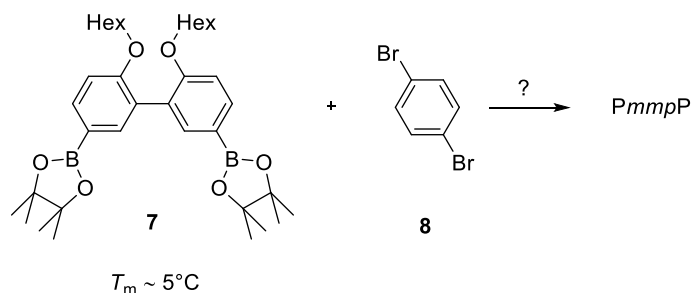


Figure 3-3: Reversed functional groups are challenging due to the low melting point of **7**. Therefore this route was not explored any further.

In order to polycondensate **2** and **3**, we selected the air stable, two-component catalytic system S-Phos and commercial Pd_2dba_3 .^[1,4,45] Initial polymerizations with Pd_2dba_3 / S-Phos only resulted in low molecular weights for *PmmpP* of $M_w \sim 30$ kg/mol. Difficulties with commercial Pd_2dba_3 have already been reported in the literature.^[46] Far better MWs up to $M_w \sim 100$ kg/mol were obtained using non-commercial Pd_2dba_3 ($\text{Pd}_2\text{dba}_3^*$) and a reaction temperature of 70 °C. Note that *PmmpP* with the same backbone regiochemistry but different side chains has recently been made from non-symmetric monomers, but toughness below the glass transition temperature (T_g) of the crude material was not reported.^[7]

Typically, kinked polyarylenes exhibit a bimodal MW distribution as in our case due to a high content of cyclic oligomers and polymers in the low molecular weight fraction (Figure 3-4).^[5,47] Purification of *PmmpP* worked best by Soxhlet extraction with cyclohexane (for other solvents, see Figure 3-6).

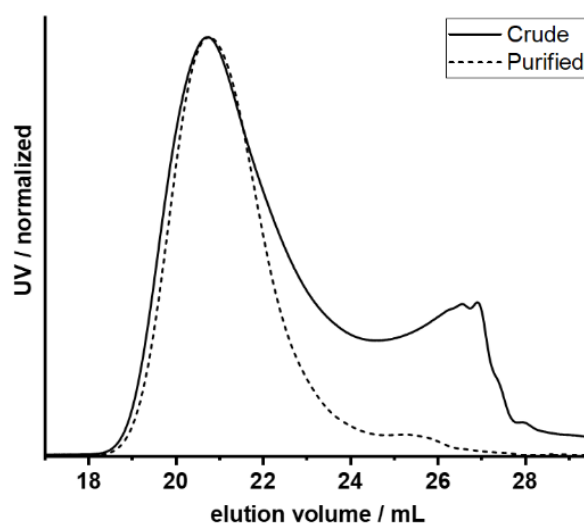
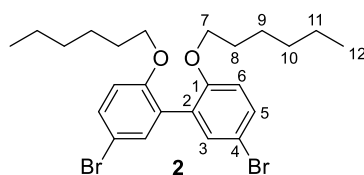


Figure 3-4: SEC of crude and purified polymer *PmmpP* **P1**. Purification was carried out by Soxhlet extraction in cyclohexane. For purification with other solvents, see Figure 3-6.

After work-up, differential scanning calorimetry (DSC) of *PmmpP* yielded a T_g around 117 °C which was slightly dependent on MW (Table 3-1). No indication for semicrystallinity was found, consistent with the rather irregular *mmp*-backbone structure and the transparent appearance of drop-cast films.

6.3. Preparation of monomers and catalyst

6.3.1. Preparation of 2

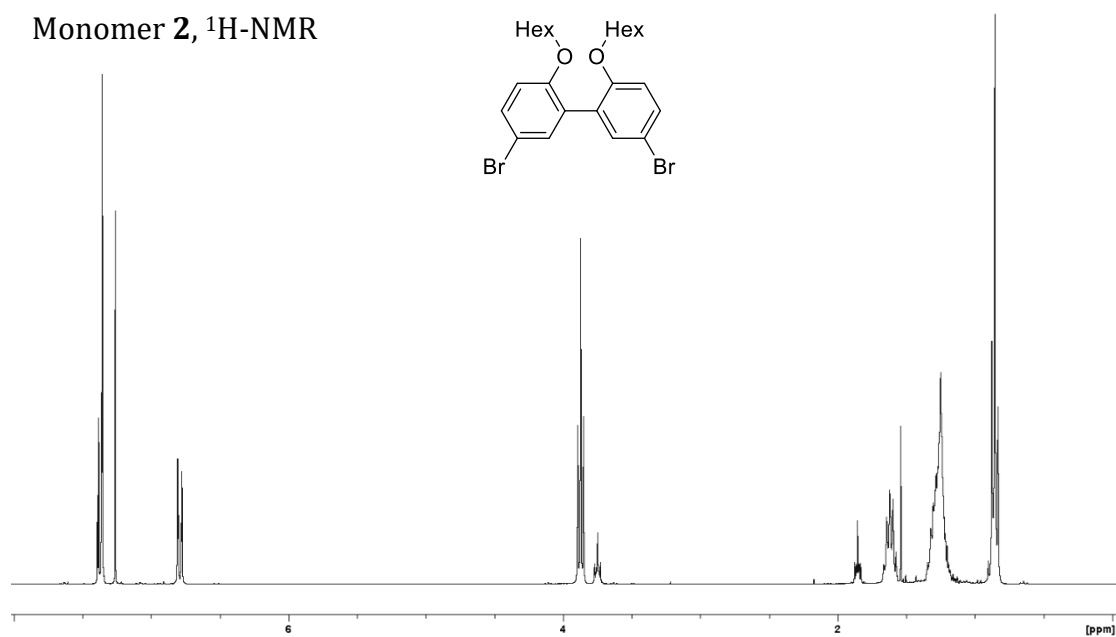
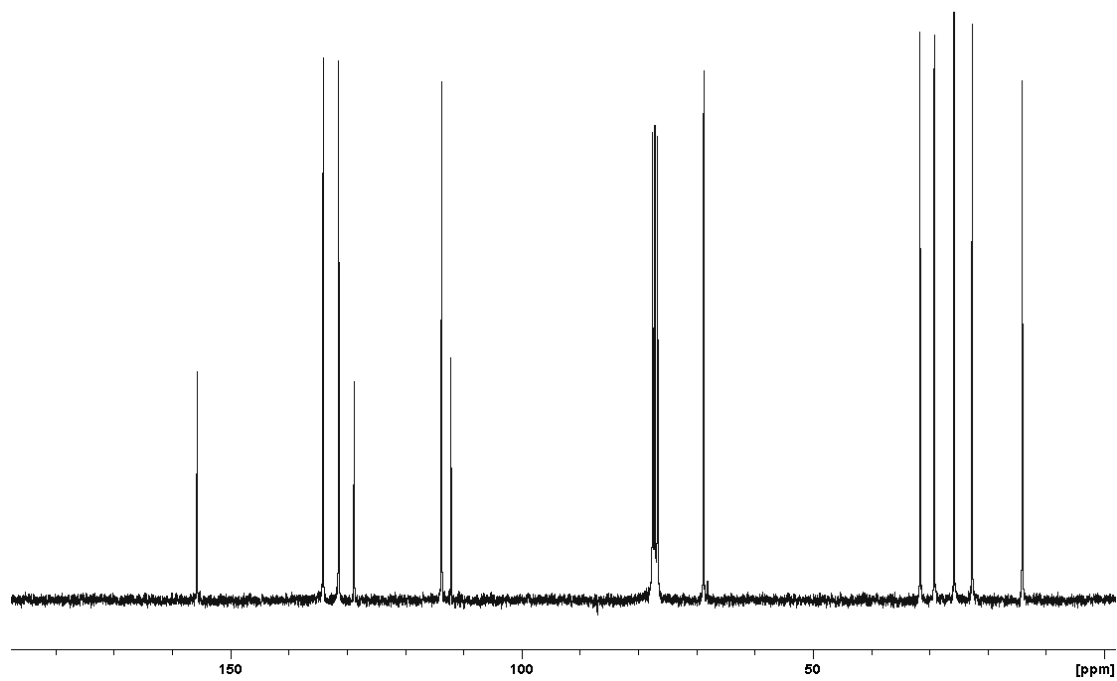


2,2'-Biphenol (10.075 g, 54.106 mmol) and K_2CO_3 (15.636 g, 113.13 mmol, 2.1 eq.) were dissolved in ACN (dry, 140 mL) under N_2 . After addition of 1-bromohexane (22.5 mL, 26.5 g, 161 mmol, 3.0 eq.) the reaction was heated under reflux for 18 h. The crude mixture was freed from precipitates by filtration under air (flushed with an additional 20 mL of ACN). Addition of NBS (19.1 g, 107 mmol, 2.0 eq.) and continuous purging with N_2 resulted in precipitation within 30 min. After an additional 30 min of mild agitation the crude product was isolated by filtration under air. Recrystallization from 2-propanol (3 x 300 mL) afforded monomer 1 as colorless crystals (8.11 g, 15.8 mmol, 29 %, mp. 65-66 °C).

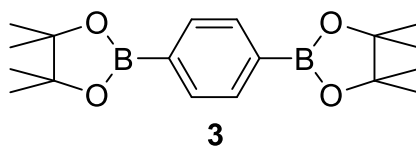
NMR: 1H (300 MHz, $CDCl_3$): δ = 0.88 (t, 6 H, H-12), 1.17-1.36 (m, 28 H, H-9/10/11), 1.62 (tt, 4 H, H-8), 3.87 (t, 4 H, H-7), 6.79 (dd, 2 H, H-6), 7.36 (br. s, 2 H, H-3), 7.37 (dd, 2 H, H-5) ppm. ^{13}C (75 MHz, $CDCl_3$): δ = 14.1 (C-12), 22.7 (C-11), 25.8 (C-10), 29.2 (C-9), 31.7 (C-8), 68.8 (C-7), 112.2 (C-4), 113.8 (C-6), 128.8 (C-2), 131.4 (C-3), 134.1 (C-5), 155.8 (C-1).

MS (ESI, $[M-H]^+$, $C_{24}H_{32}O_2Br_2$) calc. / found: m/z = 511.0842 / 511.0842, 513.0821 / 513.0820, 515.0801 / 515.0799.

EA calc. / found (deviation): C 56.27 % / 56.41 % (0.14 %), H 6.30 % / 6.30 % (0.00 %).

Monomer **2**, ^1H -NMRMonomer **2**, ^{13}C -NMR

6.3.2. Preparation of **3**



Mg (6.2380 g, 256.60 mmol, 3.0 eq.) and LiCl (7.9555 g, 187.67 mmol, 2.2 eq.) were dried inside the reaction vessel at 600 °C under high vacuum for 5 min and the vessel flooded with N₂. 1,4-Dibromobenzene (20.034 g, 84.926 mmol) and THF (dry, 400 mL) were added and the reaction heated under reflux for 3 h. The mixture was cooled to 0 °C (ice/water bath). After addition of iPrO-Bpin (CAS: 61676-62-8, 34.5 mL, 31.4 g, 169 mmol, 2.0 eq.) the reaction was stirred for 20 h, slowly reaching room temperature. After addition of NH₄Cl (sat., aq., 11.0 mL) and HCl (aq., 2 M, 42.0 mL) the mixture was extracted with Et₂O (3 × 100mL), the organic phases extracted with brine (100 mL) and dried with MgSO₄. Recrystallization from ethanol (2 × 500mL) afforded monomer **3** as a white crystalline powder (8.18 g, 86.2 mmol, 29 %).

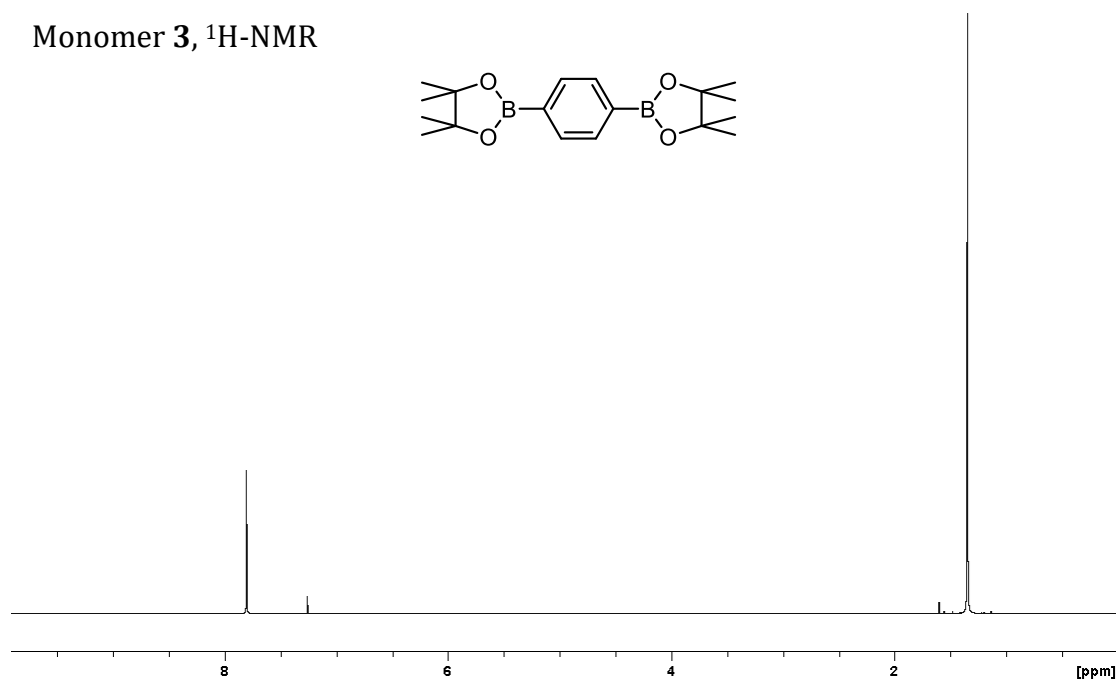
NMR: ¹H (300 MHz, CDCl₃): δ = 1.35 (s, 24 H, CH₃), 7.80 (s, 4 H, H-Ar).

NMR spectrum corresponds to literature.^[48]

MS (ESI, [M-H]⁺, C₁₈H₂₈B₂O₄): calc. / found: 330.2283/330.2284, 331.2246/331.2248.

MS (ESI, [M-NH₄]⁺, C₁₈H₂₈B₂O₄): calc. / found: m/z = 348.2512/348.2512.

EA calc. / found (deviation): C 65.51 % / 65.68 % (0.17 %), H 8.55 % / 8.49 % (0.06 %).

Monomer **3**, ^1H -NMR

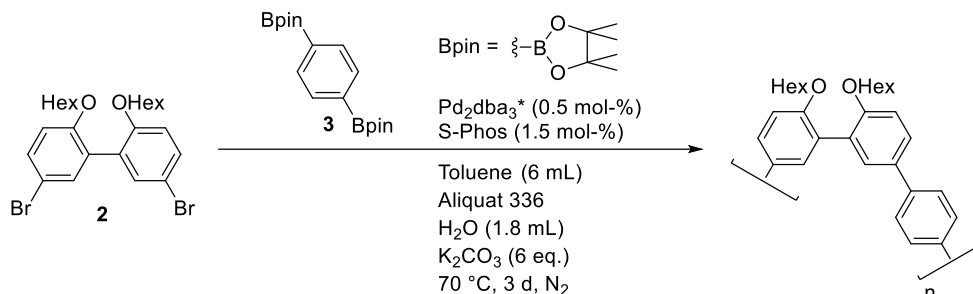
6.3.3. Pd₂dba₃*

PdCl₂(CH₃CN)₂ (350.1 mg, 1.35 mmol) was dissolved in MeOH (70 ml, p.a.) and stirred at 60 °C for 15 min. Afterwards dibenzylideneacetone (982.0 mg, 4.19 mmol, 3.1 eq.) was added. After 15 min at 60 °C, NaOAc · 3 H₂O (1.101 g, 13.42 mmol, 9.9 eq.) was added and stirred for 2 h while it was allowed to cool to room temperature. The product slowly precipitated. The solvent was removed by filtration cannula. The precipitate was washed with MeOH (3 x 30 ml), H₂O (1 x 10 ml) and again with MeOH (3 x 30 ml). Finally the precipitate was transferred into a small vial as a suspension in Et₂O (total 7.0 mL, excess Et₂O re-used). Excess Et₂O was carefully removed with a pipette. The product was carefully heated to dryness (heat-gun, 50 °C) and dried under continuous high vacuum (< 1 mbar) for 20. Pd₂dba₃* (0.483 g, 0.53 mmol, 20 %) was afforded as a brown solid.

6.4. Polymers PmmpP P1-P5

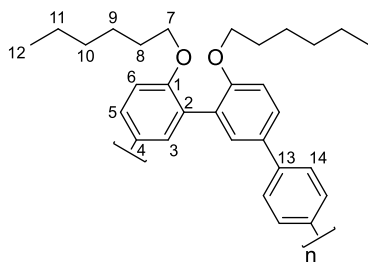
6.4.1. Preparation

6.4.1.1. PmmpP P1



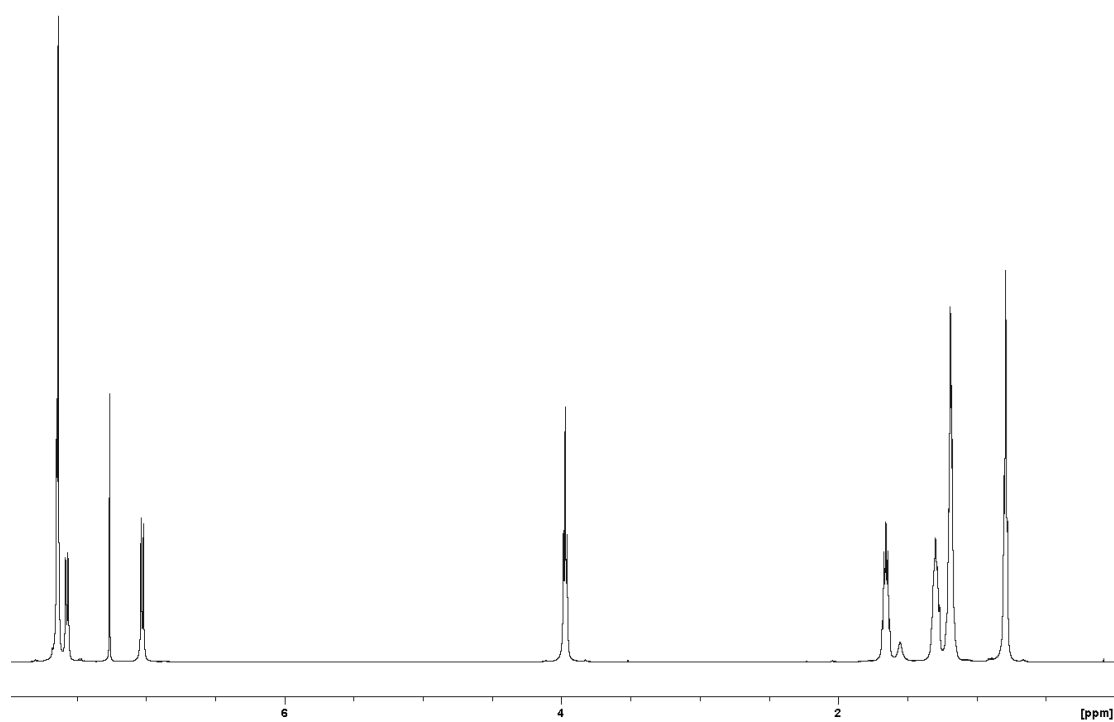
Monomer **2** (597.84 mg, 1.1669 mmol), monomer **3** (385.12 mg, 1.1669 mmol, 1.000 eq.), $\text{Pd}_2\text{dba}_3^*$ (5.45 mg, 5.95 μmol , 0.5 mol-%), S-Phos (7.31 mg, 17.8 μmol , 1.5 mol-%) and K_2CO_3 (967.52 mg, 7.0009 mmol, 6.0 eq.) were mixed. The vessel was purged for 30 min with N_2 under slight agitation. Water and toluene (with Aliquat 336 added) were purged with N_2 separately for 30 min. Toluene (6.0 mL) was added first. After 5 min, H_2O (1.8 mL) was added and the vessel heated to 70 °C for 3 d under N_2 . The polymer was precipitated dropwise from the organic phase in MeOH (300 mL), filtered off and dried under reduced pressure at 50 °C for 16 h. Soxhlet extraction was carried out with cyclohexane for 24 h. The polymer was collected from the Soxhlet extractor with DCM and the solvent removed under reduced pressure. Filtration in THF over a short Silica plug and solvent removal under reduced pressure afforded the purified polymer.

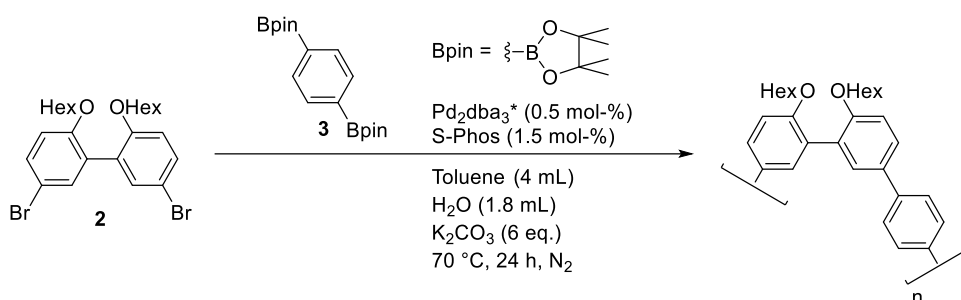
SEC (THF, 1 mL/min): $M_w = 96\,400$ g/mol, $M_n = 36\,000$ g/mol, $D = 2.7$.



NMR: ^1H (500 MHz, CDCl_3): δ = 0.78 (m, 6 H, H-12), 1.18 (m, 8 H, H-11 and H-10), 1.29 (m, 4 H, H-9), 1.65 (m, 4 H, H-8), 3.95 (t, 4 H, H-7), 7.02 (d, 2 H, H-6), 7.56 (dd, 2 H, H-5), 7.63 (s, 4 H, H-14), 7.64 (d, 2 H, H-3) ppm.

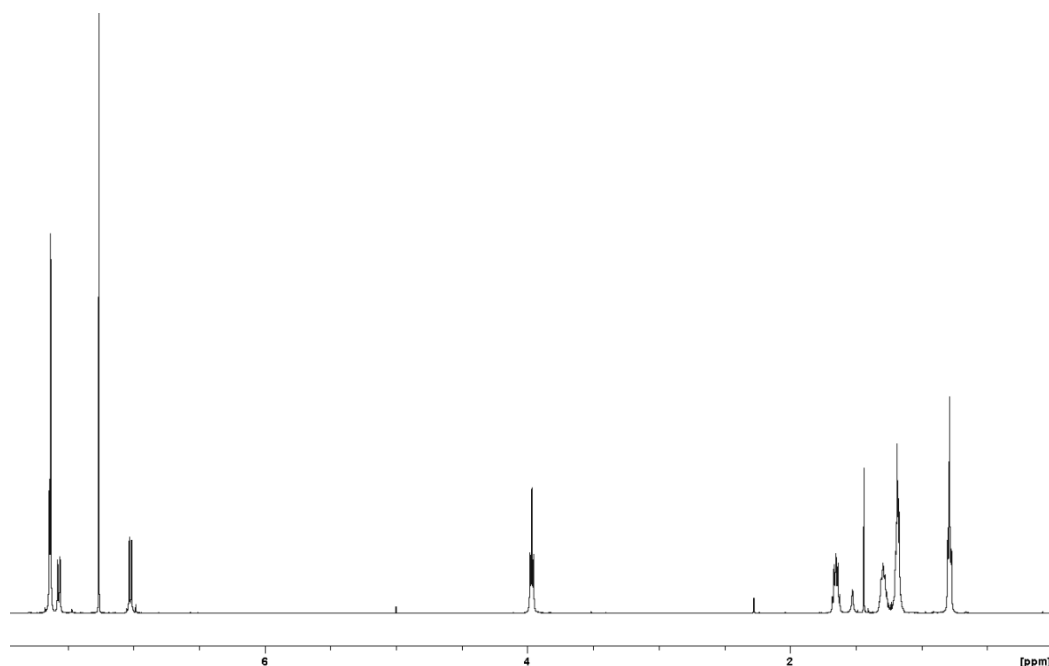
^1H -NMR *PmmpP* **P1**

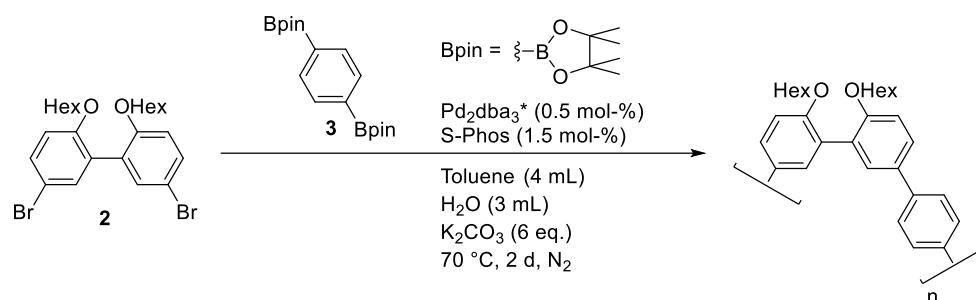


6.4.1.2. *PmmpP P2*

Monomer **2** (1195.29 mg, 2.3330 mmol), monomer **3** (770.09 mg, 2.3333 mmol, 1.000 eq.), $\text{Pd}_2\text{dba}_3^*$ (10.65 mg, 11.63 μmol , 0.5 mol-%), S-Phos (14.48 mg, 35.3 μmol , 1.5 mol-%) and K_2CO_3 (1934.8 mg, 14.000 mmol, 6.0 eq.) were mixed. The vessel was purged for 30 min with N_2 under slight agitation. Water and toluene were purged with N_2 separately for 30 min. Toluene (4.0 mL) was added first. After 5 min, H_2O (1.8 mL) was added and the vessel heated to $70\text{ }^\circ\text{C}$ for 24 h under N_2 . The polymer was precipitated dropwise from the organic phase in MeOH (300 mL), filtered off and dried under reduced pressure at $50\text{ }^\circ\text{C}$ for 16 h. Soxhlet extraction was carried out with cyclohexane for 24 h. The polymer was collected from the Soxhlet extractor with THF and the solvent removed under reduced pressure. Filtration in THF over a short Silica plug and solvent removal under high vacuum afforded the purified polymer.

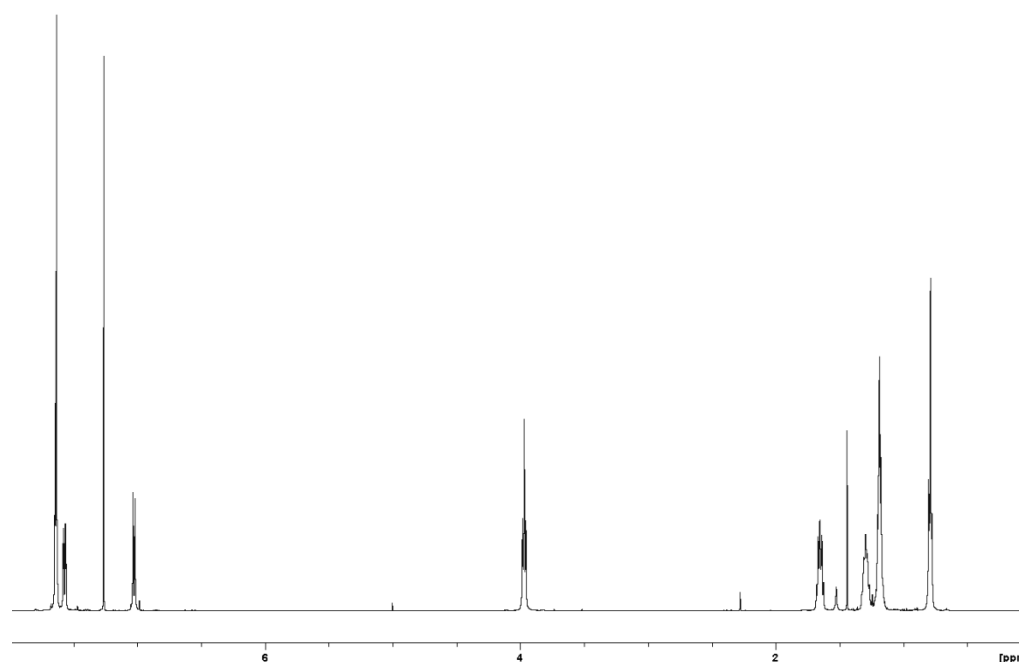
SEC (THF, 1 mL/min): $M_w = 88\,700\text{ g/mol}$, $M_n = 45\,700\text{ g/mol}$, $D = 1.9$.

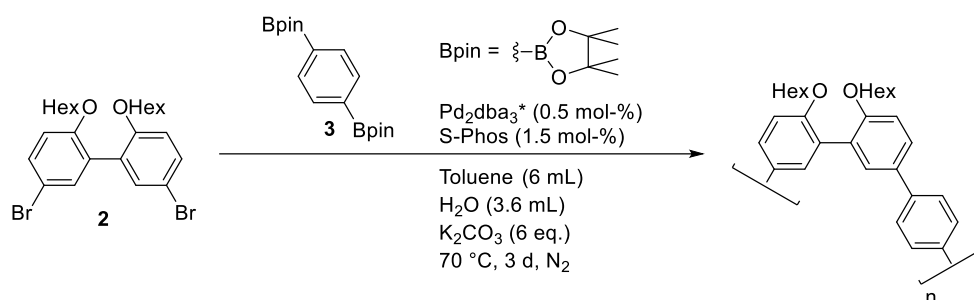
 $^1\text{H-NMR}$ *PmmpP P2*

6.4.1.3. *PmmpP P3*

Monomer **2** (1196.75 mg, 2.3359 mmol), monomer **3** (770.95 mg, 2.3359 mmol, 1.000 eq.), $\text{Pd}_2\text{dba}_3^*$ (10.72 mg, 11.71 μmol , 0.5 mol-%), S-Phos (14.32 mg, 34.9 μmol , 1.5 mol-%) and K_2CO_3 (1934.8 mg, 14.000 mmol, 6.0 eq.) were mixed. The vessel was purged for 30 min with N_2 under slight agitation. Water and toluene were purged with N_2 separately for 30 min. Toluene (4.0 mL) was added first. After 5 min, H_2O (3.0 mL) was added and the vessel heated to 70 °C for 2 d under N_2 . The polymer was precipitated dropwise from the organic phase in MeOH (300 mL), filtered off and dried under reduced pressure at 50 °C for 16 h. Soxhlet extraction was carried out with cyclohexane for 24 h. The polymer was collected from the Soxhlet extractor with THF and the solvent removed under reduced pressure. Filtration in THF over a short Silica plug and solvent removal under high vacuum afforded the purified polymer.

SEC (THF, 1 mL/min): $M_w = 70\,800$ g/mol, $M_n = 33\,500$ g/mol, $D = 2.1$.

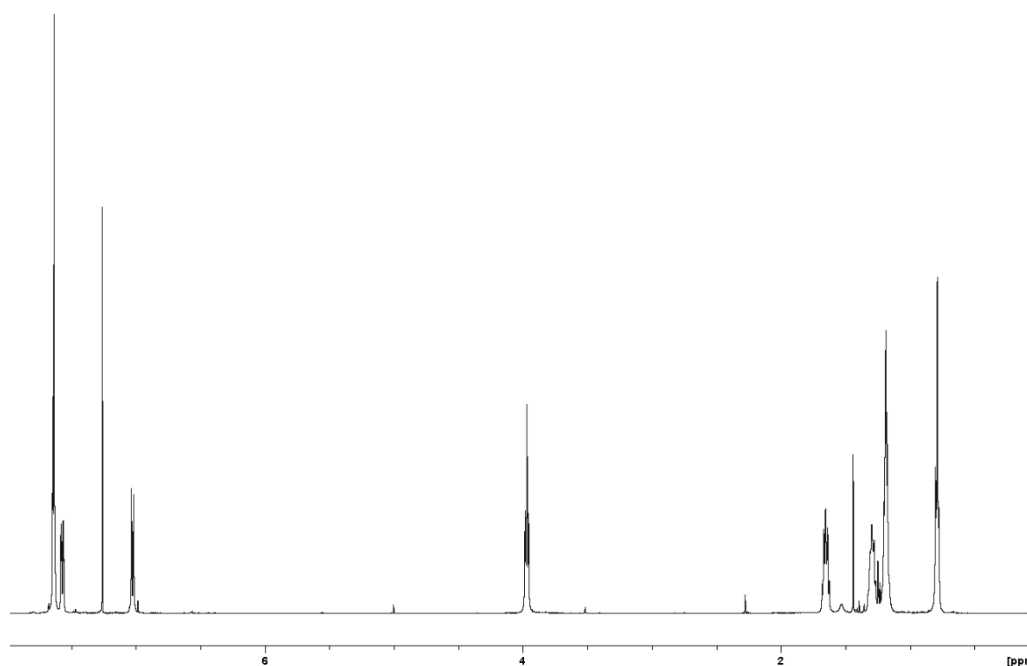
 ^1H -NMR *PmmpP P3*

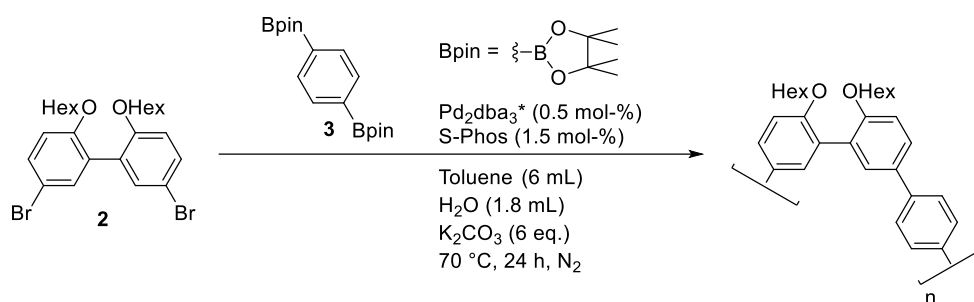
6.4.1.4. *PmmpP P4*

Monomer **2** (1195.50 mg, 2.3335 mmol), monomer **3** (770.11 mg, 2.3334 mmol, 1.000 eq.), $\text{Pd}_2\text{dba}_3^*$ (10.70 mg, 11.68 μmol , 0.5 mol-%), S-Phos (14.37 mg, 35.00 μmol , 1.5 mol-%) and K_2CO_3 (1934.6 mg, 13.999 mmol, 6.0 eq.) were mixed. The vessel was purged for 30 min with N_2 under slight agitation. Water and toluene were purged with N_2 separately for 30 min. Toluene (6.0 mL) was added first. After 5 min, H_2O (3.6 mL) was added and the vessel heated to 70°C for 3 d under N_2 . The polymer was precipitated dropwise from the organic phase in MeOH (300 mL), filtered off and dried under reduced pressure at 50°C for 16 h. Soxhlet extraction was carried out with cyclohexane for 24 h. The polymer was collected from the Soxhlet extractor with THF and the solvent removed under reduced pressure. Filtration in THF over a short Silica plug and solvent removal under high vacuum afforded the purified polymer.

SEC (THF, 1 mL/min): $M_w = 57\,100$ g/mol, $M_n = 25\,900$ g/mol, $D = 2.3$.

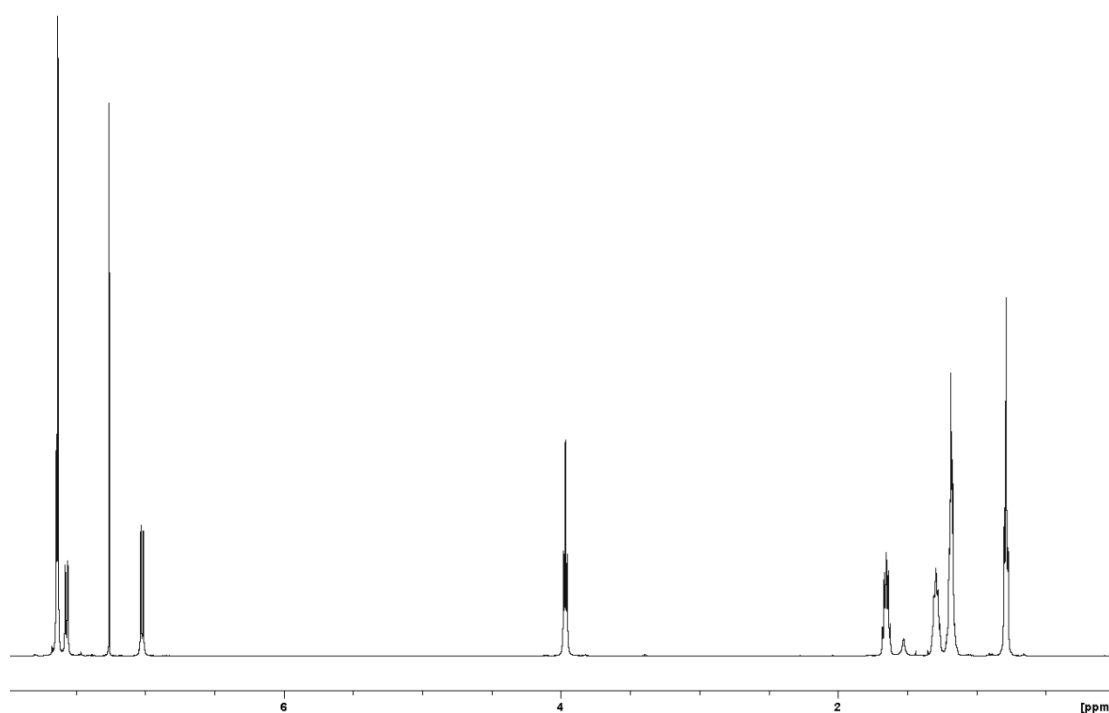
$^1\text{H-NMR}$ *PmmpP P4*



6.4.1.5. *PmmpP P5*

Monomer **2** (1210.28 mg, 2.3623 mmol), monomer **3** (779.69 mg, 2.3624 mmol, 1.000 eq.), $\text{Pd}_2\text{dba}_3^*$ (10.69 mg, 11.67 μmol , 0.5 mol-%), S-Phos (14.31 mg, 34.86 μmol , 1.5 mol-%) and K_2CO_3 (1936.1 mg, 14.009 mmol, 6.0 eq.) were mixed. The vessel was purged for 30 min with N_2 under slight agitation. Water and toluene were purged with N_2 separately for 30 min. Toluene (6.0 mL) was added first. After 5 min, H_2O (1.8 mL) was added and the vessel heated to 70°C for 24 h under N_2 . The polymer was precipitated dropwise from the organic phase in MeOH (300 mL), filtered off and dried under reduced pressure at 50°C for 16 h. Soxhlet extraction was carried out with cyclohexane for 24 h. The solvent was removed under high vacuum.

SEC (THF, 1 mL/min): $M_w = 56\,100\text{ g/mol}$, $M_n = 32\,100\text{ g/mol}$, $D = 1.8$.

 $^1\text{H-NMR}$ *PmmpP P5*

6.4.1.6. Mechanical properties of *PmmpP* **P1-P5**

To probe the mechanical properties of *PmmpP* as a function of MW, uniaxial stress-strain experiments were performed on selected samples *PmmpP* **P1-P5** with M_w between 56 and 96 kg/mol (Figure 3-5, Table 3-1). Generally, mechanical properties improved both upon purification and with increasing MW, with *PmmpP* **P1** exhibiting a maximum Young's modulus $E = 0.9$ GPa and a strain at break $\epsilon_{\text{break}} = 300$ %. This is a much higher strain and a similar modulus compared to the best polyarylenes reported to date ($\epsilon \approx 120$ %, $E \approx 1$ GPa).^[3]

Table 3-1: Mechanical and molecular weight data.

<i>PmmpP</i>	Young's modulus / MPa	σ_{yield} / MPa	ϵ_{break} / %	M_w / kg mol ⁻¹	\bar{D}	T_g / °C
P1	897	50.5	304	96.4	2.7	118
P2	655	37.7	287	88.7	1.9	117
P3	812	36.6	281	70.8	2.1	117
P4	661	26.7	100	57.1	2.3	112
P5	617	30.0 ^[a]	8 ^[a]	56.1	1.8	n.d.

[a] Disintegrates at yield point.

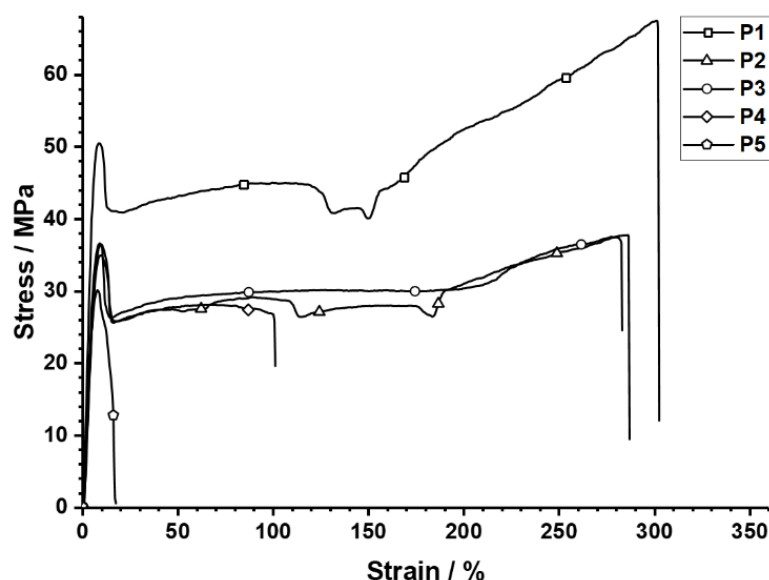


Figure 3-5: Stress-strain experiments on purified polymers **P1 - P5** (10 mm/min). Specimen cut from rigid thin film (DIN 53504 type 3) after solvent-cast from dichloromethane.

6.5. Soxhlet fractionation: Solvent screening

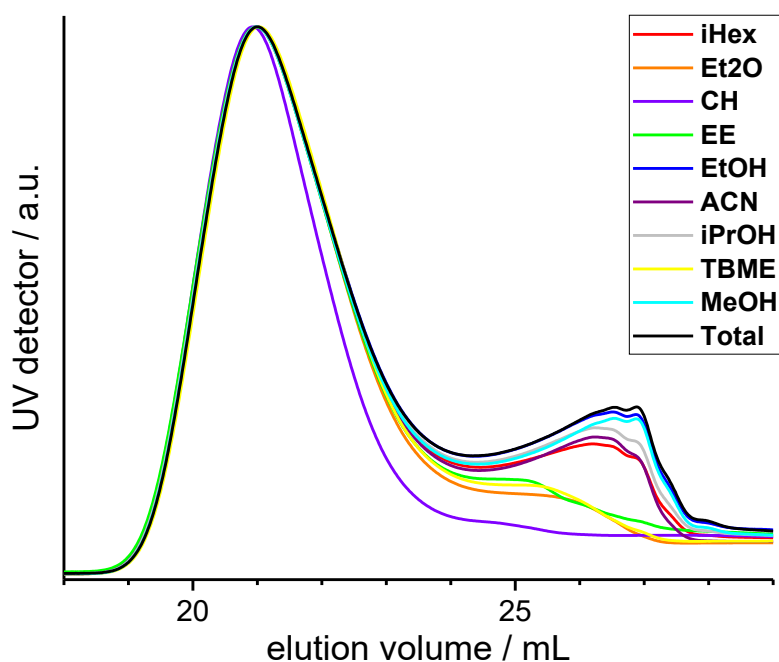


Figure 3-6: Soxhlet extraction of Polymer **S1** for 16 h. iHex: Isohexane, Et₂O: diethyl ether, CH: cyclohexane, EE: ethyl acetate, EtOH: ethanol, ACN: acetonitrile, iPrOH: Isopropanol, TBME: *tert*-butyl methyl ether, MeOH: methanol.

6.6. Screening of monomer ratio

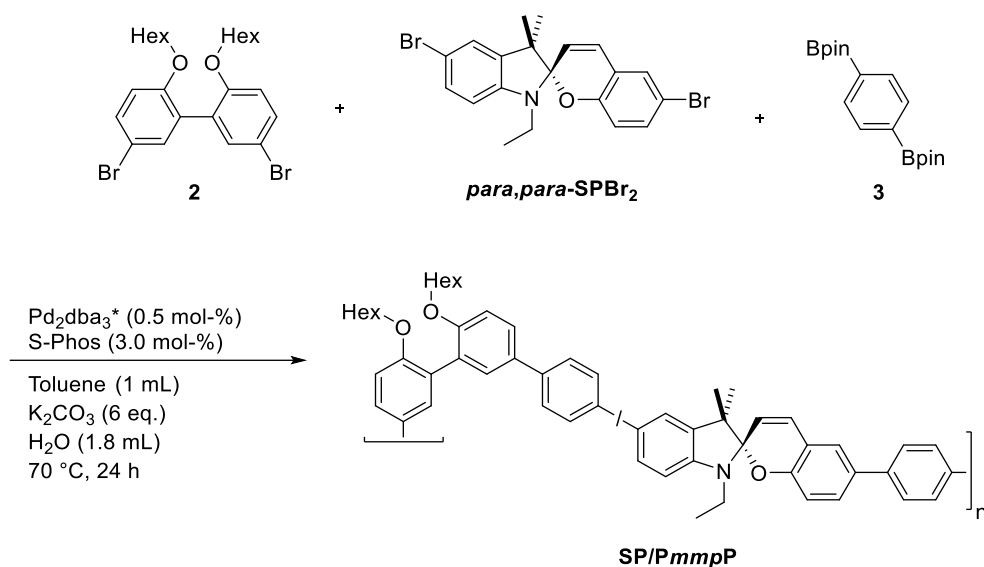
The molecular weight was optimized by changing the ratio of monomers **3** and **2**. Polymerization was carried out with conditions as for *PmmpP 2* (see section 6.4.1.2), but with a concentration of 250 mg of final Polymer in 1 mL toluene. The best monomer ratio was 1 : 1.000 (Table 3-2).

Table 3-2: Molecular weight data for screening of monomer ratio.

Code	Bpin : Br	M_w / g/mol	\bar{D}
S2	0.990	83 000	5.3
S3	0.995	84 000	5.5
S4	1.000	99 000	5.7
S5	1.005	98 000	5.1
S6	1.010	82 000	4.1

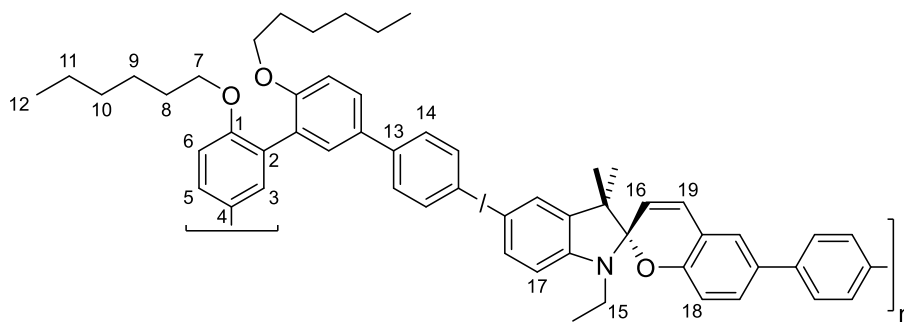
6.7. SP/PmmpP copolymer

6.7.1. Preparation



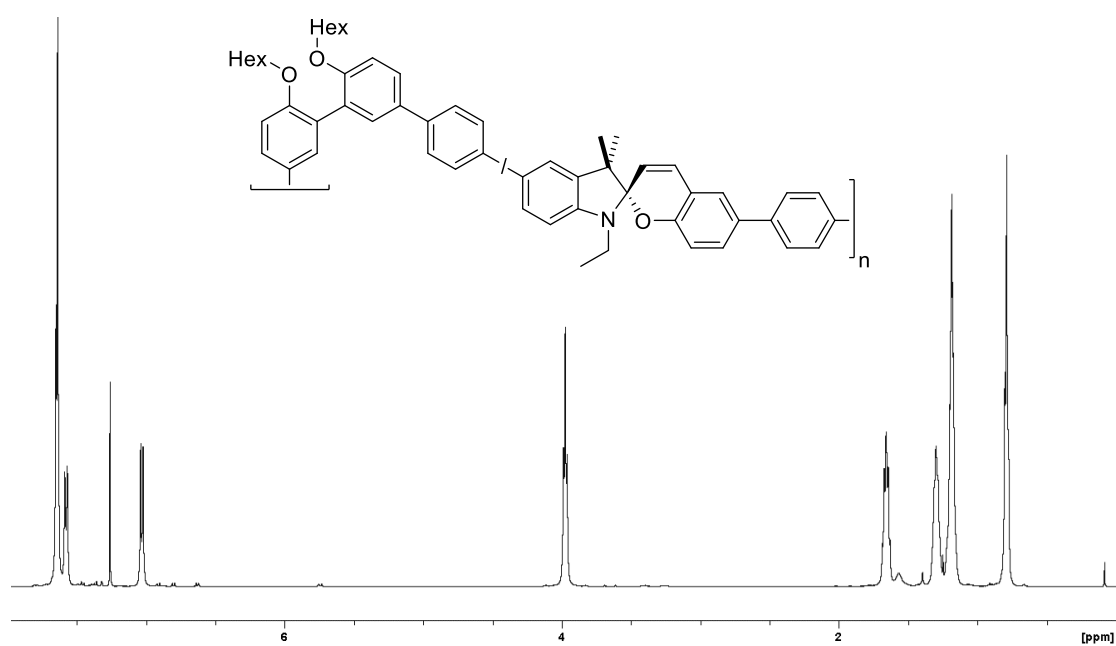
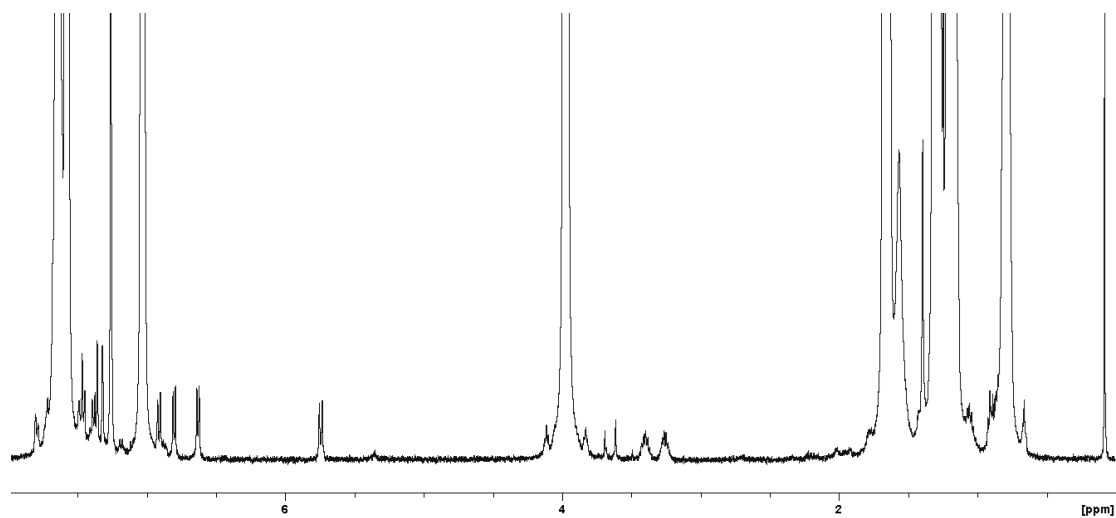
Monomer **2** (286.88 mg, 559.95 μmol , 0.95849 eq.), *para,para*-SPBr₂ (10.44 mg, 23.24 μmol , 0.03978 eq.), monomer **3** (192.81 mg, 584.20 μmol), Pd₂dba₃* (2.89 mg, 3.16 μmol , 0.5 mol-%), S-Phos (6.90 mg, 16.8 μmol , 3 mol-%) and K₂CO₃ (495.91 mg, 3.5884 mmol, 6.1 eq.) were mixed. The vessel was purged for 30 min with N₂ under slight agitation. Water and toluene were purged with N₂ separately for 30 min. Toluene (6.0 mL) was added first. After 5 min, H₂O (1.8 mL) was added and the vessel heated to 70 °C for 24 h under N₂. The polymer was precipitated dropwise from the organic phase in MeOH (300 mL), filtered off and dried under reduced pressure at 50 °C for 16 h. Soxhlet extraction was carried out with Et₂O for 24 h. The solvent was removed under reduced pressure.

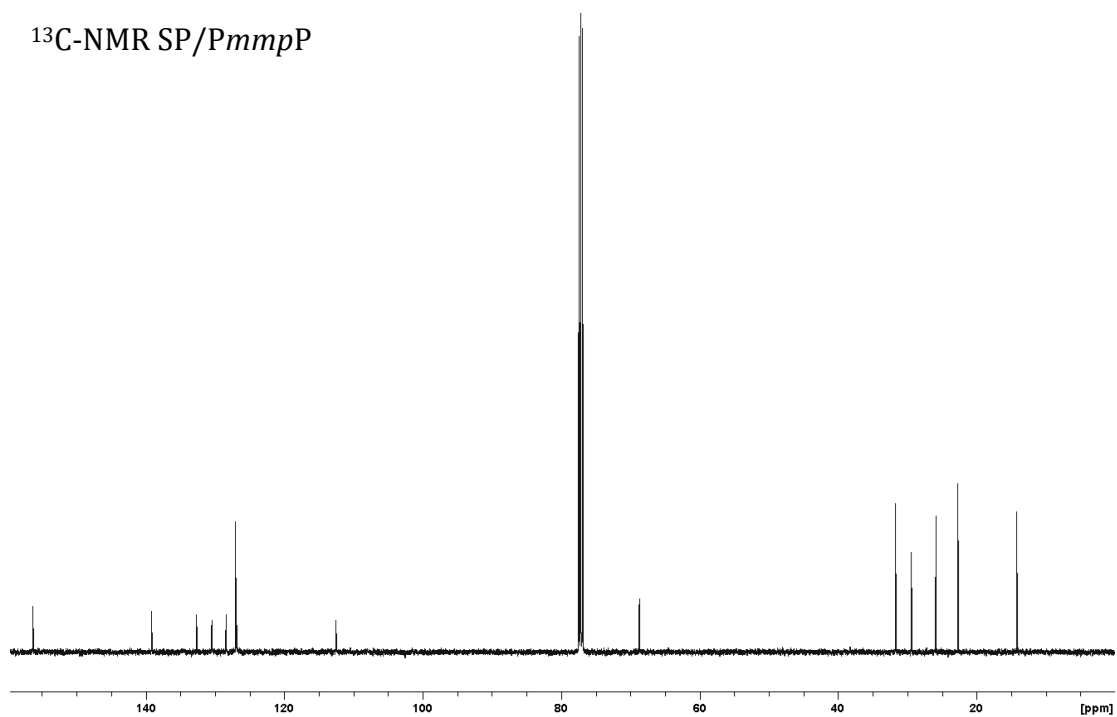
SEC (THF, 1 mL/min): $M_w = 128\,900$ g/mol, $M_n = 20\,100$ g/mol, $D = 6.4$.



^1H (500 MHz, CDCl_3): δ = 0.78 (m, 6 H, H-12), 1.18 (m, 8 H, H-11 and H-10), 1.29 (m, 4 H, H-9), 1.65 (m, 4 H, H-8), 3.05-3.38 (m, ABX_3 -signal, 15-H), 3.95 (t, 4 H, H-7), 5.74 (d, 16-H), 6.63 (d, 17-H), 6.80 (d, 18-H), 6.91 (d, 19-H), 7.02 (d, 2 H, H-6), 7.56 (dd, 2 H, H-5), 7.63 (s, 4 H, H-14), 7.64 (d, 2 H, H-3) ppm. ^{13}C (125 MHz, CDCl_3): δ = 14.0 (C-12), 22.5 (C-11), 25.7 (C-9), 29.3 (C-8), 31.5 (C-10), 68.6 (C-7), 112.5 (C-6), 126.7 (C-5), 126.9 (C-14), 128.4 (C-2), 130.3 (C-3), 132.6 (C-4), 139.1 (C-13), 156.2 (C-1) ppm.

Spiropyran chemical shifts correspond to literature.^[49]

^1H -NMR SP/PmmpP ^1H -NMR SP/PmmpP (Zoom into baseline)

^{13}C -NMR SP/*PmmpP*

6.8. Stress-strain experiment

The film was cast in a glass petri dish (inner diameter 40 mm) from dichloromethane (p.a., 4.0 mL) with 233 mg of copolymer. After 24 h the film was stored under continuous high vacuum (< 1 mbar) at room temperature for 15 h. The resulting film thickness was $187.7\ \mu\text{m}$. The specimen for the stress-strain experiment was punched from the film with a “double bell”-shaped cutting tool. Elongation speed was $10\ \text{mm/s}$ (positive and negative).

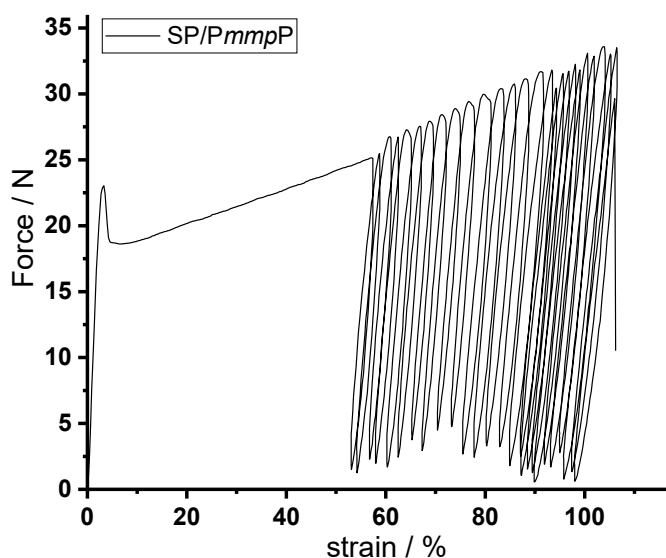


Figure 3-7: Force-strain graph of SP/PmmpP copolymer isomerization experiment.

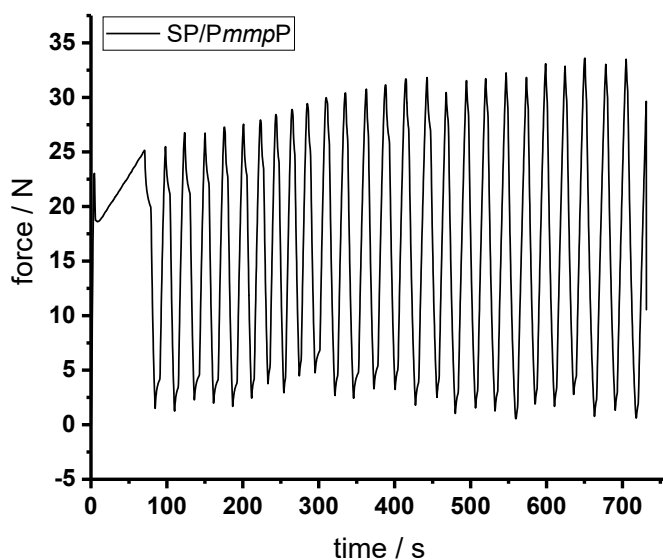


Figure 3-8: Force-time graph of SP/PmmpP copolymer isomerization experiment.

6.9. Video Analysis

Video was recorded with a Samsung Galaxy S5 (Model SM-G900F, Android 6). Settings: White balance mode *fluorescent*, flash/light *on*. Video quality: 30 fps, 1920 x 1080 Pixel, 24 bit color depth. The provided video was cropped on all sides. Video analysis was carried out in a 15 x 32 bit box (Figure 3-9). All values inside the box were averaged separately for the red, green and blue color channel (Figure 3-10).

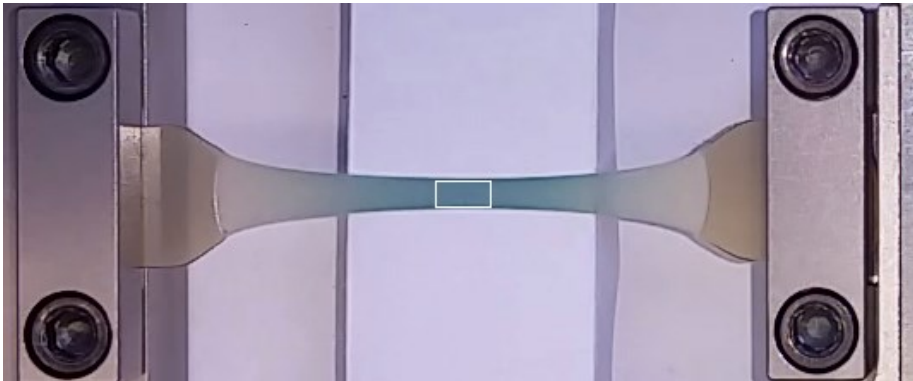


Figure 3-9: Picture from video indicating area of color analysis (white box).

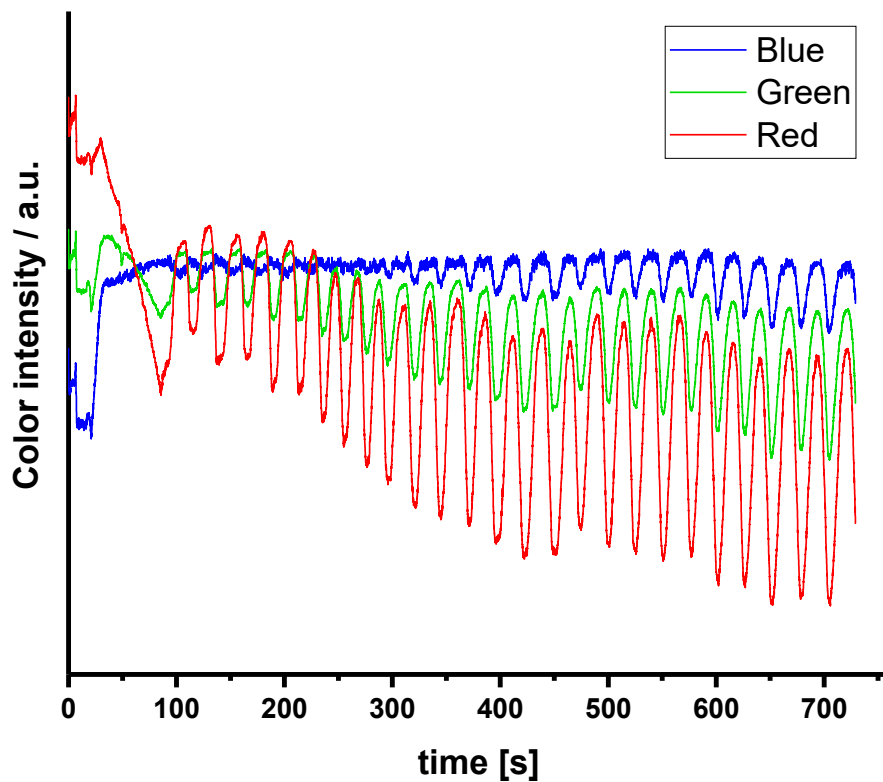


Figure 3-10: Video analysis for three separate color channels.

6.10. Differential scanning calorimetry

6.10.1. DSC analysis of *PmmpP* P1

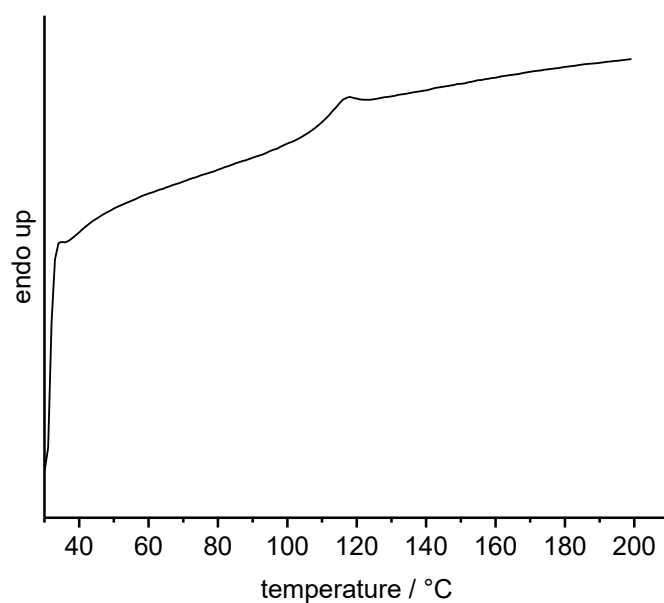


Figure-3-11: DSC of *PmmpP* P1, 10 K / min, 2. heating.

6.10.2. DSC analysis of *PmmpP* P2

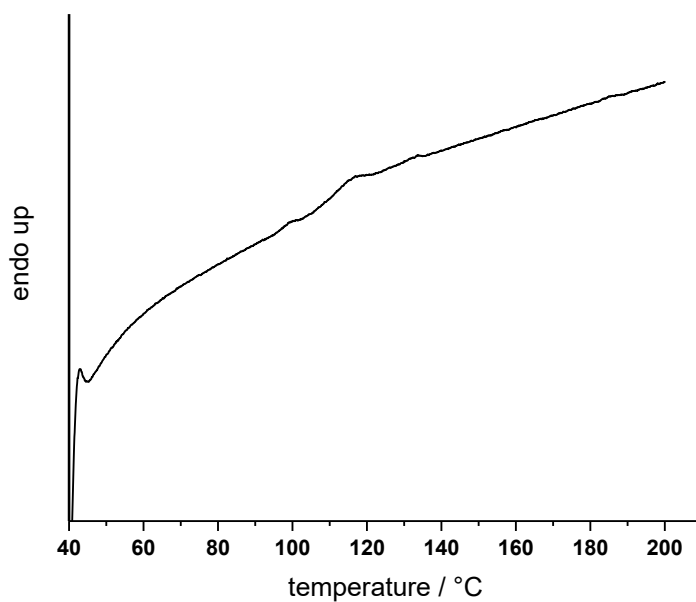


Figure 3-12: DSC of *PmmpP* P2, 10 K / min, 2. heating.

6.10.3. DSC analysis of *PmmpP* P3

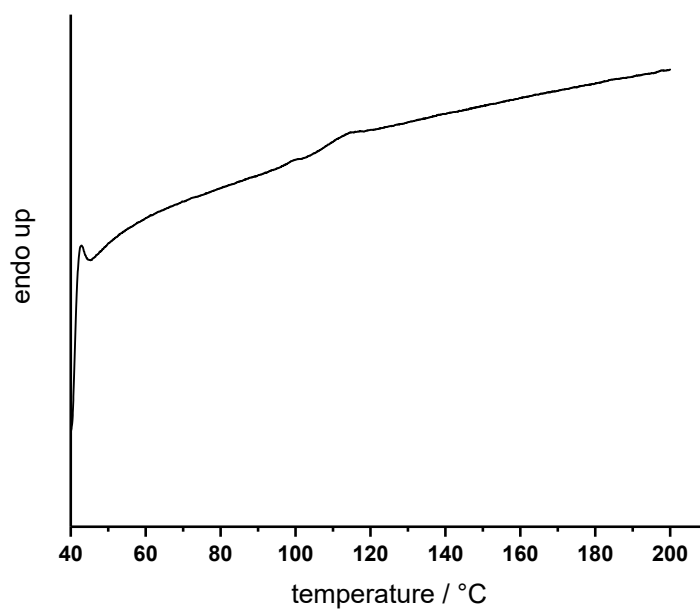


Figure 3-13: DSC *PmmpP* P3, 10 K / min, 2. heating.

6.10.4. DSC analysis of *PmmpP* P4

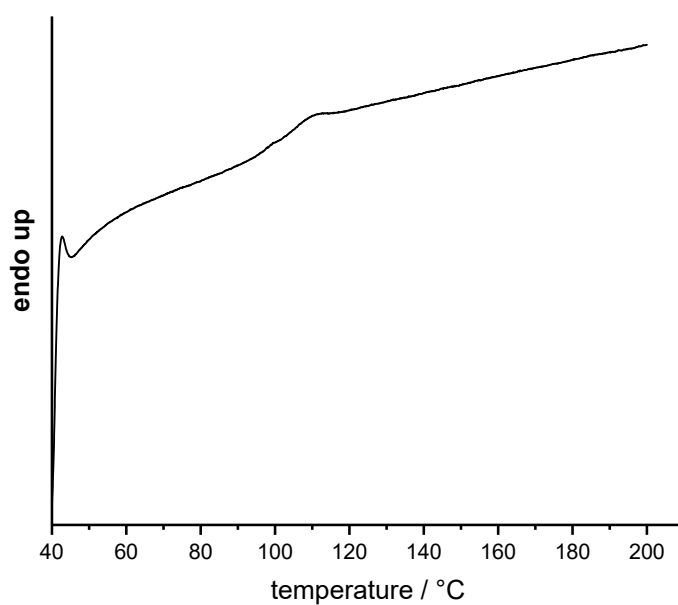


Figure 3-14: DSC of *PmmpP* P4, 10 K / min, 2. heating.

6.11. UV/VIS spectroscopy

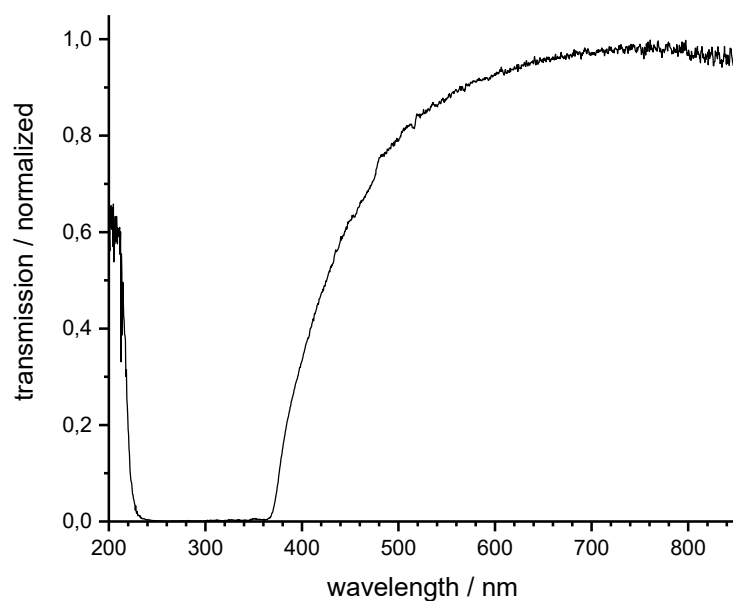


Figure 3-15: Transmission of **P3** (film). Normalized to maximum transmission.

6.12. Thermogravimetry

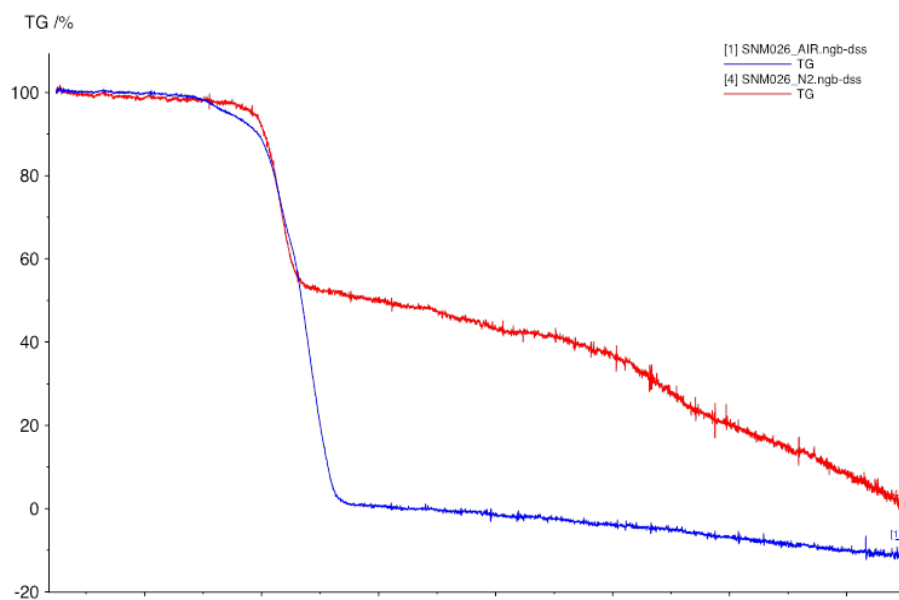
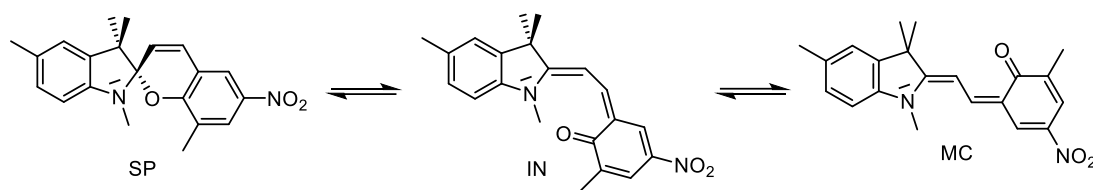


Figure 3-16: Thermogravimetric analysis of **P1**. 10 K / min. Blue: Air atmosphere; Red: Nitrogen atmosphere.

6.13. Theoretical methods



Scheme 3-2: Transition between spiropyran (SP) and CTC-merocyanine (MC) over the intermediate form (IN).

In order to obtain the force needed for the transition from SP to MC, we applied a two-dimensional Constrained Geometries Simulate External Force (COGEF) method, where the energy barriers in dependence of F_{ext} are determined. In the first step, the distance d between the pulling points and the central C-O bond length b that transforms SP to MC were varied independently (see Figure 3-2a,b in the main text). All other degrees of freedom are relaxed without further symmetry constraints. Including a vibrational analysis results in the Gibbs free energy $G_0(d, b)$.^[29,50]

The influence of a given external force F_{ext} is taken into account by the additional work via $G(d, b; F_{\text{ext}}) = G_0(d, b) - dF_{\text{ext}}$ ^[22] resulting in an energy landscape that depends on F_{ext} with a reactant minimum energy $G_R(F_{\text{ext}})$, a transition state energy $G_{TS}(F_{\text{ext}})$ and product energy $G_P(F_{\text{ext}})$. These energies define the reaction barriers in forward direction towards cleavage of the central C-O bond $\Delta G_f = G_{TS} - G_R$ and the corresponding backward reaction $\Delta G_b = G_{TS} - G_P$. The dependence on F_{ext} was suppressed for clarity. Although the C-O bond is opened in the product state, the molecule does not adopt the planar structure of MC yet, thus the product represents an instable intermediate state ("IN" in Scheme 3-2). To arrive at the final *cis,trans,cis*-MC (CTC-MC)^[51] form requires to overcome the additional barrier for *cis-trans* isomerization by rotation of the dihedral angle β (Figure 3-2a,b, main text). This defines another two dimensional energy landscape $G(d, \beta; F_{\text{ext}})$ with corresponding forward and backward barriers (Figure 3-17).

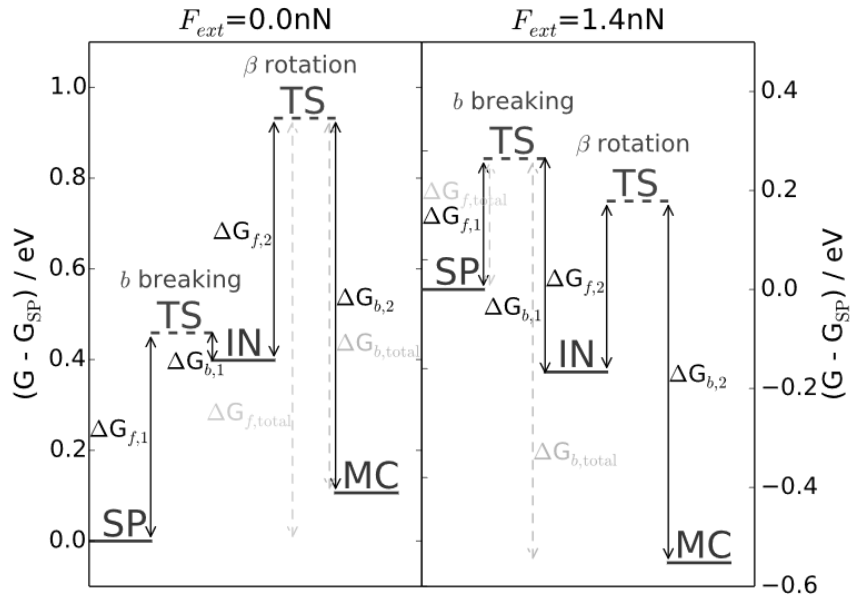


Figure 3-17: Energetics for two different external forces.

In order to calculate the dependency on time of the probabilities of the spiropyran P_{SP} , intermediate P_{IN} and merocyanine P_{MC} form, we calculated the rate constants $k_{i,j}(F_{ext})$ of the two forward and two backward transitions with the Eyring equation (Equation (1), main text) at room temperature $T = 298$ K and solved numerically the following coupled rate equations for two different applications,

$$\frac{dP_{SP}}{dt} = k_{IN,SP}P_{IN} - k_{SP,IN}P_{SP}, \quad (3)$$

$$\frac{dP_{IN}}{dt} = k_{SP,IN}P_{SP} + k_{MC,IN}P_{MC} - (k_{IN,SP} + k_{IN,MC})P_{IN}, \quad (4)$$

$$\frac{dP_{MC}}{dt} = k_{IN,MC}P_{IN} - k_{MC,IN}P_{MC}, \quad (5)$$

where $k_{i,j}$ is the rate constant for the transition from state i to state j . In order to investigate the de-coloration process at zero force we set initially $P_{MC}=1$, $P_{IN}=0$ and $P_{SP}=0$. The probability of the colored form in dependence of time is $P_c(t)=1-P_{SP}(t)$ as only the spiropyran form is uncolored. Solving the differential equations for $k_{i,j}$ ($F_{ext} = 0$) leads to the result for SP/*Pmmp*P and SP-NO₂ as shown in Figure 3-18.

In order to obtain the average rupture force we set initially $P_{SP}=1$, $P_{IN}=0$ and $P_{MC}=0$. We assume that the external force is initially zero and increases with constant loading rate $\alpha = dF_{ext}/dt$. The coloration process $P_c(t)$ can then be calculated with the same differential equations (3) – (5) and the average rupture force F follows

from equation (2) from the main text. The error bars given in Figure 3-2d in the main text are the uncertainty s_F of F which we define as the force range around F which contains 68.3% probability for coloration by analogy with the Gaussian distribution,

$$\int_{F-s_F}^{F+s_F} \frac{dP_c(F_{ext})}{dF_{ext}} dF_{ext} = 68.3\% . \quad (6)$$

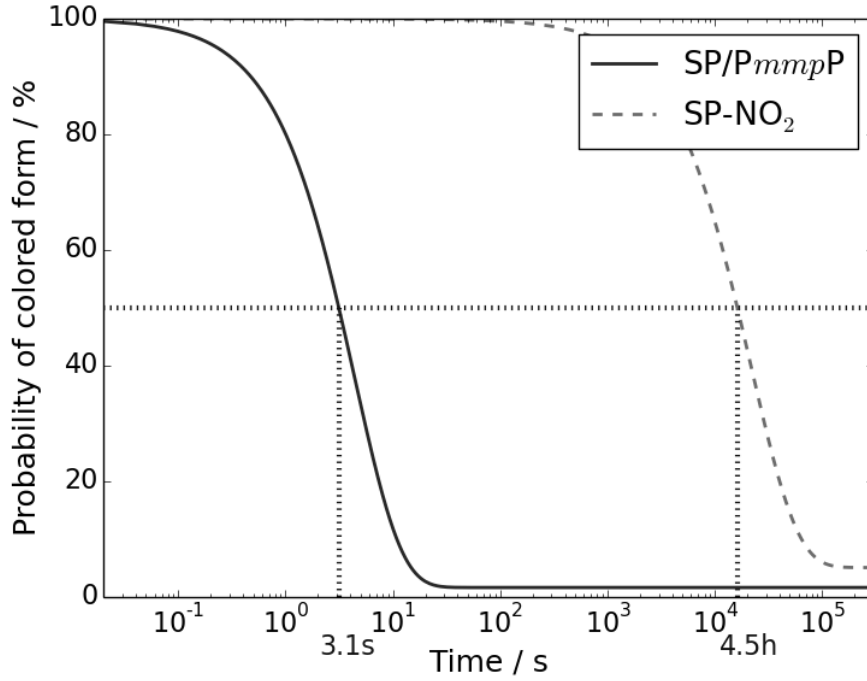


Figure 3-18: Discoloration process at zero force starting from 100% colored MC form (solid and dashed lines) and the resulting half times. The probability of MC converges for large time values against the equilibrium value which is the Boltzmann factor associated to the energy difference between MC and SP at zero force.

7. References

- [1] J. Sakamoto, M. Rehahn, G. Wegner, A. D. Schlüter, *Macromol. Rapid Commun.* **2009**, *30*, 653–687.
- [2] C. C. C. Johansson Seechurn, M. O. Kitching, T. J. Colacot, V. Snieckus, *Angew. Chem.* **2012**, *124*, 5150–5174.
- [3] R. Kandre, K. Feldman, H. E. H. Meijer, P. Smith, A. D. Schlüter, *Angew. Chem. Int. Ed.* **2007**, *46*, 4956–4959.
- [4] R. Kandre, A. D. Schlüter, *Macromol. Rapid Commun.* **2008**, *29*, 1661–1665.
- [5] S. Jakob, A. Moreno, X. Zhang, L. Bertschi, P. Smith, A. D. Schlüter, J. Sakamoto, *Macromolecules* **2010**, *43*, 7916–7918.
- [6] B. Deffner, A. D. Schlüter, *Polym. Chem.* **2015**, *6*, 7833–7840.
- [7] B. Deffner, S. Jimaja, A. Kroeger, A. D. Schlüter, *Macromol. Chem. Phys.* **2017**, *218*, 1600561–1600561.
- [8] M. Sommer, H. Komber, *Macromol. Rapid Commun.* **2013**, *34*, 57–62.
- [9] H. Komber, S. Müllers, F. Lombeck, A. Held, M. Walter, M. Sommer, *Polym. Chem.* **2013**, *5*, 443–453.
- [10] L. Metzler, T. Reichenbach, O. Brüchner, H. Komber, F. Lombeck, S. Müllers, R. Hanselmann, H. Hillebrecht, M. Walter, M. Sommer, *Polym. Chem.* **2015**, *6*, 3694–3707.
- [11] D. a Davis, A. Hamilton, J. Yang, L. D. Cremer, D. Van Gough, S. L. Potisek, M. T. Ong, P. V. Braun, T. J. Martínez, S. R. White, J. S. Moore, N. R. Sottos, *Nature* **2009**, *459*, 68–72.
- [12] M. M. Caruso, D. A. Davis, Q. Shen, S. A. Odom, N. R. Sottos, S. R. White, J. S. Moore, *Chem. Rev.* **2009**, *109*, 5755–5798.
- [13] G. O'Bryan, B. M. Wong, J. R. McElhanon, *ACS Appl. Mater. Interfaces* **2010**, *2*, 1594–600.
- [14] R. Klajn, *Chem Soc Rev* **2014**, *43*, 148–184.
- [15] B. S. Lukyanov, M. B. Lukyanova, *Chem. Heterocycl. Compd.* **2005**, *41*, 281–311.
- [16] H. Zhang, Y. Chen, Y. Lin, X. Fang, Y. Xu, Y. Ruan, W. Weng, *Macromolecules* **2014**, *47*, 6783–6790.
- [17] G. R. Gossweiler, G. B. Hewage, G. Soriano, Q. Wang, G. W. Welshofer, X. Zhao, S. L. Craig, *ACS Macro Lett.* **2014**, *3*, 216–219.
- [18] O. Brüchner, T. Reichenbach, M. Sommer, M. Walter, *J. Phys. Chem. A* **2017**, *121*, 2683–2687.
- [19] I. V. Pobelov, K. P. Lauritzen, K. Yoshida, A. Jensen, G. Mészáros, K. W. Jacobsen, M. Strange, T. Wandlowski, G. C. Solomon, *Nat. Commun.* **2017**, *8*, 15931–15937.
- [20] M. F. Pill, S. W. Schmidt, M. K. Beyer, H. Clausen-Schaumann, A. Kersch, *J. Chem. Phys.* **2014**, *140*, 44321–44332.
- [21] F. Hanke, H. J. Kreuzer, *Phys. Rev. E* **2006**, *74*, 31909–31914.
- [22] J. Ribas-Arino, D. Marx, *Chem. Rev.* **2012**, *112*, 5412–5487.

- [23] D. A. Davis, A. Hamilton, J. Yang, L. D. Cremer, D. Van Gough, S. L. Potisek, M. T. Ong, P. V. Braun, T. J. Martínez, S. R. White, J. S. Moore, N. R. Sottos, *Nature* **2009**, *459*, 68–72.
- [24] G. R. Gossweiler, T. B. Kouznetsova, S. L. Craig, *J. Am. Chem. Soc.* **2015**, *137*, 6148–6151.
- [25] J. J. Mortensen, L. B. Hansen, K. W. Jacobsen, *Phys. Rev. B* **2005**, *71*, 035109.
- [26] J. Enkovaara, C. Rostgaard, J. J. Mortensen, J. Chen, M. Dułak, L. Ferrighi, J. Gavnholt, C. Glinsvad, V. Haikola, H. A. Hansen, H. H. Kristoffersen, M. Kuisma, A. H. Larsen, L. Lehtovaara, M. Ljungberg, O. Lopez-Acevedo, P. G. Moses, J. Ojanen, T. Olsen, V. Petzold, N. A. Romero, J. Stausholm-Møller, M. Strange, G. A. Tritsarlis, M. Vanin, M. Walter, B. Hammer, H. Häkkinen, G. K. H. Madsen, R. M. Nieminen, J. K. Nørskov, M. Puska, T. T. Rantala, J. Schiøtz, K. S. Thygesen, K. W. Jacobsen, *J. Phys. Condens. Matter* **2010**, *22*, 253202–253227.
- [27] J. P. Perdew, K. Burke, M. Ernzerhof, *Phys. Rev. Lett.* **1996**, *77*, 3865–3868.
- [28] J. Ribas-Arino, M. Shiga, D. Marx, *Angew. Chem. Int. Ed.* **2009**, *48*, 4190–4193.
- [29] Christopher J. Cramer, *Essentials of Computational Chemistry: Theories and Models*, John Wiley & Sons Ltd, The Atrium, Southern Gate, Chichester, West Sussex PO19 8SQ, England, **2004**.
- [30] M. Sakuragi, K. Aoki, T. Tamaki, K. Ichimura, *Bull. Chem. Soc. Jpn.* **1990**, *63*, 74–79.
- [31] G. Baillet, G. Giusti, R. Guglielmetti, *J. Photochem. Photobiol. Chem.* **1993**, *70*, 157–161.
- [32] G. Ballet, *Mol. Cryst. Liq. Cryst. Sci. Technol. Sect. Mol. Cryst. Liq. Cryst.* **1997**, *298*, 75–82.
- [33] V. W. Kern, W. Gruber, W. Heitz, H. O. Wirth, I. Ziegler, *Makromol. Chem.* **1962**, *51*, 1–14.
- [34] G. Wegner, *Macromol. Chem. Phys.* **2003**, *204*, 347–357.
- [35] M. Rehahn, A.-D. Schlüter, G. Wegner, W. J. Feast, *Polymer* **1989**, *30*, 1060–1062.
- [36] M. G. A. Vieira, M. A. da Silva, L. O. dos Santos, M. M. Beppu, *Eur. Polym. J.* **2011**, *47*, 254–263.
- [37] J. L. Musfeldt, J. R. Reynolds, D. B. Tanner, J. P. Ruiz, J. Wang, M. Pomerantz, *J. Polym. Sci. Part B Polym. Phys.* **1994**, *32*, 2395–2404.
- [38] M.-H. Xu, Z.-M. Lin, L. Pu, *Tetrahedron Lett.* **2001**, *42*, 6235–6238.
- [39] H. Zhang, L. He, X. Liu, Y. Li, Y. Ma, J. Shen, *Synth. Met.* **2003**, *135–136*, 207–208.
- [40] H. Q. Zhang, B. Yang, Y. Zheng, F. Z. Shen, L. L. Liu, Y. G. Ma, G. D. Yang, X. F. Chen, *Thin Solid Films* **2005**, *477*, 119–124.
- [41] D. R. Armstrong, R. J. Breckenridge, C. Cameron, D. C. Nonhebel, P. L. Pauson, P. G. Perkins, *Tetrahedron Lett.* **1983**, *24*, 1071–1074.
- [42] P. K. Chhattise, A. V. Ramaswamy, S. B. Waghmode, *Tetrahedron Lett.* **2008**, *49*, 189–194.
- [43] E. Zysman-Colman, K. Arias, J. S. Siegel, *Can. J. Chem.* **2009**, *87*, 440–447.
- [44] B. A. Haag, C. Sämann, A. Jana, P. Knochel, *Angew. Chem. Int. Ed.* **2011**, *50*, 7290–7294.
- [45] S. D. Walker, T. E. Barder, J. R. Martinelli, S. L. Buchwald, *Angew. Chem. Int. Ed.* **2004**, *43*, 1871–1876.

- [46] S. S. Zalesskiy, V. P. Ananikov, *Organometallics* **2012**, *31*, 2302–2309.
- [47] B. Hohl, L. Bertschi, X. Zhang, A. D. Schlüter, J. Sakamoto, *Macromolecules* **2012**, *45*, 5418–5426.
- [48] C. Kleeberg, L. Dang, Z. Lin, T. B. Marder, *Angew. Chem. Int. Ed.* **2009**, *48*, 5350–5354.
- [49] S. B. Schmidt, F. Kempe, O. Brüchner, M. Walter, M. Sommer, *Polym. Chem.* **2017**, *8*, 5407–5414.
- [50] A. H. Larsen, J. J. Mortensen, J. Blomqvist, I. E. Castelli, R. Christensen, Marcin Dułak, J. Friis, M. N. Groves, B. Hammer, C. Hargus, E. D. Hermes, P. C. Jennings, P. B. Jensen, J. Kermode, J. R. Kitchin, E. L. Kolsbjerg, J. Kubal, Kristen Kaasbjerg, S. Lysgaard, J. B. Maronsson, T. Maxson, T. Olsen, L. Pastewka, Andrew Peterson, C. Rostgaard, J. Schiøtz, O. Schütt, M. Strange, K. S. Thygesen, Tejs Vegge, L. Vilhelmsen, M. Walter, Z. Zeng, K. W. Jacobsen, *J. Phys. Condens. Matter* **2017**, *29*, 273002–273063.
- [51] V. I. Minkin, *Chem. Rev.* **2004**, *104*, 2751–2776.

Chapter 4 Semifluorinated, kinked polyarylenes via direct arylation polycondensation

Fabian Kempe,^a Felix Riehle,^b Hartmut Komber,^c Rukiya Matsidik,^a Michael Walter ^d
and Michael Sommer ^{*a}

^a TU Chemnitz, Str. der Nationen 62, 09111 Chemnitz, Germany

^b Institute for Macromolecular Chemistry, University of Freiburg, Stefan-Meier-Str. 31,
79104 Freiburg, Germany

^c Leibniz Institute of Polymer Research, Hohe Str. 6, 01069 Dresden, Germany

^d Freiburg Center for Interactive Materials and Bioinspired Technologies (FIT), University of Freiburg,
Georges-Koehler-Allee 105, 79110 Freiburg, Germany

Reproduced from *Polym. Chem.* **2020**, *11*, 6928–6934 with permission from the
Royal Society of Chemistry.

<https://doi.org/10.1039/D0PY00973C>

1. Abstract

Semifluorinated, amorphous polyarylenes *PmmpF4* with kinked backbone structure were prepared from a *meta*-substituted, biphenol-based monomer with varying alkoxy substituents R and 1,2,4,5-tetrafluorobenzene (*pF4*) via direct arylation polymerization (DAP). The chemistry employed is simple, scalable and does not rely on tedious purification techniques. Polycondensation occurs cleanly without major side reactions. Despite the clean polycondensation reaction, high molar mass materials are difficult to obtain, which is ascribed to an unusual solubility behavior compared to non-fluorinated analogues and similar tetrafluorobenzene copolymers based on fluorene or carbazole. In order to investigate this phenomenon further, the side chain-dependent properties *PmmpF4* are investigated using linear, branched and cyclic side-chains. While the glass transition temperature of *PmmpF4* is a strong function of R and can be varied between 50 °C and 197 °C for constant backbone structure and molecular weight, solubility cannot be improved by using longer linear or branched side chains. Density functional theory calculations suggest significant polarization-type non-covalent interactions between tetrafluorobenzene and the biphenol-based monomer as origin for the observed limited solubility, which guide the design of both kinked and straight conjugated polymers with high molar mass and solubility.

2. Introduction

Polyarylenes offer unique thermal and chemical stability compared to most aliphatic polymers.^[1,2] Other aromatic polymers like aromatic polyesters, polyaramides or aromatic polycarbonates contain heteroatom-bonding in their backbone and therefore lack the inherent stability of aryl-aryl bonds. Aromatic carbon bonds are stable against common acids, bases and redox agents that other polymers may suffer from due to their backbones containing functional groups such as esters, carbonates, amides and ethers.^[3,4] The presence of aromatic rings in the repeat unit also causes high glass transition temperatures in polyarylenes, as generally observed when cyclic units are incorporated into polymer backbones.^[5] High glass transition temperatures (T_g s) are caused by the lower degree of freedom of planar (aromatic) rings in which individual atoms can only move simultaneously by rotation as a single unit.^[6] This low degree of freedom is often accompanied by liquid crystallinity or

even fully crystalline properties.^[2,5] However, high T_g s and high crystallinity may cause brittleness of materials. This may be mitigated by addition of aliphatic side chains to an aromatic polymer backbone. Thereby solubility improves due to addition of degrees of freedom in the flexible side chain while maintaining a durable polymer backbone. Nonetheless, *para*-polyarylenes are brittle materials due to their low entanglement density caused by their rigidity and rod-like shape.^[7,8] However, pioneering work by Schlüter *et al.* on polyarylenes with *meta*-comonomers proved that sufficient entanglement could be generated at very high molecular weights.^[7,9,10] These poly(*meta*-/*para*-phenylenes) (PmpP) are tough, amorphous materials on par with aromatic polycarbonates. Yet improved mechanical properties can be achieved by incorporating a “double *meta*-” motif developed by our group.^[11] Here the resulting poly(*meta*-/*meta*-/*para*-phenylenes) (PmmpP) are tough materials without prior purification starting from affordable and scalable building blocks.

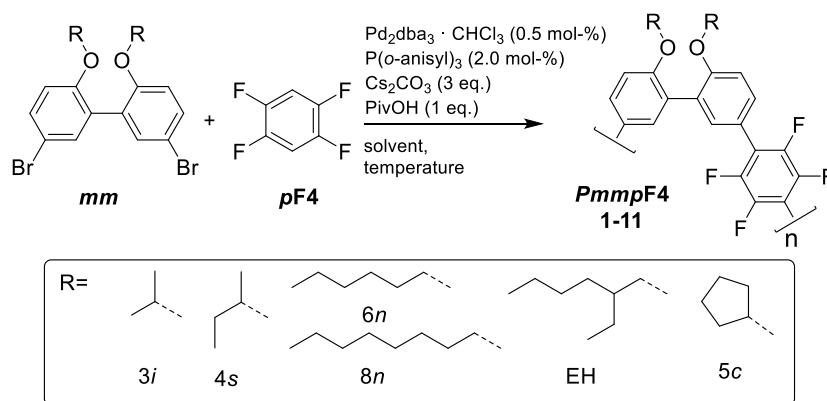
The typical cross-coupling variant for the transition metal-catalyzed polycondensation of phenylene-based monomers is the Suzuki-Miyaura reaction.^[12] Monomers are typically aryl halides coupled with a main group metal coupling partner. Polyarylenes prepared by direct arylation polymerization (DAP) are especially efficient with respect to atom economy compared to other cross coupling reactions.^[13–16] Aryl halides are coupled directly with C-H activated aryls without the need for additional functional groups. 1,2,4,5-Tetrafluorobenzene (*p*F4) has been successfully employed in this regard in order to synthesize copolymers of fluorene or carbazole.^[17,18] We were interested in kinked, semifluorinated polyarylenes as the envisaged chemistry involving DAP appears highly attractive in terms of improved atom economy, simple monomers and selective regiochemistry. Usage of F4 as the nucleophile in DAP is also expected to lead to less degradation of functional groups during polycondensation such as protio- or oxidative deborylation.^[19–23] Regarding properties, backbone fluorination is generally expected to significantly change material properties in terms of chain rigidity, solubility and order, and thus novel property profiles may become accessible.^[24–26] We therefore investigated the copolymerization of commercially available F4 with a series of 2,2'-biphenol bromide-based monomers having a double *meta* motif and different side chains developed by our group. The monomer synthesis employed

here includes three simple steps only, does not rely on chromatography or distillation and is easily scalable. The molecular and thermal properties of the resulting polymers *PmmpF4* are investigated. Density functional theory calculations are finally employed to understand and explain the unexpected, rather limited solubility of *PmmpF4*, and these result may guide the design of other polyarylenes or conjugated polymers in general as well.

3. Results and Discussion

3.1. Synthesis

We have screened the copolymerization of F4 with differently substituted 2,2'-biphenol monomers with respect to the solvent, concentration and temperature. The catalytic system itself was Pd₂dba₃/ P(*o*-anisyl)₃/ pivalic acid, a system that has emerged as a universal combination for the synthesis of many conjugated polymers via DAP.^[13] The side chains R used were isopropyl (3i), *sec*-butyl (4s), cyclopentyl (5c), *n*-hexyl (6n), *n*-octyl (8n) and 2-ethylhexyl (EH) (Scheme 4-1). All entries showed precipitation at different, limited molecular weights. This is in stark contrast to *PmmpP*, which is the non-fluorinated analog that shows excellent solubility for *M_w* up to ~100 kg/mol. We prefer to report *M_w* values here as *M_n* values are strongly influenced by oligomer content (see size exclusion chromatography (SEC) curves shown as Figure 4-5 and Figure 4-6).^[11] Therefore, molecular weight is indicative of solubility of the copolymer at the temperature of the reaction. Interestingly, longer side-chins did not generally improve solubility. The introduction of branched side chains was beneficial to improve solubility in some cases (4s vs. 5c and 3i). Interestingly, usage of EH instead of 6n or also 8n did not improve solubility. These observations are in stark contrast to conjugated polymers where side chain branching is key to increase solubility significantly and for many examples to enable processing at all.^[27]



Scheme 4-1: Synthesis of kinked, semifluorinated *PmmpF4* via DAP.

Good solvents for *PmmpF4* are chloroform, dichloromethane and 1,2-dichloroethane, all of which are unsuitable for cross coupling reactions. Chlorobenzene (CB) is a good solvent for *PmmpF4* but leads to phenyl-endcapping (see Figure 4-19). The highest molar mass was achieved for Toluene (Tol) as solvent, 100 °C reaction temperature and a monomer concentration of 0.8 M (entries 1-5, Table 4-1). Despite screening for solvents, side chains and temperature, only moderate molecular weights up to $M_{w,SEC} \sim 22$ kg/mol were achieved (entry 2), which could be somewhat increased to $M_{w,SEC} \sim 31$ kg/mol by fractionation (entry 2a). In general, *meta*-substituted polyarylenes show better solubility compared to *para*-substituted ones.^[28]

PmmpF4 was characterized by ^1H and ^{19}F NMR spectroscopy (Figure 4-1a, Figure 4-14 to Figure 4-19). Additionally, the ^{13}C NMR spectrum was recorded for the hexyl derivative (entry 2, Figure 4-1b). The rather clean ^1H NMR spectra without obvious end group signals suggest good molecular weights. The only proven end groups are $-\text{C}_6\text{F}_4\text{-H}$ and $-\text{C}_6\text{F}_4\text{-Ph}$, which result in characteristic signals of low intensity in the ^{19}F NMR spectra (Figure 4-14b to Figure 4-19b). The $-\text{C}_6\text{F}_4\text{-Ph}$ end group is only observed when CB was used as solvent for polymerization (Figure 4-18b). Considering that the reaction mixture became highly viscous in all cases, gelated or precipitation occurred during polycondensation, and that some of the samples were only partially soluble in CHCl_3 at room temperature, solubility appeared to be the limiting factor that prevented the formation of higher molecular weights. We therefore used the best conditions and varied the side chain to elucidate whether an increase in molecular weight could be achieved, and finally to vary properties. However, molecular weight could not be increased for none of the different

monomers used, as gelation or precipitation occurred in most cases (entries 6-11, Table 4-1).

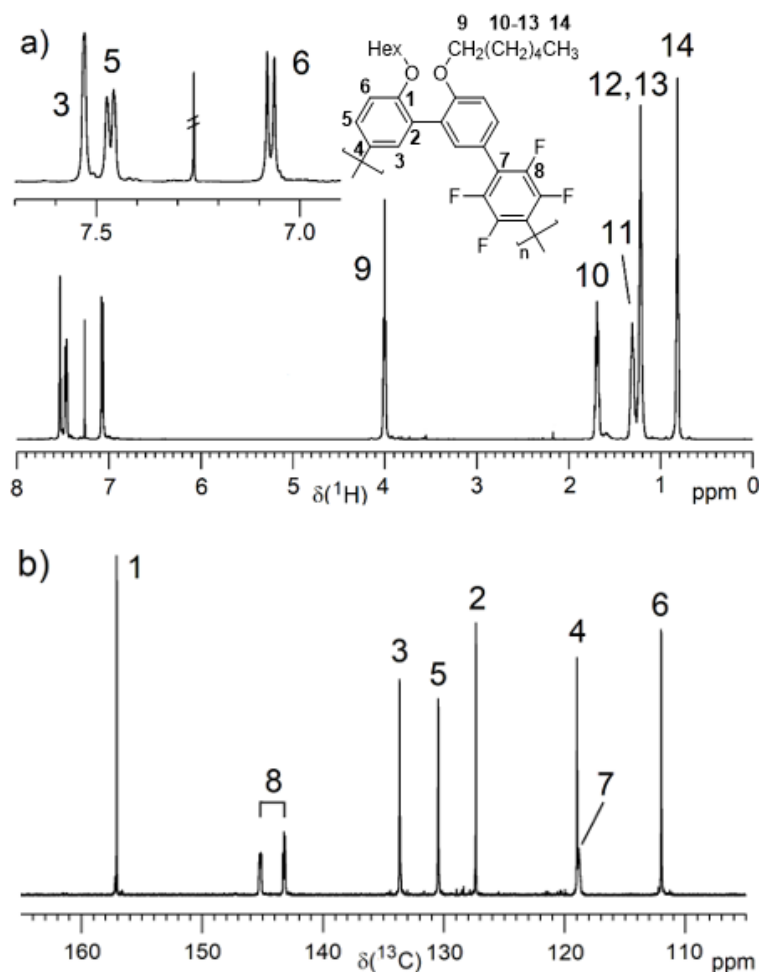


Figure 4-1: ^1H (a) and ^{13}C (b) NMR spectra of *PmmpF4* (entry 2) in CDCl_3 with assignments.

3.2. Thermal properties

The thermal properties of our polymer were investigated next (Figure 4-2). Figure 4-2a shows the dependence of T_g of *PmmpF4* with *n*-hexyl side chains on molecular weight. A trend showing saturation at 90 °C for $M_n/M_w \sim 10/20$ kg/mol is seen, which is expected for conjugated polymers (Figure 4-2a).^[29] The dependence of the T_g of *PmmpF4* on the side chain for similar molecular weight is shown in Figure 4-2b and Table 4-2. Usually, longer side-chains decrease the T_g of conjugated polymers.^[29–32] This is also seen here, with the T_g of *PmmpF4* with 8*n* being lower (50 °C) than of *PmmpF4* with 6*n* (83 °C) as expected.^[32] *PmmpF4* with EH side chains exhibits a higher T_g (68 °C) compared to 8*n* (50 °C, Figure 4-2b, Table 4-2). The moderate increase of T_g for linear *versus* branched side chains but a constant number of carbons in the side chain is again similar to e.g. polythiophenes, where

for poly(3-octylthiophene) and poly(3-(2-ethylhexyl)thiophene) glass transition temperatures of -13 °C and 24 °C, respectively, have been reported.^[30,33] The T_g of *PmmpF4* further increases more strongly when moving to cyclic side chains. Upon attaching 5c side chains a T_g of 197 °C is measured. Clearly, cyclic side chains increase T_g much stronger than linear ones. While cyclic side chains are rather uncommon for conjugated polymers, the comparison of the T_g s of poly(1-hexene) (-63 °C)^[34] and polyvinylcyclohexane (80 °C)^[35] also indicates a strong increase in T_g for linear versus cyclic side chains at constant side chain fraction. We also attempted to install *n*-decyl side chains, in which case very low molar mass *PmmpF4* was obtained, as well as cyclohexyl side chains, which failed at the monomer synthesis stage (not shown). Thus, the T_g of *PmmpF4* can be varied by as much as ~150 K for the herein investigated range of side chains.

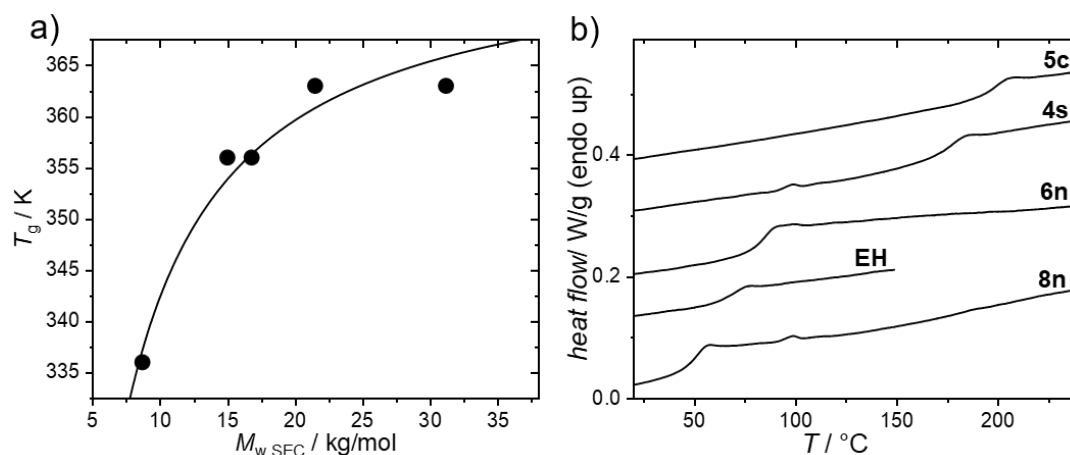


Figure 4-2: Glass transition temperature of *PmmpF4* with 6n as a function of molecular weight (a) and for varying side chains including entry 5 (b). Conditions: 2nd heating, 10 K/min, N₂.

Table 4-1: Optimization of reaction conditions for *n*-hexyl side chain.

entry	M1	M2	Solvent	Temp./ °C	conc./ M	M_n / kg/mol	M_w / kg/mol
1	6 <i>n</i>	<i>p</i> F4	Tol	70	1.0	3.9	8.7
2	6 <i>n</i>	<i>p</i> F4	Tol	100	0.8	10.8	21.5
2a ^a	6 <i>n</i>	<i>p</i> F4	Tol	100	0.8	15.8	31.2
3	6 <i>n</i>	<i>p</i> F4	Tol	120	0.8	3.9	5.5
4	6 <i>n</i>	<i>p</i> F4	THF	100	0.8	7.9	16.8
5	6 <i>n</i>	<i>p</i> F4	dioxane	100	0.5	6.4	15.0
6	EH	<i>p</i> F4	Tol	100	1.2	10.2	14.8
7	4 <i>s</i>	<i>p</i> F4	Tol	100	0.8	10.1	17.1
8	3 <i>i</i>	<i>p</i> F4	Tol	100	0.8	1.9	2.5
9	5 <i>c</i>	<i>p</i> F4	Tol	100	0.8	6.6	11.8
10	8 <i>n</i>	<i>p</i> F4	Tol	100	1	6.1	12.6
11	8 <i>n</i>	<i>p</i> F4	CB	90	1	6.2	13.0

^a obtained from entry 2 after additional Soxhlet extraction with ethyl acetate.

Table 4-2: Glass transition temperatures of polyarylenes with different side chains.

Entry #	R =	T_g / °C	M_w / kg/mol	\bar{D}
2a	<i>n</i> -hexyl	90	31.2	1.5
2	<i>n</i> -hexyl	90	21.5	2.0
4	<i>n</i> -hexyl	83	16.8	2.1
5	<i>n</i> -hexyl	83	15.0	2.3
1	<i>n</i> -hexyl	63	8.7	2.2
7	<i>s</i> -butyl	173	17.1	1.7
9	cyclopentyl	197	11.8	1.8
11	<i>n</i> -octyl	50	13.0	2.1
6	(2-ethyl) hexyl	68	14.8	1.5

With *PmmpP* being highly soluble^[11], it is tempting to explain the limited solubility of *PmmpF4* by the replacement of Ph by F4. However, the mere presence of an F4 moiety alone cannot explain the limited solubility. Other alternating F4 copolymers with fluorene (PF8F4) or carbazole show excellent solubility with molecular weights of PF8F4 of up to $M_{n,SEC} = 347$ kg/mol.^[17] With PF8F4 exhibiting stiff and coplanar dioctylfluorene units in combination with *p*F4, it appears counterintuitive that the herein investigated twisted and kinked *PmmpF4* with a similar amount of side chains exhibits a lower solubility than PF8F4 for the same range of solvents. We therefore assumed attractive interactions between segments of *PmmpF4* to be present. Possible interactions anticipated include oxygen/lone pair-F4 interactions, which may be comparable to anion/lone pair- π -interactions, and π - π interactions (Figure 4-3a,b).^[36,37]

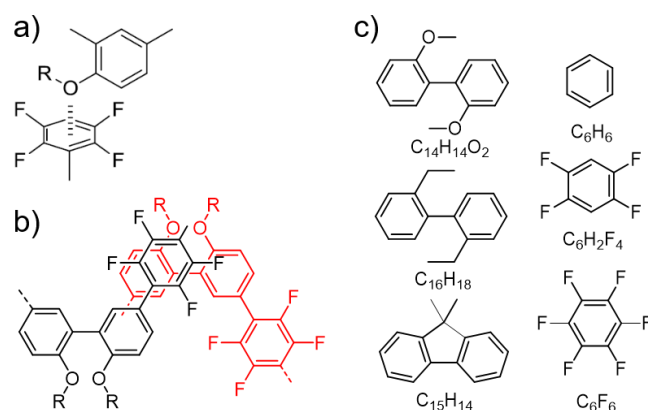


Figure 4-3: a,b) Possible chain chain interactions of *PmmpF4* and c) model compounds used for DFT calculations.

However, F4-oxygen interactions as depicted in Figure 4-3a are difficult to prove. The fact that the solubility of *PmmpF4* in THF was even lower than in Tol did also not point to such a motif. Interactions including π - π -stacked configurations as depicted in Figure 4-3b were therefore investigated theoretically.

3.3. Density functional theory calculations

In order to further investigate a possible origin for the reduced solubility of *PmmpF4*, we have performed an extensive theoretical study of the weak interactions between its building blocks. The absence of effects due to the side chains suggests that strong interactions between different parts of the *PmmpF4* backbone might be responsible for the decreased solubility relative to *PmmpP* observed. We were

particularly interested in the effect of fluorination of the phenyl-based comonomer and the role of substitution of the biphenyl comonomer on the aggregation behavior. We therefore studied the interaction of building blocks of *PmmpF4* as well as differently substituted derivatives. Figure 4-3c shows chemical structures of all compounds involved, namely C_6H_6 , $C_6H_2F_4$, C_6F_6 , $C_{15}H_{14}$, $C_{16}H_{18}$ and $C_{14}H_{14}O_2$.

DFT calculations were performed in the projector augmented wave method^[38] as implemented in the GPAW package.^[39,40] The smooth Kohn-Sham wave functions were represented on real space grids with a grid spacing of 0.2 Å and the electron density on grids of 0.1 Å spacing. The exchange-correlation energy was approximated as devised by Perdew, Burke and Ernzerhof (PBE)^[41] and the corrections proposed by Tkatchenko and Scheffler (TS09)^[42] were included to describe dispersive interactions. The results were cross checked using the vdW-DF2^[43] functional. The structures were set up using the atomic simulation environment^[40] and the simulation box was ensured to contain at least 4 Å of space around each atom. Molecules were placed in random relative orientations and structures subsequently relaxed to the next local minimum. This resulted in 190-650 relaxed structures for each pairing from which we have obtained the configurations of lowest energy. The configurations were accepted if at least two lowest energy structures were found within the range of 4 kJ/mol representing chemical accuracy (see Figure 4-20).^[44] Interactions involving $C_6H_2F_4$ required considerably more pairs than those containing C_6H_6 or C_6F_6 to achieve this goal. This effect can be attributed to the lower symmetry of $C_6H_2F_4$, which results in a larger structural entropy in the pairs.

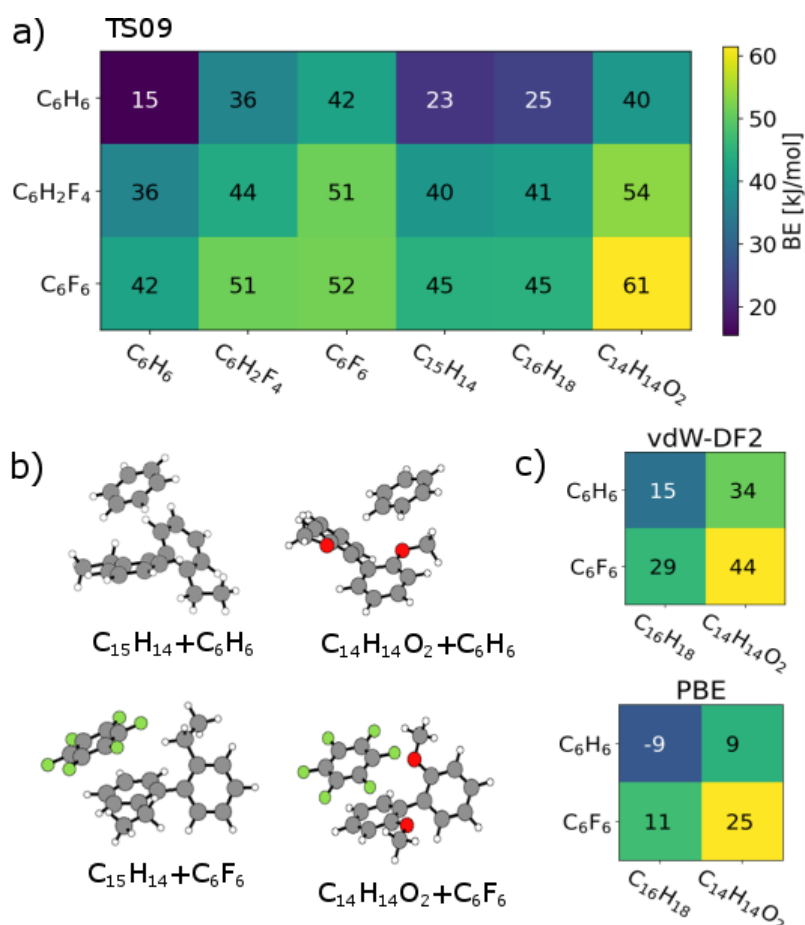


Figure 4-4: a) Scheme of binding energies between the model fragments of *PmmpF4*, for chemical structures see Figure 4-3c. b) Selected lowest energy structures. c) Binding energies in vdW-DF2 and PBE in the TS09 relaxed structure.

Figure 4-4a) displays the binding energies (BEs, positive values indicate attraction) of the energetically best pairs found. There is a clear trend of enhanced attraction between fluorinated species as compared to benzene. The lowest BE is found for the benzene pair with 15 kJ/mol in the parallel-displaced configuration (see Figure 4-21). This value is slightly higher than the CCSD(T) value of 11-12 kJ/mol^[45,46] and the difference can be assigned to the tendency of the TS09 approximation to overestimate the interactions^[47], while keeping the relative ordering correct.^[48] We find the C_6H_6 - C_6F_6 pair to bind with 42 kJ/mol in good agreement to MP2 value of 39 kJ/mol.^[49] The overall highest binding energy is found for the C_6F_6 pair with 52 kJ/mol. All combinations involving C_6H_6 , $C_6H_2F_4$ and C_6F_6 prefer parallel-displaced configurations.

Regarding relaxed structures between C_6H_6 , $C_6H_2F_4$ and C_6F_6 with $C_{15}H_{14}$, $C_{16}H_{18}$ and $C_{14}H_{14}O_2$, there is a large variety of relative configurations with the tendency to parallel stacked configurations of the fluorinated benzenes with the biphenyl model compounds (see Figure 4-3b, Figure 4-4b and Figure 4-21). Also here, the binding

energies follow clear trends of stronger interactions with increasing number of fluorine substituents for each biphenyl derivative. Pairs involving $C_{14}H_{14}O_2$ in combination with C_6H_6 and $C_6H_2F_4$ are found to form CH-O hydrogen bonds (see Figure 4-21) with bond lengths between 2.7 Å and 2.9 Å for the two best structures of each pair, which obviously are not relevant for the polymer under scrutiny. However, from a general perspective, this structure factor is remarkable despite of the weakness of this bond that should be less than 10 kJ/mol.^[50,51] Most importantly, however, is the finding that all three benzene derivatives exhibit the strongest interactions with $C_{14}H_{14}O_2$. A higher binding energy is found for $C_{14}H_{14}O_2$ and C_6H_6 , $C_6H_2F_4$ as well as C_6F_6 in comparison to the coplanar fluorene derivative $C_{15}H_{14}$. A cross check with the conceptually different description of dispersive interactions by the vdW-DF2 functional leads to slightly lower binding energies, but the same relative ordering as seen in Fig. 4c. Similar ordering is already obtained at the PBE level (evaluated for TS09 relaxed structures), which indicates that the effect is rather due to polarization than dispersion.^[52] Bader analysis^[53,54] did not reveal any significant charge transfer in these structures. The larger BE values of the couple $C_{14}H_{14}O_2$ / C_6F_6 compared to $C_{15}H_{14}$ / C_6F_6 reflect both the rather good solubility of PF8F4^[17] as well as the limited solubility of *Pmmp*F4. From a structural design point of view, the combination of the F4 motif with alkoxyated biphenyls apparently makes a large difference by increasing chain-chain interactions and reducing solubility.

4. Conclusion

We have successfully prepared kinked polyarylenes by a straightforward and simple direct arylation approach with high atom economy. The glass transition temperature of these semifluorinated aromatic copolymers can be varied between 50 and 200 °C depending on type and size of the side chain. Molar mass is limited by solubility and not by termination reactions, which is surprising considering the kinked backbone structure and the exceptionally good solubility of the non-fluorinated analog *Pmmp*P. DFT calculations on model systems reveal strong attractive interactions between the fluorinated and dialkoxyated comonomers, which continuously increases with the degree of fluorination. This effect is caused mainly by an increased polarization interaction rather than changes in dispersion

or charge transfer. It is thus the combination of the alkoxy side chains with the F4 unit that causes the experimentally observed limited solubility, which should be avoided if copolymers with high molar mass and solubility are the target.

5. Acknowledgements

M. S. and F. K. thank M. Raisch for the synthesis of 5,5'-dibromo-2,2'-bis(2-ethylhexyloxy)biphenol. M.W. acknowledges computational resources provided by the state of Baden-Württemberg through bwHPC via the JUSTUS cluster.

6. Experimental Methods

6.1. General methods

All chemicals were obtained from Sigma Aldrich and used without further treatment unless specified.

DSC measurements were acquired on a DSC 2500 (TA Instruments) under a nitrogen atmosphere at a heating and cooling rate of 10 K / min. Fox-Flory fit was carried out with $T_g = T_{g,\infty} - (A/M_w)$. Here, the fit parameters are $T_{g,\infty}$ (T_g at a hypothetical infinite molecular weight) and A (general fit parameter).

NMR measurements were carried out on an Advance III 500 NMR spectrometer (Bruker) at 500.13 MHz (^1H), 125.76 MHz (^{13}C) and 470.59 MHz (^{19}F). The spectra were recorded in CDCl_3 and DMSO-d_6 at 30 °C or in $\text{C}_2\text{D}_2\text{Cl}_4$ at 120 °C. The spectra were referenced to the solvent signal (CDCl_3 : $\delta(^1\text{H}) = 7.26$ ppm, $\delta(^{13}\text{C}) = 77.0$ ppm; DMSO-d_6 : $\delta(^1\text{H}) = 2.50$ ppm, $\delta(^{13}\text{C}) = 39.6$ ppm; $\text{C}_2\text{D}_2\text{Cl}_4$: $\delta(^1\text{H}) = 5.98$ ppm). The ^{19}F NMR spectra recorded in CDCl_3 were referenced to external C_6F_6 ($\delta(^{19}\text{F}) = -163$ ppm). Signal assignments were confirmed by $^1\text{H} - ^1\text{H}$ and $^1\text{H} - ^{13}\text{C}$ correlated spectra.

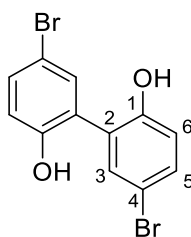
TGA measurements were done on a TGA/DSC3+ (Mettler-Toledo) under nitrogen at a heating rate of 10 K / min.

SEC measurements in CHCl_3 were carried out on three MZ-Gel SD plus 5 μm columns and a pre-column, with pore sizes of 10^3 , 10^4 and 10^5 Å (MZ-Analysentechnik GmbH) connected in series with a SPD20AV UV detector (Shimadzu) and calibrated with polystyrene standards. CHCl_3 (HPLC grade) was used as eluent at 30 °C at a flow rate of 1.0 mL / min. SEC measurements in THF were carried out on three SDV gel 5 μm columns and a pre-column, with pore sizes ranging from 10^3 to 10^5 Å (PSS), connected in series with a 254 nm UV detector and calibrated with polystyrene standards. THF (HPLC grade) was used as eluent at 30 °C at a flow rate of 1.0 mL / min.

6.2. Preparation of monomers

The preparation of the linear side chain monomer 6n was reported previously.^[11] The procedure was modified for the syntheses of the following monomers.

6.2.1. 5,5'-Dibromobiphenyl-2,2'-diol

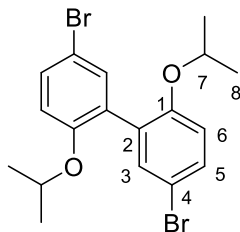


2,2'-Biphenol (10.001 g, 53.703 mmol, 1.0 eq.) and *p*-toluenesulfonic acid (12.211 g, 70.911 mmol, 1.3 eq.) were dissolved in acetonitrile (100 mL). Subsequently N-bromosuccinimide (19.168 g, 107.68 mmol, 2.00 eq.) was added and the mixture agitated for 1 h. The suspension was filtered and remaining solids recrystallized from ethanol. The product was a colorless solid (6.0 g, 17.5 mmol, 33 %).

Melting point: 176-178 °C

¹H NMR (500 MHz, DMSO-*d*₆, ppm): 9.63 (br s, 2H; OH), 7.30 (dd, 8.6 Hz, 2.6 Hz, 2H; H₅), 7.26 (d, 2.6 Hz, 2H; H₃), 6.86 (d, 8.6 Hz, 2H; H₆).

¹³C NMR (125 MHz, CDCl₃, ppm): 154.1 (C₁), 133.5 (C₃), 131.1 (C₅), 126.6 (C₂), 117.8 (C₆), 109.6 (C₄).

6.2.2. 5,5'-Dibromo-2,2'-bis(isopropoxy)biphenyl

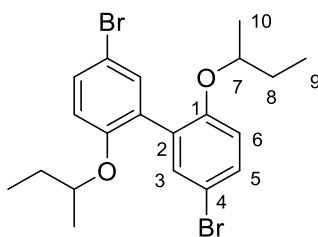
5,5'-Dibromobiphenyl-2,2'-diol (10.029 g, 29.125 mmol, 1.0 eq.), 2-bromopropane (16.4 mL, 21.5 g, 175 mmol, 6.0 eq.) and K_2CO_3 (12.059 g, 87.258 mmol, 3.0 eq.) were stirred in acetonitrile (dry, 100 mL) and stirred at 90 °C for 24 h. Volatiles were removed under reduced pressure. Solid residue were extracted with *iso*-hexanes (60 mL) and washed with water (60 mL) and brine (25 mL). Aqueous phases were extracted with Et_2O (3 x 60 mL) and all combined organic phases dried over Na_2SO_4 . Solvents were removed under reduced pressure and the product recrystallized from 2-propanol. The title compound (7.13 g, 16.66 mmol, 57 %) was a colorless solid.

Melting point: 66-69 °C

1H NMR (500 MHz, $CDCl_3$, ppm): 7.36 (4H; H_3 , H_5), 6.82 (m, 2H; H_6), 4.34 (sept, 6.1 Hz, 2H; H_7), 1.19 (d, 6.1 Hz, 12H; H_8).

^{13}C NMR (125 MHz, $CDCl_3$, ppm): 154.5 (C_1), 134.3 (C_3), 131.1 (C_5), 130.2 (C_2), 116.3 (C_6), 112.2 (C_4), 71.3 (C_7), 21.9 (C_8).

6.2.3. 5,5'-Dibromo-2,2'-bis(sec-butoxy)biphenyl

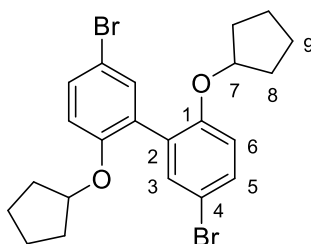


5,5'-Dibromobiphenyl-2,2'-diol (10.008 g, 28.594 mmol, 1.0 eq.), 2-bromobutane (19.0 mL, 23.9 g, 174 mmol, 6.0 eq.) and K_2CO_3 (12.051 g, 87.200 mmol, 3.0 eq) were stirred in acetonitrile (dry, 100 mL) at 90 °C for 24 h. Volatiles were removed under reduced pressure. Solid residues were dissolved in *iso*-hexanes (60 mL), washed with H_2O (25 mL) and brine (25 mL) and dried over Na_2SO_4 . Solvents were removed under reduced pressure and the product recrystallized from 2-propanol. The title compound (7.77 g, 17.0 mmol, 58 %) was a colorless solid.

Melting point: 64-67 °C

^1H NMR (500 MHz, CDCl_3 , ppm): 7.35 (4H; H_3 , H_5), 6.80 (d, 8.3 Hz, 2H; H_6), 4.13 (2H; H_7), 1.57 and 1.48 (2 x m, 4H; H_8), 1.15 and 1.14 (2 x d, 6.0 Hz, 6H; H_{10}), 0.83 and 0.82 (2 x t, 7.4 Hz, 6H; H_9). Note: The reaction product is the mixture of the two diastereomers.

^{13}C NMR (125 MHz, CDCl_3 , ppm): 154.6 (C_1), 134.4 (C_3), 131.1 (C_5), 130.1 (C_2), 116.1 (C_6), 112.0 (C_4), 76.1 (C_7), 29.0 (C_8), 18.9 (C_{10}), 9.4 (C_9).

6.2.4. 5,5'-Dibromo-2,2'-bis(cyclopentoxy)biphenyl

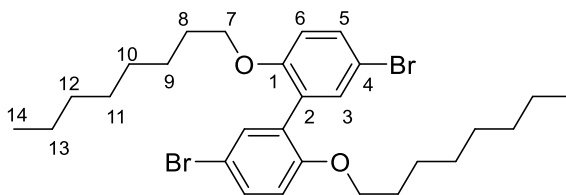
5,5'-Dibromobiphenyl-2,2'-diol (6.006 g, 17.44 mmol, 1.0 eq.), DMF (1 mL), bromocyclopentane (23.0 mL, 33.9 g, 227 mmol, 13 eq.) and K_2CO_3 (7.271 g, 52.61 mmol, 3.1 eq.) were stirred at 95 °C for 18 h. The mixture was quenched with H_2O (25 mL) and washed with brine (25 mL). Aqueous phases were extracted with Et_2O (3 × 25 mL) and the organic phase dried with $MgSO_4$. Volatiles were removed under reduced pressure. Solid residues were purified in a Kugelrohr apparatus under high vacuum (0.6 bar, 280 °C). The product was recrystallized from 2-propanol. The title compound (3.78 g, 7.87 mmol, 45 %) was a colorless solid.

Melting point: 133-136 °C.

1H NMR (500 MHz, $CDCl_3$, ppm): 7.34 (4H; H_3, H_5), 6.79 (m, 2H; H_6), 4.65 (m, 2H; H_7), 1.85-1.70 (8H; H_8), 1.70-1.50 (8H; H_{10}).

^{13}C NMR (125 MHz, $CDCl_3$, ppm): 154.5 (C_1), 134.1 (C_3), 131.0 (C_5), 129.5 (C_2), 115.3 (C_6), 111.8 (C_4), 80.2 (C_7), 32.7 (C_8), 23.8 (C_9).

6.2.5. 5,5'-Dibromo-2,2'-bis(octyloxy)biphenyl



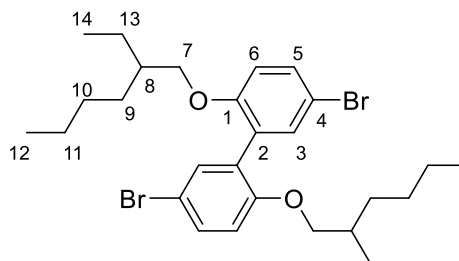
2,2'-Biphenol (10.016 g, 53.789 mmol, 1 eq.) and K_2CO_3 (15.601 g, 112.88 mmol, 2.1 eq.) were stirred in acetonitrile (dry, 150 mL) under N_2 . After addition of 1-bromooctane (28.0 mL, 25.0 g, 129.66 mmol, 2.4 eq.) the reaction was heated under reflux for 18 h. The crude mixture was freed from precipitates by filtration under air (flushed with an additional 20 mL of ACN). Addition of N-bromosuccinimide (19.1 g, 107 mmol, 2.0 eq.) and continuous purging with N_2 resulted in precipitation within 30 min. After an additional 30 min of mild agitation the crude product was isolated by filtration under air. Recrystallization from ethanol afforded the monomer as colorless crystals (17.90 g, 31.49 mmol, 59 %).

Melting point: 66-67 °C

1H NMR (500 MHz, $CDCl_3$, ppm): 7.37 (d, 8.5 Hz, 2H; H_5), 7.36 (s, 2H; H_3), 6.79 (d, 8.5 Hz, 2H; H_6), 3.87 (t, 6.4 Hz, 4H; H_7), 1.62 (m, 4H; H_8), 1.35-1.15 (20H; H_9 - H_{13}), 0.88 (t, 7.4 Hz, 6H; H_{14}).

^{13}C NMR (125 MHz, $CDCl_3$, ppm): 155.6 (C_1), 134.0 (C_3), 131.3 (C_5), 128.7 (C_2), 113.7 (C_6), 112.1 (C_4), 68.7 (C_7), 31.8 (C_{12}), 29.2 (C_8, C_{10}, C_{11}), 26.0 (C_9), 22.7 (C_{13}), 14.1 (C_{14}).

6.2.6. 5,5'-Dibromo-2,2'-bis(2-ethylhexyloxy)biphenol



5,5'-Dibromobiphenyl-2,2'-diol (10.025 g, 29.143 mmol, 1.0 eq.), 2-ethylhexylbromide (31.0 mL, 33.7 g, 174 mmol, 6.0 eq.) and K_2CO_3 (12.044 g, 87.143 mmol, 3.0 eq.) were stirred in acetonitrile (dried over 3 Å mol sieve / 4 d, p.a., 100 mL) and heated under reflux for 18 h. The solvent was removed under reduced pressure. Residues were dissolved in *iso*-hexanes (50 mL) and washed with H_2O (2 x 25 mL). Aqueous phases were extracted with Et_2O (2 x 30 mL) and combined organic phases dried over $MgSO_4$. Volatiles were removed under reduced pressure. The viscous residue was purified twice with a Kugelrohr apparatus under high vacuum (0.6 bar, 260-280 °C). The title compound (6.104 g, 10.74 mmol, 37 %) was a yellow oil.

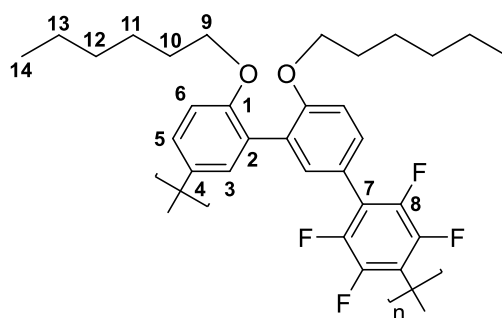
1H NMR (500 MHz, $CDCl_3$, ppm): 7.37 (4H; H_3 , H_5), 6.80 (m, 2H; H_6), 3.75 (d, 5.6 Hz, 4H; H_7), 1.55 (m, 4H; H_8), 1.28 (m, 4H; H_{13}), 1.25-1.10 (12H; H_9 - H_{11}), 0.84 (t, 7.2 Hz, 6H; H_{12}), 0.81 (t, 7.4 Hz, 6H; H_{14}).

^{13}C NMR (125 MHz, $CDCl_3$, ppm): 155.8 (C_1), 134.0 (C_3), 131.2 (C_5), 128.6 (C_2), 113.6 (C_6), 111.9 (C_4), 71.1 (C_7), 39.4 (C_8), 30.6 (C_9), 29.0 (C_{10}), 23.8 (C_{13}), 23.0 (C_{11}), 14.1 (C_{12}), 11.1 (C_{14}).

6.3. Preparation of polymers and SEC curves

Polymerization was carried out in a head-space vial with an elliptical rare earth magnetic stirrer bar. Into a screw-cap vial Pd₂dba₃ (0.5 mol-%), tris(*o*-methoxyphenyl)phosphine (2 mol-%), cesium carbonate (3.0 eq.), pivalic acid (1.0 eq.) and 2,2-bromo-4,4-dihexylbiphenol was added, and the mixture purged with nitrogen. The solvent and tetrafluorobenzene were separately purged with nitrogen and added via syringe to the vial. The mixture was stirred for one day at the indicated temperature or until gelation occurred. Precipitation into methanol and Soxhlet extraction with methanol gave the polycondensates as white powders.

NMR data are reported for 6n as an example:



¹H NMR (500 MHz, CDCl₃, ppm): 7.53 (s; H₃), 7.46 (d, 8.5 Hz; H₅), 7.07 (d, 8.5 Hz; H₆), 4.00 (t, 6.5 Hz; H₉), 1.69 (m; H₁₀), 1.31 (m; H₁₁), 1.22 (H₁₂, H₁₃), 0.82 (H₁₄).

¹H NMR (500 MHz, C₂D₂Cl₄, 120 °C, ppm): 7.55 (s; H₃), 7.49 (d, 8.7 Hz; H₅), 7.11 (d, 8.7 Hz; H₆), 4.04 (t, 6.5 Hz; H₉), 1.71 (m; H₁₀), 1.36 (m; H₁₁), 1.29 (H₁₂, H₁₃), 0.88 (H₁₄).

¹³C NMR (125 MHz, CDCl₃, ppm): 157.1 (C₁), 144.2 (m, ¹J_{CF} = 250 Hz, C₈), 133.7 (C₃), 130.5 (C₅), 127.4 (C₂), 119.0 (C₄), 118.8 (m, C₇), 112.0 (C₆), 68.6 (C₉), 31.4 (C₁₂), 29.0 (C₁₀), 25.7 (C₁₁), 22.5 (C₁₃), 13.9 (C₁₄); -C₆H₄Ph end group observed for nOct: 127.7 (Ph_i), 130.2 (Ph_o), 128.6 (Ph_m), 129.0 (Ph_p).

¹⁹F NMR (470 MHz, CDCl₃, ppm): -146.0 (s, F₈); -C₆F₄H end group: -140.9 (F *ortho* to H), -145.1 (F *meta* to H); -C₆F₄Ph end group observed for nOct: -145.5 (F *ortho* to Ph), -146.05 (F *meta* to Ph)

¹⁹F NMR (470 MHz, C₂D₂Cl₄, 120 °C, ppm): -144.7 (s, F₈); -C₆F₄H end group: -140.0 (F *ortho* to H), -143.7 (F *meta* to H).

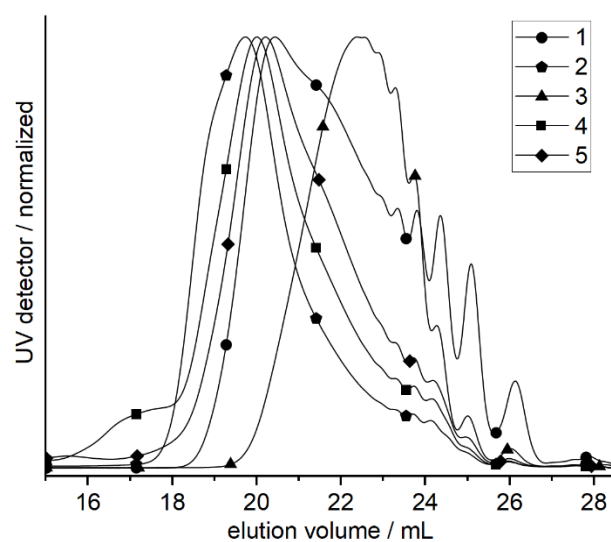


Figure 4-5: SEC eluograms of entries 1 – 5.

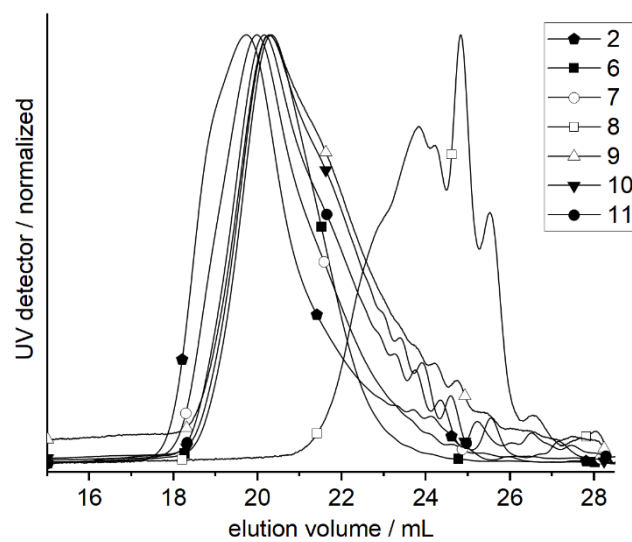


Figure 4-6: SEC eluograms of entries 6 – 11 compared to entry 2.

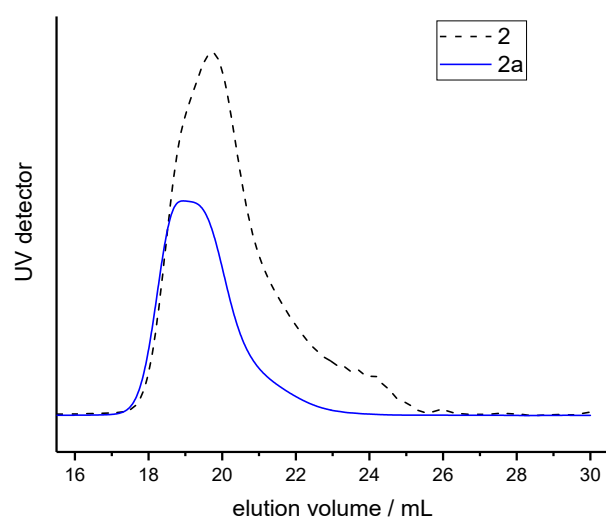


Figure 4-7: SEC eluograms of entries 2 and 2a, which was derived from entry 2 by soxhlet extraction with ethyl acetate.

6.4. NMR spectra of monomers

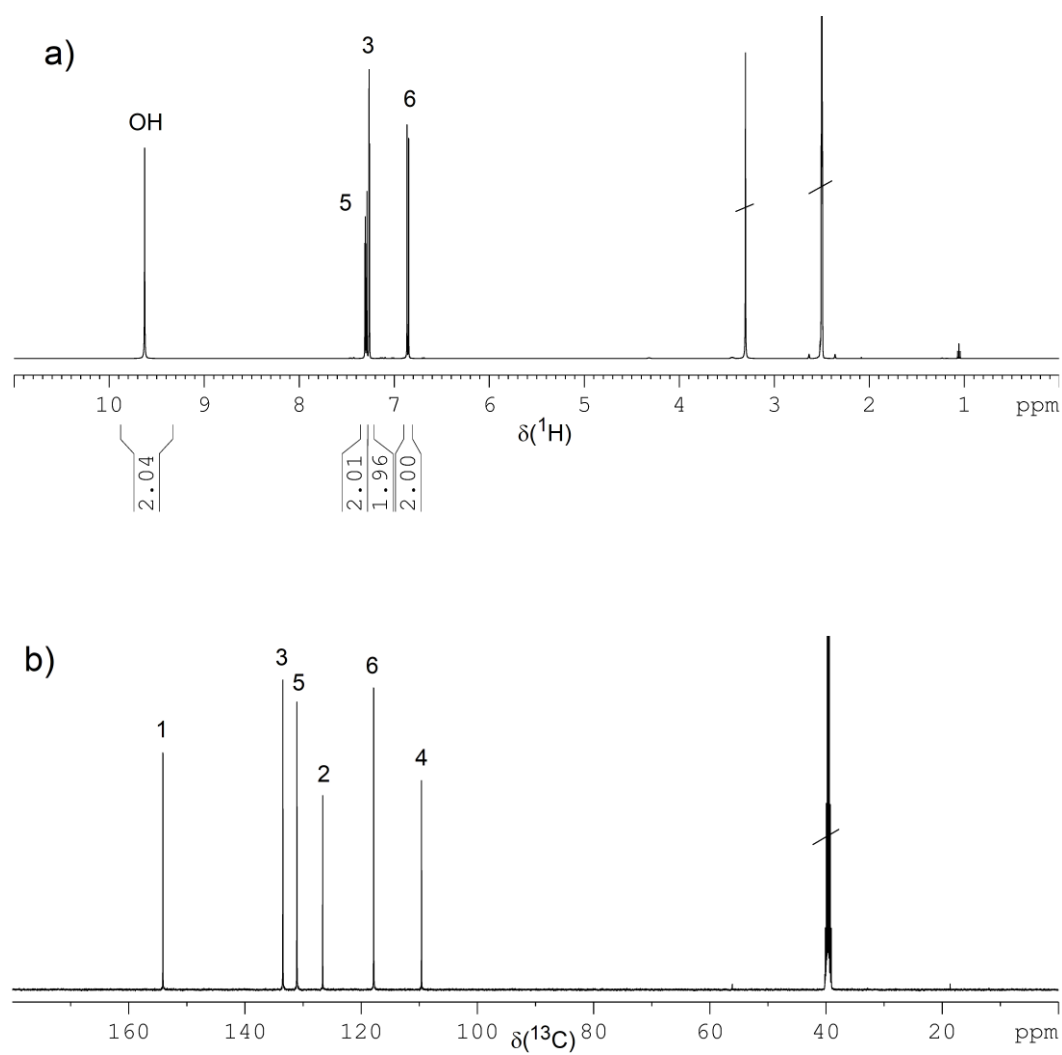


Figure 4-8: ¹H (a) and ¹³C NMR spectrum (b) of 5,5'-dibromobiphenyl-2,2'-diol in DMSO-d₆.

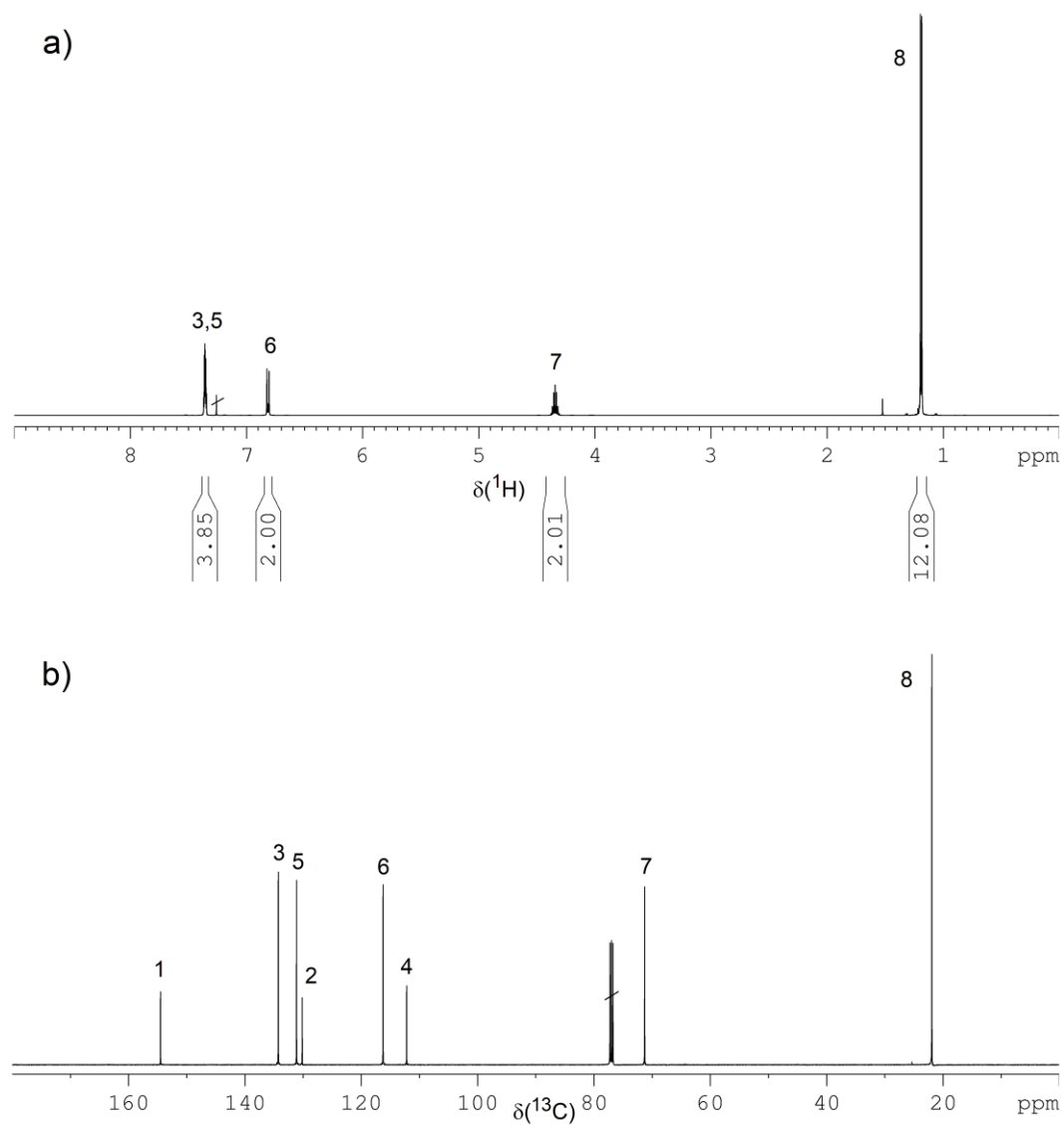


Figure 4-9: ^1H (a) and ^{13}C NMR spectrum (b) of 5,5'-dibromo-2,2'-bis(isopropoxy)biphenyl in CDCl_3 .

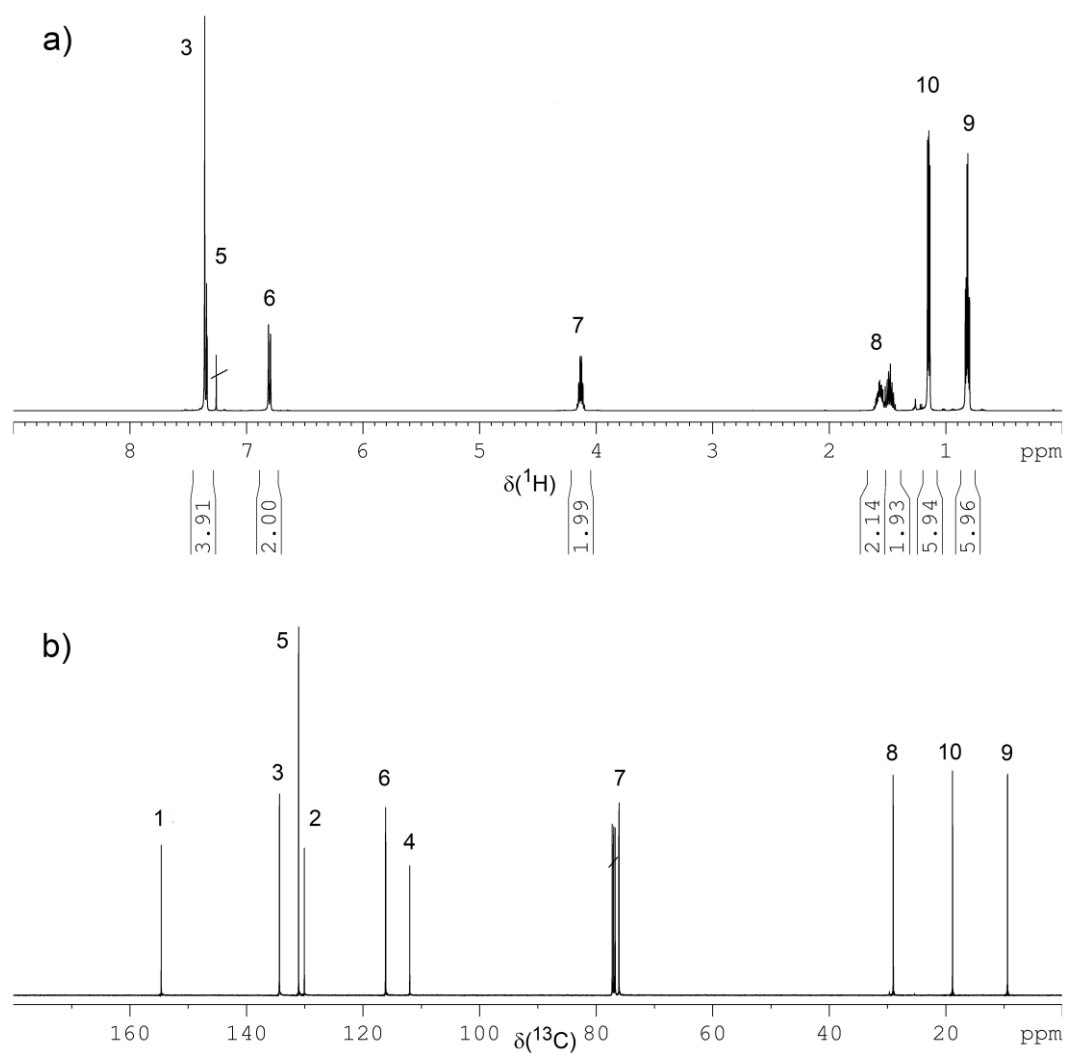


Figure 4-10: ^1H (a) and ^{13}C NMR spectrum (b) of 5,5'-dibromo-2,2'-bis(sec-butoxy)biphenyl in CDCl_3 .

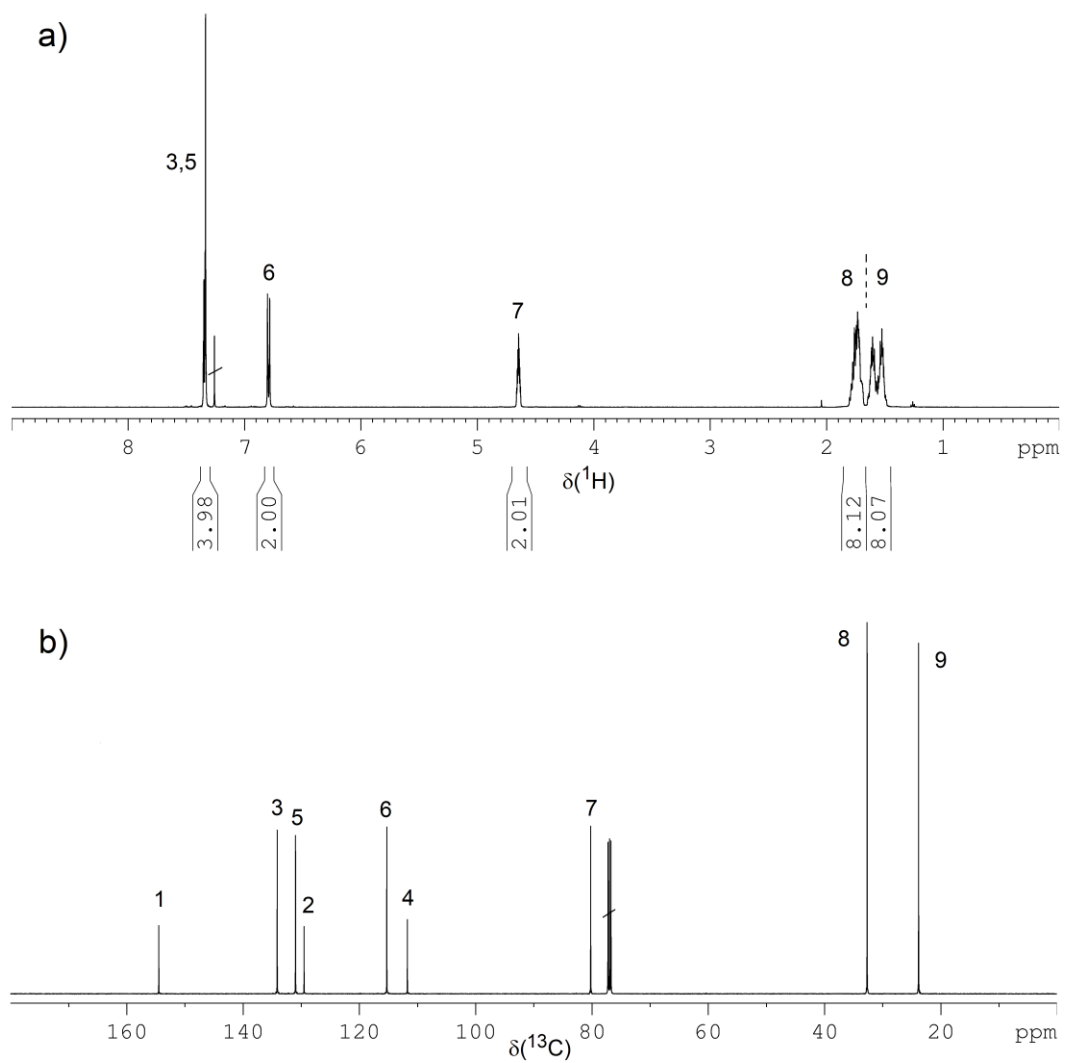


Figure 4-11: ^1H (a) and ^{13}C NMR spectrum (b) of 5,5'-dibromo-2,2'-bis(cyclopentoxo)biphenyl in CDCl_3 .

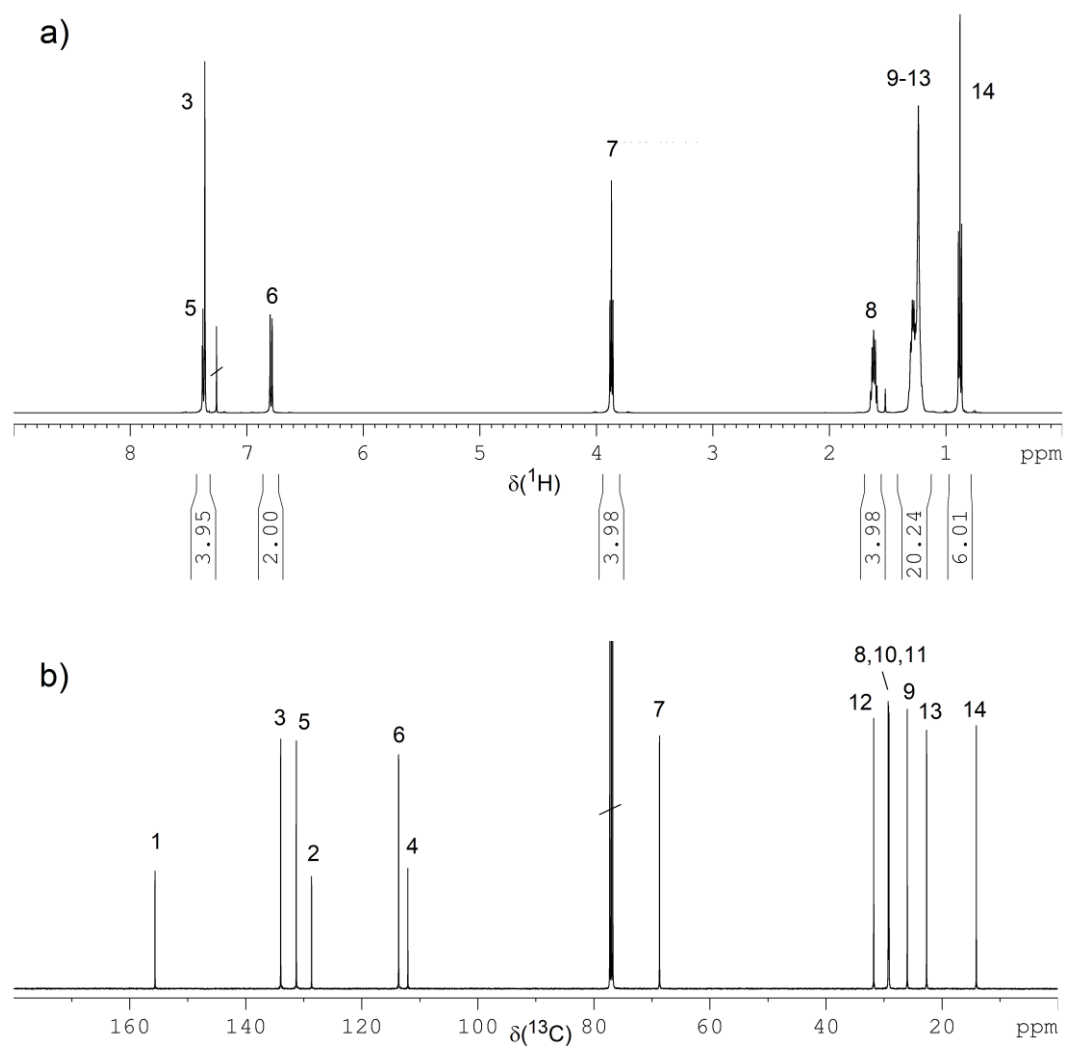


Figure 4-12: ^1H (a) and ^{13}C NMR spectrum (b) of 5,5'-dibromo-2,2'-bis(octyloxy)biphenyl in CDCl_3 .

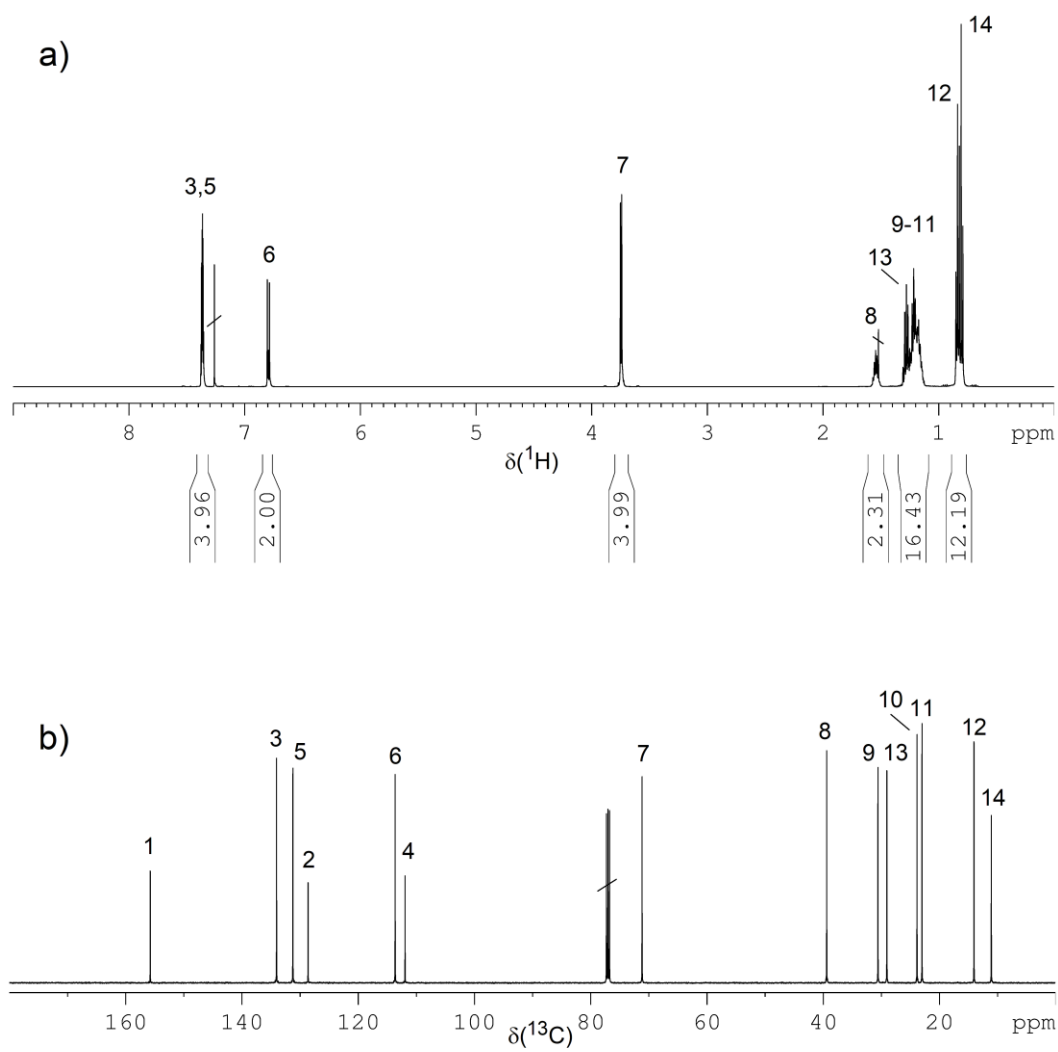
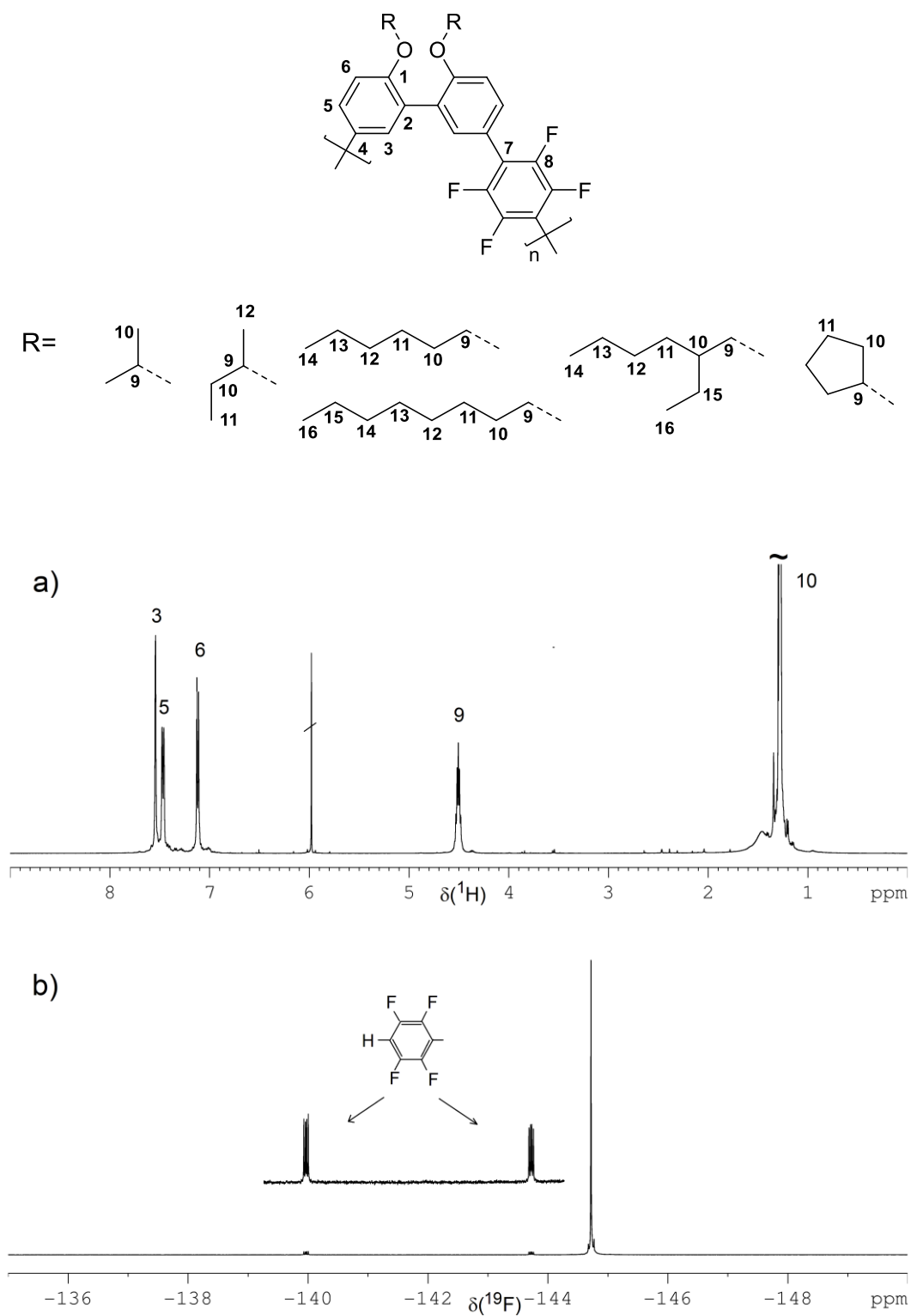


Figure 4-13: ^1H (a) and ^{13}C NMR spectrum (b) 5,5'-dibromo-2,2'-bis(2-ethylhexyloxy)biphenyl in CDCl_3 .

6.5. NMR spectra of polymers

Figure 4-14: ^1H (a) and ^{19}F NMR spectrum (b) of entry 8 (3i) ($\text{C}_2\text{D}_2\text{Cl}_4$; 120 °C)

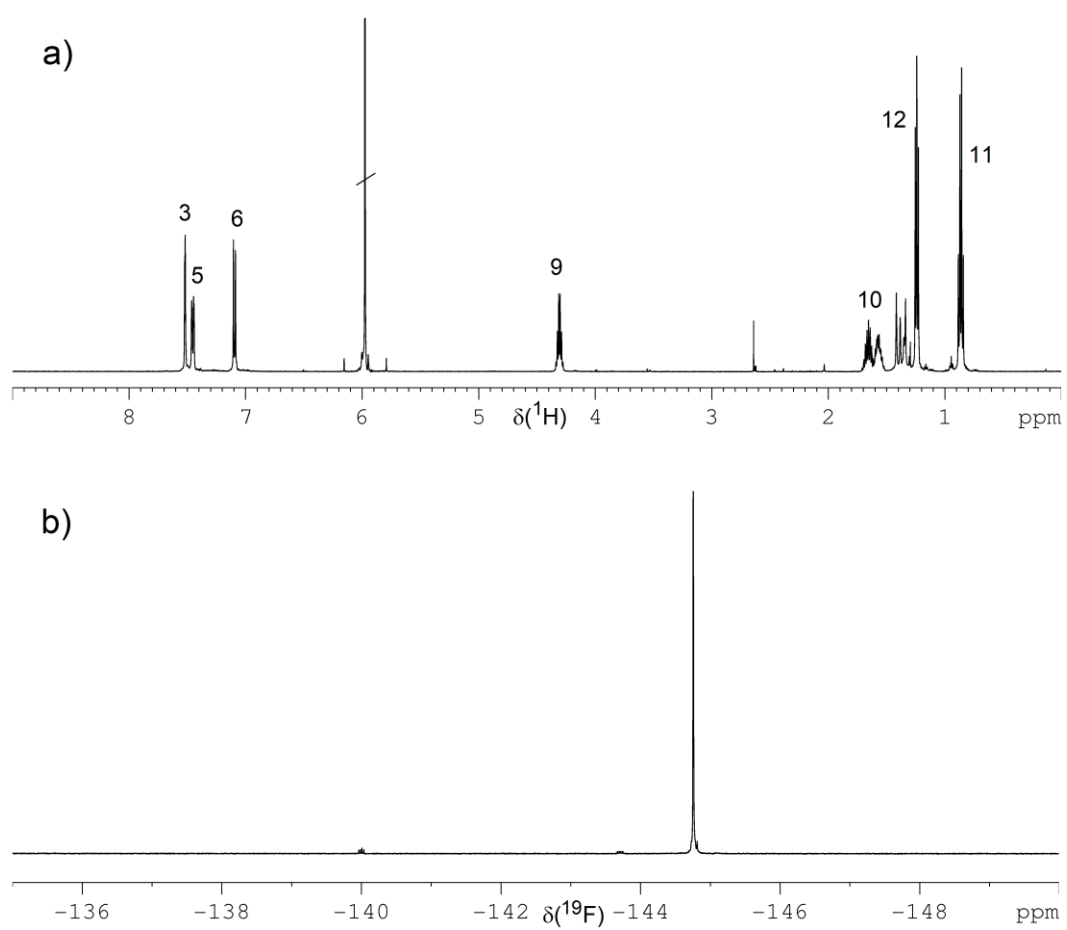


Figure 4-15: ^1H (a) and ^{19}F NMR spectrum (b) of entry 7 (4s) ($\text{C}_2\text{D}_2\text{Cl}_4$; 120 $^\circ\text{C}$).

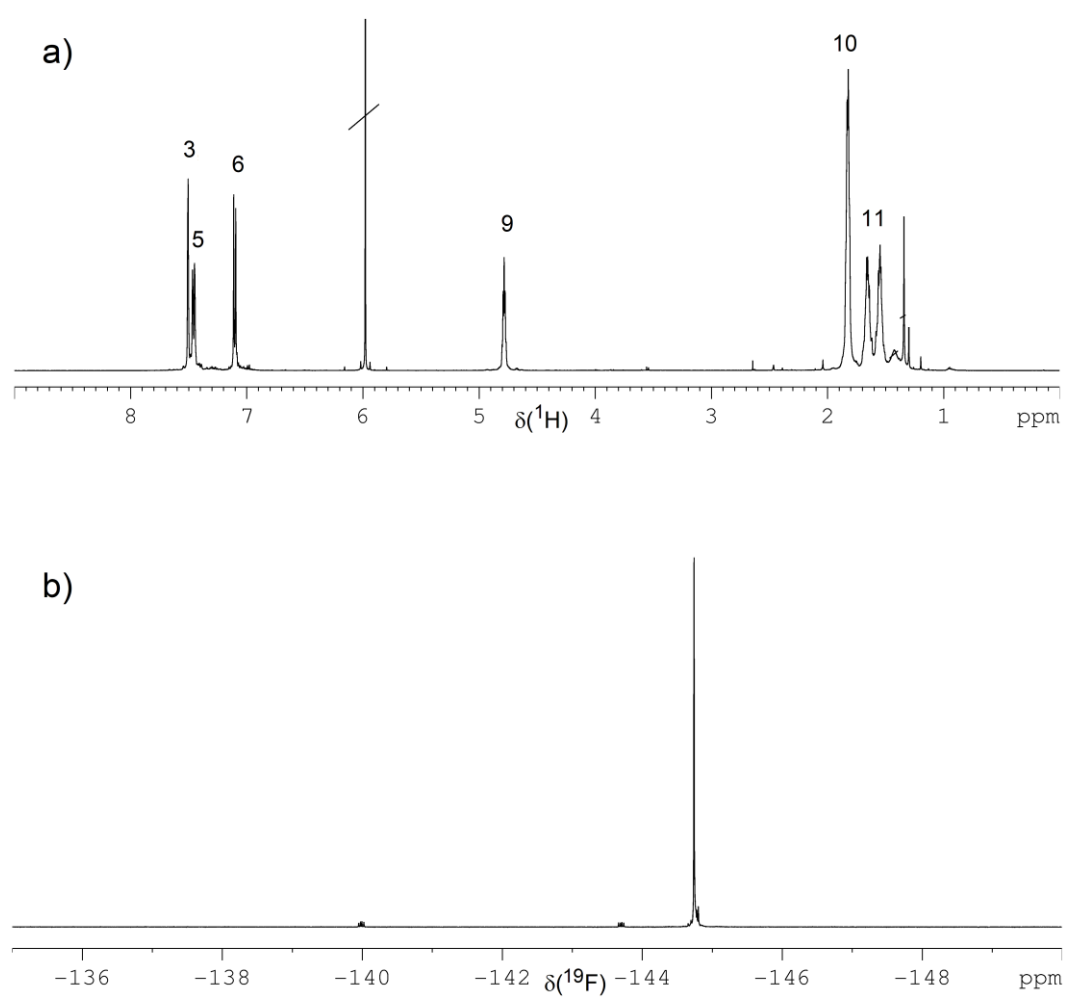


Figure 4-16: ^1H (a) and ^{19}F NMR spectrum (b) of entry 9 (5c) ($\text{C}_2\text{D}_2\text{Cl}_4$; 120 °C).

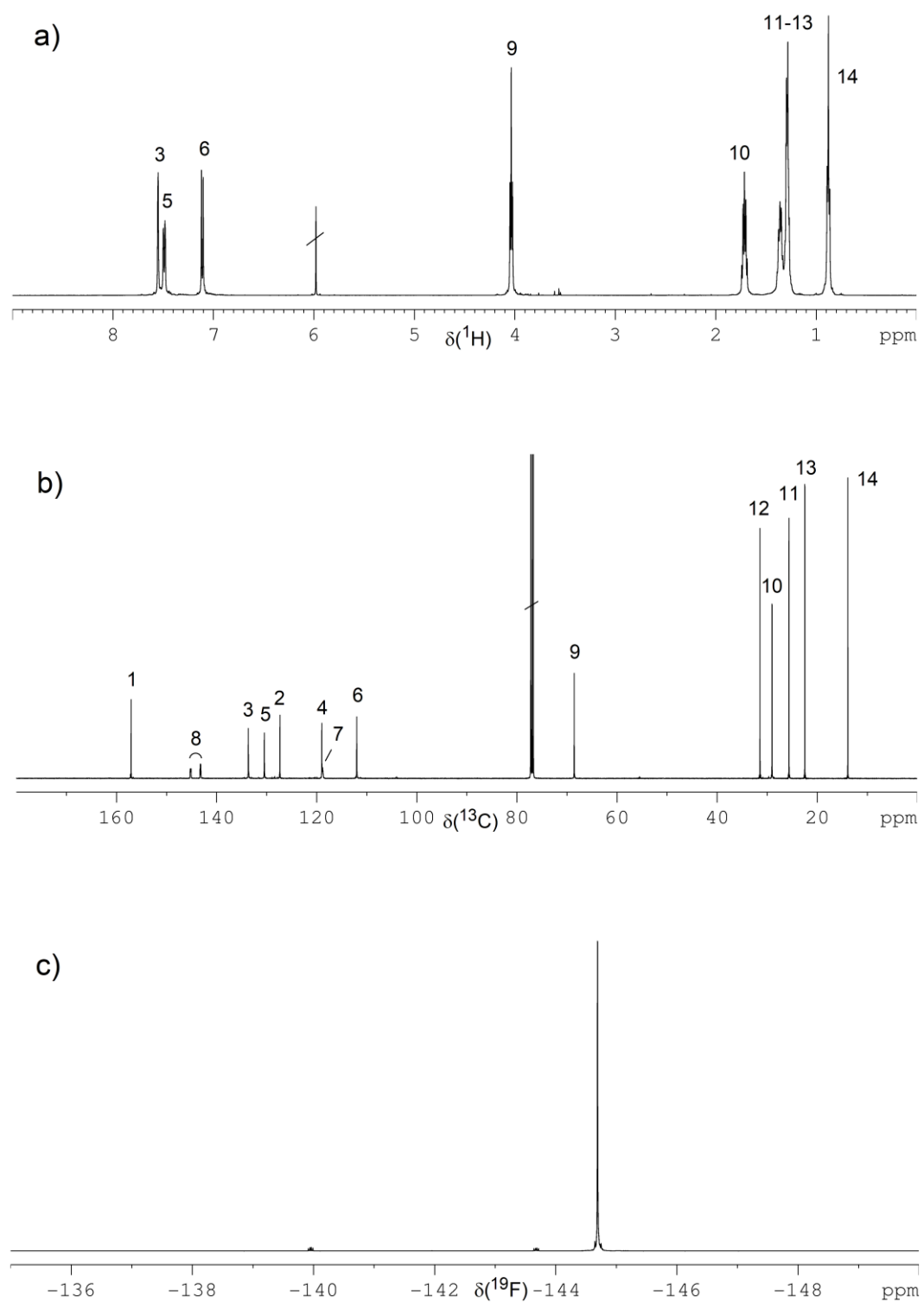


Figure 4-17: ^1H (a), ^{13}C (b) and ^{19}F NMR spectrum (c) of entry 2 (6n) (a,c: $\text{C}_2\text{D}_2\text{Cl}_4$; 120 $^\circ\text{C}$ and b: CDCl_3 , 30 $^\circ\text{C}$).

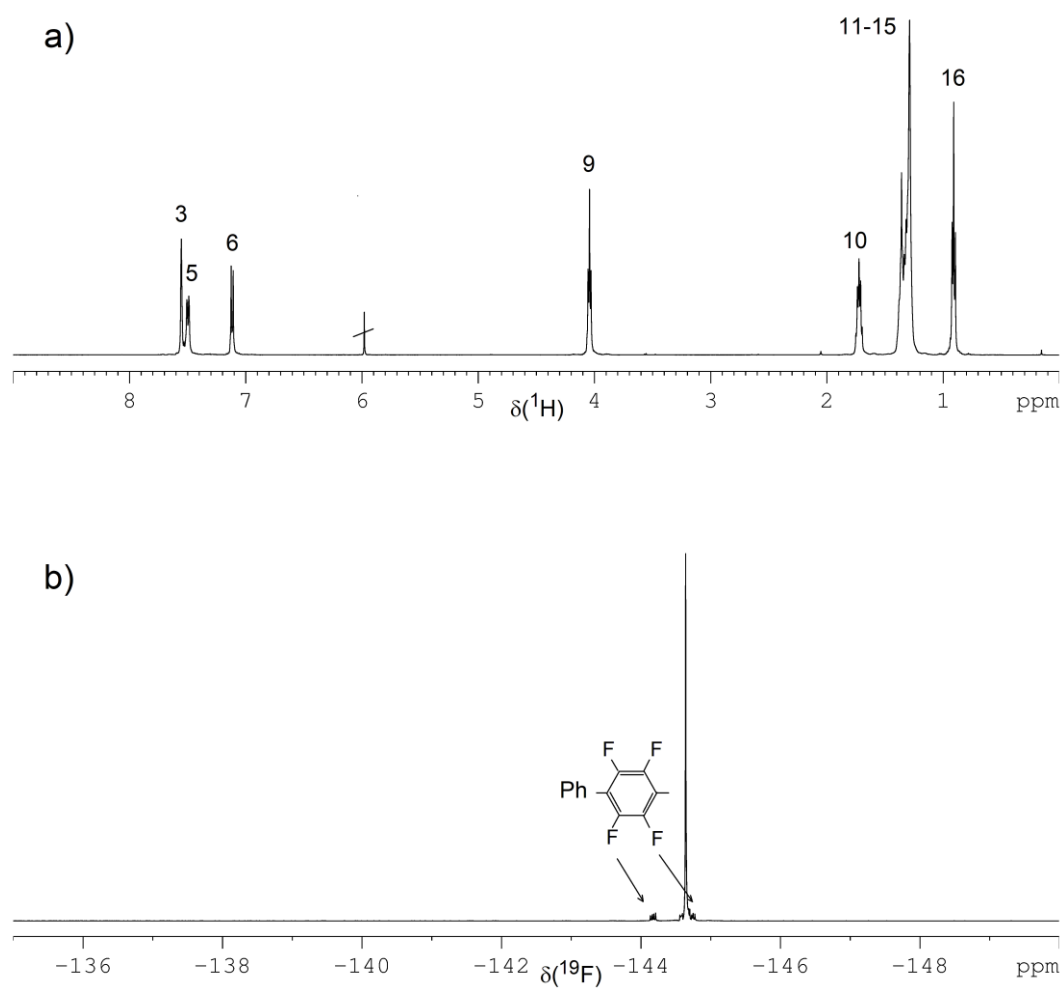


Figure 4-18: ^1H (a) and ^{19}F NMR spectrum (b) of entry 11 (8n) ($\text{C}_2\text{D}_2\text{Cl}_4$; 120°C).

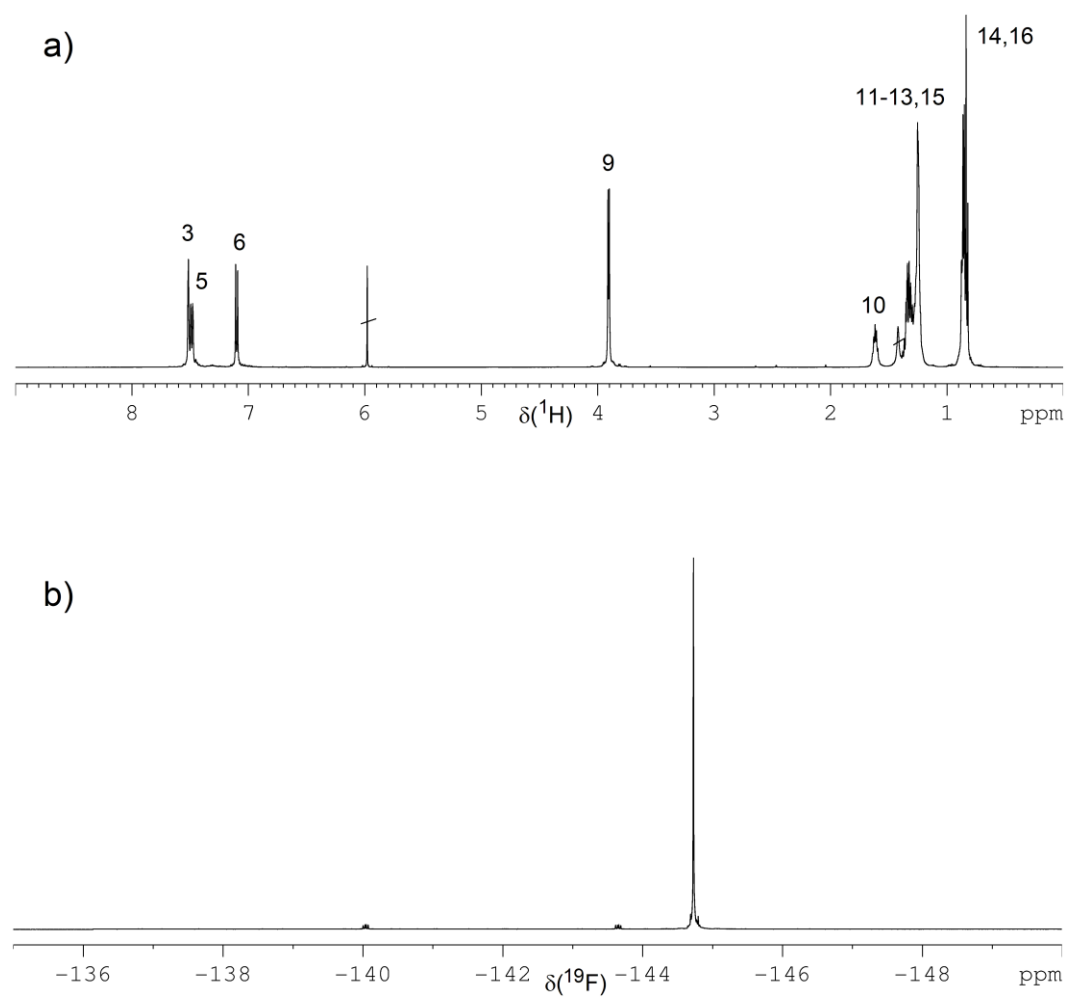


Figure 4-19: ^1H (a) and ^{19}F NMR spectrum (b) of entry 6 (EH) ($\text{C}_2\text{D}_2\text{Cl}_4$; 120 °C).

6.6. Theoretical methods

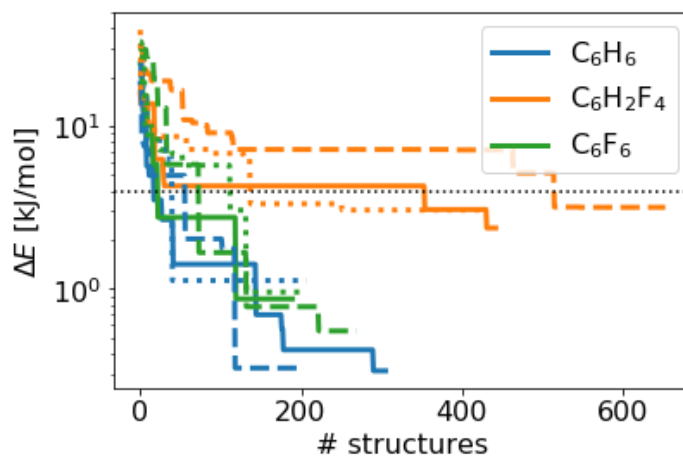


Figure 4-20: Development of the energetic distance ΔE between the best and the second best structure with number of structures tried for $C_{15}H_{14}$ (solid), $C_{16}H_{18}$ (dashed) and $C_{14}H_{14}O_2$ (dotted) in interaction with the color-coded smaller molecules. The dotted horizontal line indicates 4 kJ/mol. The structures involving $C_6H_2F_4$ show slower convergence than C_6H_6 or C_6F_6 .

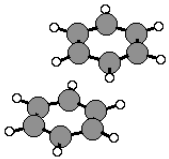
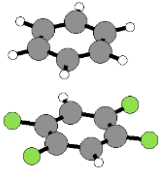
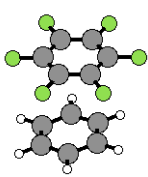
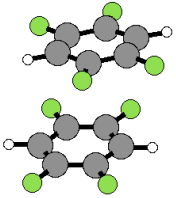
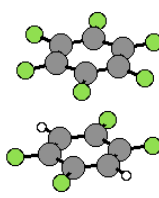
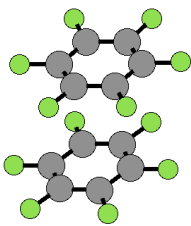
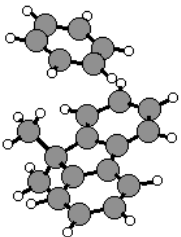
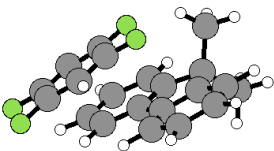
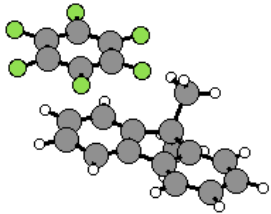
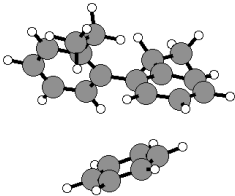
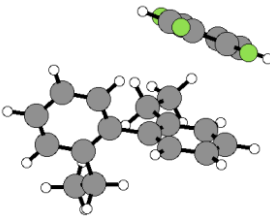
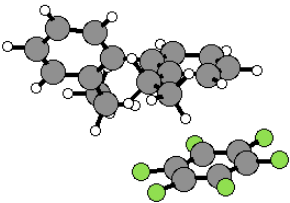
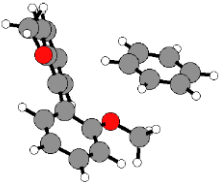
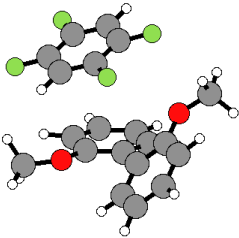
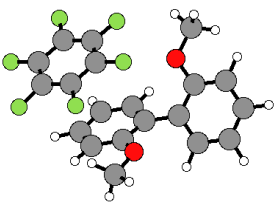
	C₆H₆	C₆H₂F₄	C₆F₆
C₆H₆			
C₆H₂F₄			
C₆F₆			
C₁₅H₁₄			
C₁₆H₁₈			
C₁₄H₁₄O₂			

Figure 4-21: Lowest energy structures found. C: grey, O: red, H: white, F: green.

7. References

- [1] E. J. Park, Y. S. Kim, *J. Mater. Chem. A* **2018**, 6, 15456–15477.
- [2] M. Friedman, G. Walsh, *Polym. Eng. Sci.* **2002**, 42, 1756–1788.
- [3] A. D. Mohanty, S. E. Tignor, J. A. Krause, Y.-K. Choe, C. Bae, *Macromolecules* **2016**, 49, 3361–3372.
- [4] S. Noh, J. Y. Jeon, S. Adhikari, Y. S. Kim, C. Bae, *Acc. Chem. Res.* **2019**, 52, 2745–2755.
- [5] J. A. Reglero Ruiz, M. Trigo-López, F. C. García, J. M. García, *Polymers* **2017**, 9, 414–458.
- [6] I. A. Ronova, S. S. A. Pavlova, *High Perform. Polym.* **2016**, 10, 309–329.
- [7] R. Kandre, K. Feldman, H. E. H. Meijer, P. Smith, A. D. Schlüter, *Angew. Chem. Int. Ed.* **2007**, 46, 4956–4959.
- [8] S. Jakob, A. Moreno, X. Zhang, L. Bertschi, P. Smith, A. D. Schlüter, J. Sakamoto, *Macromolecules* **2010**, 43, 7916–7918.
- [9] R. Kandre, A. D. Schlüter, *Macromol. Rapid Commun.* **2008**, 29, 1661–1665.
- [10] B. Hohl, L. Bertschi, X. Zhang, A. D. Schlüter, J. Sakamoto, *Macromolecules* **2012**, 45, 5418–5426.
- [11] F. Kempe, O. Brügger, H. Buchheit, S. N. Momm, F. Riehle, S. Hameury, M. Walter, M. Sommer, *Angew. Chem. Int. Ed.* **2018**, 57, 997–1000.
- [12] J. Sakamoto, M. Rehahn, G. Wegner, A. D. Schlüter, *Macromol. Rapid Commun.* **2009**, 30, 653–687.
- [13] M. Wakioka, F. Ozawa, *Asian J. Org. Chem.* **2018**, 7, 1206–1216.
- [14] J.-R. Pouliot, F. Grenier, J. T. Blaskovits, S. Beaupré, M. Leclerc, *Chem. Rev.* **2016**, 116, 14225–14274.
- [15] J. Kuwabara, T. Kanbara, *Bull. Chem. Soc. Jpn.* **2018**, 92, 152–161.
- [16] R. M. Pankow, B. C. Thompson, *Polym. Chem.* **2020**, 11, 630–640.
- [17] M. Wakioka, Y. Kitano, F. Ozawa, *Macromolecules* **2013**, 46, 370–374.
- [18] W. Lu, J. Kuwabara, T. Kanbara, *Macromolecules* **2011**, 44, 1252–1255.
- [19] A. D. Schlüter, J. P. Rabe, *Angew. Chem. Int. Ed.* **2000**, 39, 864–883.
- [20] M. Sommer, H. Komber, S. Huettner, R. Mulherin, P. Kohn, N. C. Greenham, W. T. S. Huck, *Macromolecules* **2012**, 45, 4142–4151.
- [21] S. Kappaun, M. Zelzer, K. Bartl, R. Saf, F. Stelzer, C. Slugovc, *J. Polym. Sci. Part Polym. Chem.* **2006**, 44, 2130–2138.
- [22] T. Kirschbaum, R. Azumi, E. Mena-Osteritz, P. Bäuerle, *New J. Chem.* **1999**, 23, 241–250.
- [23] M. Jayakannan, J. L. J. van Dongen, R. A. J. Janssen, *Macromolecules* **2001**, 34, 5386–5393.
- [24] K. D. Deshmukh, R. Matsidik, S. K. K. Prasad, N. Chandrasekaran, A. Welford, L. A. Connal, A. C. Y. Liu, E. Gann, L. Thomsen, D. Kabra, J. M. Hodgkiss, M. Sommer, C. R. McNeill, *ACS Appl. Mater. Interfaces* **2018**, 10, 955–969.
- [25] X. Liao, F. Wu, Y. An, Q. Xie, L. Chen, Y. Chen, *Macromol. Rapid Commun.* **2017**, 38, 1600556.

- [26] A. Nitti, F. Debattista, L. Abbondanza, G. Bianchi, R. Po, D. Pasini, *J. Polym. Sci. Part Polym. Chem.* **2017**, *55*, 1601–1610.
- [27] M. L. Tang, Z. Bao, *Chem. Mater.* **2011**, *23*, 446–455.
- [28] R. Pinal, *Org. Biomol. Chem.* **2004**, *2*, 2692–2699.
- [29] C. Müller, *Chem. Mater.* **2015**, *27*, 2740–2754.
- [30] S. Pankaj, E. Hempel, M. Beiner, *Macromolecules* **2009**, *42*, 716–724.
- [31] Z. Qian, Z. Cao, L. Galuska, S. Zhang, J. Xu, X. Gu, *Macromol. Chem. Phys.* **2019**, *220*, 1900062.
- [32] R. Xie, A. R. Weisen, Y. Lee, M. A. Aplan, A. M. Fenton, A. E. Masucci, F. Kempe, M. Sommer, C. W. Pester, R. H. Colby, E. D. Gomez, *Nat. Commun.* **2020**, *11*, 1–8.
- [33] L. Yu, E. Davidson, A. Sharma, M. R. Andersson, R. Segalman, C. Müller, *Chem. Mater.* **2017**, *29*, 5654–5662.
- [34] M. H. Jandaghian, A. Soleimannezhad, S. Ahmadjo, S. M. M. Mortazavi, M. Ahmadi, *Ind. Eng. Chem. Res.* **2018**, *57*, 4807–4814.
- [35] J. S. Grebowicz, *Polym. Eng. Sci.* **1992**, *32*, 1228–1235.
- [36] N. J. Singh, H. M. Lee, I.-C. Hwang, K. S. Kim, *Supramol. Chem.* **2007**, *19*, 321–332.
- [37] S. Kozuch, *Phys. Chem. Chem. Phys.* **2016**, *18*, 30366–30369.
- [38] P. E. Blöchl, *Phys. Rev. B* **1994**, *50*, 17953–17979.
- [39] J. J. Mortensen, L. B. Hansen, K. W. Jacobsen, *Phys. Rev. B* **2005**, *71*, 035109.
- [40] J. Enkovaara, C. Rostgaard, J. J. Mortensen, J. Chen, M. Du\lak, L. Ferrighi, J. Gavnholt, C. Glinsvad, V. Haikola, H. A. Hansen, H. H. Kristoffersen, M. Kuisma, A. H. Larsen, L. Lehtovaara, M. Ljungberg, O. Lopez-Acevedo, P. G. Moses, J. Ojanen, T. Olsen, V. Petzold, N. A. Romero, J. Stausholm-Møller, M. Strange, G. A. Tritsarlis, M. Vanin, M. Walter, B. Hammer, H. Häkkinen, G. K. H. Madsen, R. M. Nieminen, J. K. Nørskov, M. Puska, T. T. Rantala, J. Schiøtz, K. S. Thygesen, K. W. Jacobsen, *J. Phys. Condens. Matter* **2010**, *22*, 253202–253227.
- [41] J. P. Perdew, K. Burke, M. Ernzerhof, *Phys. Rev. Lett.* **1996**, *77*, 3865–3868.
- [42] A. Tkatchenko, M. Scheffler, *Phys. Rev. Lett.* **2009**, *102*, 73005–73008.
- [43] K. Lee, É. D. Murray, L. Kong, B. I. Lundqvist, D. C. Langreth, *Phys. Rev. B* **2010**, *82*, 081101–081104.
- [44] J. A. Pople, *Rev. Mod. Phys.* **1999**, *71*, 1267–1274.
- [45] Y. C. Park, J. S. Lee, *J. Phys. Chem. A* **2006**, *110*, 5091–5095.
- [46] E. Miliordos, E. Aprà, S. S. Xantheas, *J. Phys. Chem. A* **2014**, *118*, 7568–7578.
- [47] A. Tkatchenko, R. A. DiStasio, R. Car, M. Scheffler, *Phys. Rev. Lett.* **2012**, *108*, 236402–236406.
- [48] M. Hassan, M. Walter, M. Moseler, *Phys. Chem. Chem. Phys.* **2013**, *16*, 33–37.
- [49] S. Tsuzuki, T. Uchimaru, M. Mikami, *J. Phys. Chem. A* **2006**, *110*, 2027–2033.
- [50] S. Scheiner, T. Kar, J. Pattanayak, *J. Am. Chem. Soc.* **2002**, *124*, 13257–13264.
- [51] D. Ž. Veljković, G. V. Janjić, S. D. Zarić, *CrystEngComm* **2011**, *13*, 5005–5010.
- [52] Jan Badorrek, Michael Walter, Marie-Pierre Laborie, *J Renew. Mater.* **2018**, *6*, 325–335.

- [53] R. F. W. Bader, *Atoms in Molecules: A Quantum Theory*, Clarendon Press, Oxford England : New York, **1994**.
- [54] W. Tang, E. Sanville, G. Henkelman, *J. Phys. Condens. Matter* **2009**, *21*, 084204.

Chapter 5 Conclusion

1. Summary Chapter 2

In order to investigate substituent effects and regiochemistry of SP main-chain copolymers, bis(hydroxymethyl)spiropyrans have been synthesized as bifunctional initiators. The SP initiators were used in the ring-opening polymerization of ϵ -caprolactone (Figure 5-1), which places SP towards the middle part of the polymer chain.

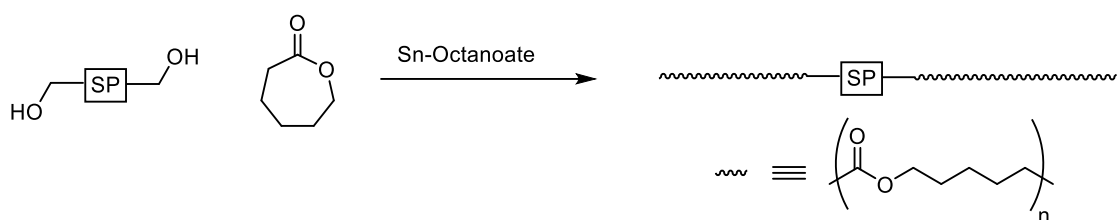


Figure 5-1: Bifunctional SP as initiator in the ROP of ϵ -caprolactone.

There were four derivatives of SP-PCL copolymers synthesized (Figure 5-2). These differ in regiochemistry (*ortho* vs. *para*-linkage) and substitution (NO_2 or H).

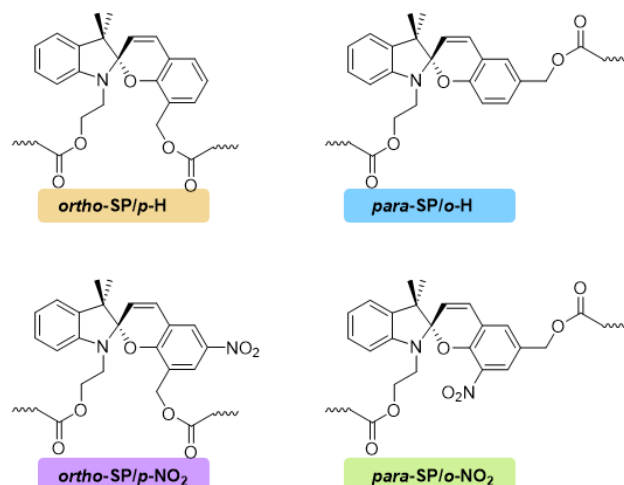


Figure 5-2: Structures of the 4 spiropyran-PCL copolymers synthesized in this investigation.

The copolymers were doctor bladed from the melt. The resulting thin films were investigated by light absorption measurement during uniaxial strain (Figure 5-3a).

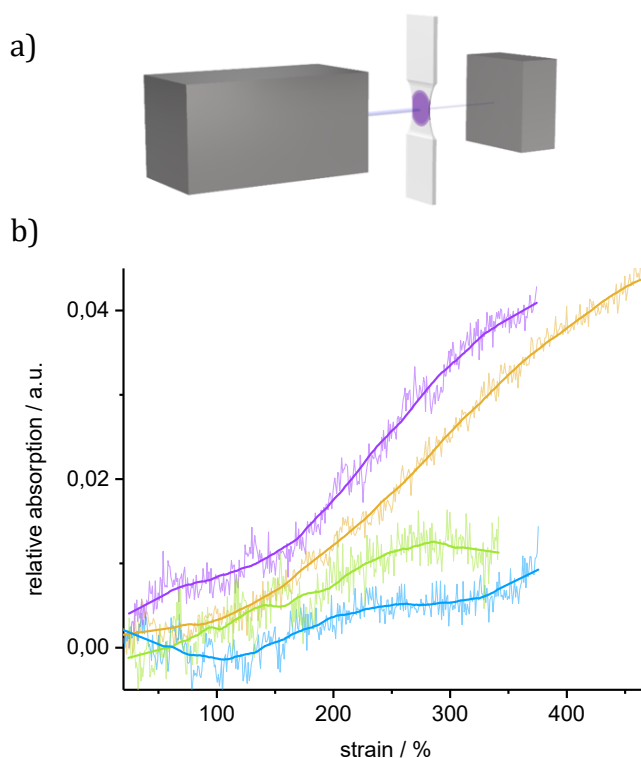


Figure 5-3: a) Schematic experimental setup for in-situ VIS spectroscopy during stress-strain of films. After the yield point polycaprolactone becomes sufficiently translucent for visible light (450 – 800 nm). b) In situ visible light absorption after the yield point.

The absorption after the yield point is shown in Figure 5-3b. Only *ortho*-SP/*p*-NO₂ (purple) immediately isomerizes after the yield point is reached. Without the NO₂ group (*ortho*-SP/*p*-H, orange) the onset of isomerization is delayed up until a strain of 100 %. This is likely due to the difference size of the π -system due to the absence of NO₂. The larger π -system in presence of NO₂ seems to lower the activation barrier for isomerization. Overall, the *ortho*-SP copolymers isomerize more readily compared to their *para*-counterparts. Therefore both *ortho*-linkage and NO₂ substitution improve the mechanochromic response of SP copolymers.

2. Summary Chapter 3

In order to investigate phenyl-substituted spiropyran copolymers a high strength, tough polyarylene was developed. This polyarylene with a meta-meta-para backbone (*PmmpP*) exhibits a tensile strength at yield of up to 50 MPa, a young's modulus of 0.9 GPa and a strain at break of 300 %. This allowed for the copolymerization of *para,para*-SP. The resulting phenyl-substituted SP showed transient mechanochromism after the yield point and was switchable for 25 force-release cycles.

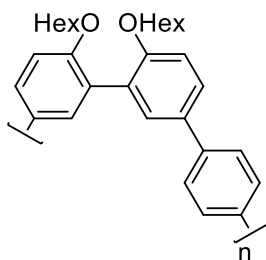


Figure 5-4: Structure of the newly developed *PmmpP*.

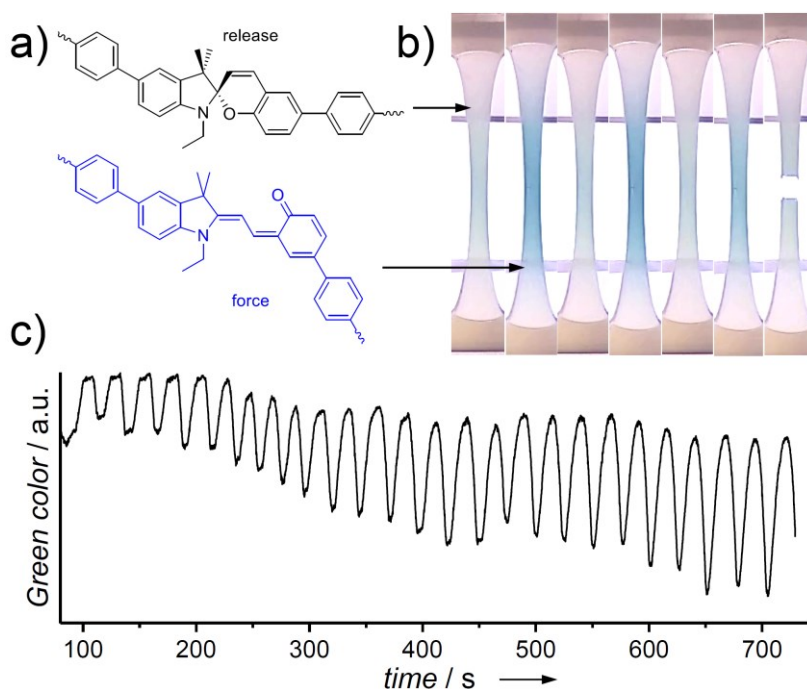


Figure 5-5: Tensile experiment of *PmmpP* containing 2 mol-% *p,p*-SPBr₂. a) Structures of SP (top) and MC (bottom) in the *PmmpP* matrix. b) Pictures of repeated strained and released samples. Pictures were adjusted for brightness and contrast. c) Intensity of green color in the mid-section of the specimen during repeated force build-up and release.

DFT calculations indicated that the transient mechanochromism was enabled by the short lifetime of the colored MC ($t_{1/2} = 3.1$ s). This MC lifetime is magnitudes shorter than that of NO₂-SP in chapter 2 ($t_{1/2} = 4.5$ h). Therefore *PmmpP* allowed SP to be used as a true tensile force sensor.

3. Summary Chapter 4

In order to simplify access to kinked polyarylenes, direct arylation polymerization of the biphenol monomer with 1,4-tetrafluorobenzene was investigated. The resulting semifluorinated polyarylenes (*PmmpF4*) were investigated with 6 different side-chains (Figure 5-6). Highest molecular weight of $M_w = 21\,500$ g/mol was achieved with a hexyl side-chain. This was

increased to $M_w = 31\,000$ g/mol by soxhlet extraction with ethyl acetate. All derivatives were limited by solubility during polymerization. NMR analysis did not find any indication for significant side reactions. Hence, the low molecular weight of some side-chains was caused primarily by limited solubility. Even using 1,3-tetrafluorobenzene in order to synthesize an all-*meta* PmmmF4 did not alleviate this limitation. This phenomenon is rather atypical for semifluorinated polymers and is not observed for copolymers of 1,4-tetrafluorobenzene with fluorene or carbazol. DFT calculations suggest that the combination of tetrafluorobenzene and the very electron-rich biphenol monomer causes increased interactions due to polarization and thus lead to low solubility.

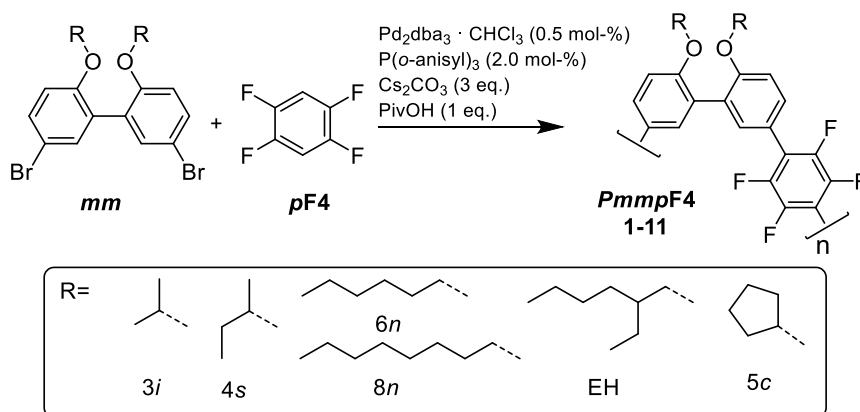


Figure 5-6: Synthesis of kinked, semifluorinated PmmpF4 via DAP.

Overall, the different side chain derivatives show a large range of T_g s from 50 to ca. 200 °C. This shows that a large variety of materials can be derived by simple direct arylation polymerization from 1,4-tetrafluorobenzene in an efficient and atom economic fashion.

Declaration of self-reliance

Thereby, I declare that I wrote this work independently, and that I did not use anything other than the designated sources and tools. Any section of text or content that was extracted or quoted from another author has been explicitly specified. I have not submitted or used this work for other purposes in same or similar form and this dissertation has not been published.

Chemnitz, 28.08.2020 _____

Fabian Kempe

Curriculum Vitae

Since 04/2017	Ph.D. studies (Prof. Dr. Michael Sommer) at TU Chemnitz
09/2015 – 03/2017	Start of Ph.D. studies (Dr. Sommer / Prof. Dr. Rolf Mülhaupt) at Albert-Ludwigs-University Freiburg
10/2012 – 08/2015	M.Sc., Chemistry, Albert-Ludwigs-University Freiburg
10/2011 – 09/2012	M.Sc. (research), Chemistry, Durham University, UK
10/2008 – 09/2011	B.Sc., Chemistry, Albert-Ludwigs-University Freiburg
07/2008	Abitur, Sächsisches Landesgymnasium St. Afra zu Meißen

Awards

Scholarship by the German Academic Foundation (2009-2014)

Award for excellence in B.Sc. studies by the Alumni Association (2011)

Young Scientist (Jugend forscht) special federal award (2008)

Publications, posters and talks

“Glass transition temperature from the chemical structure of conjugated polymers”

R. Xie, A. R. Weisen, Y. Lee, M. A. Aplan, A. M. Fenton, A. E. Masucci, **F. Kempe**, M. Sommer, C. W. Pester, R. H. Colby, E. D. Gomez, *Nat. Commun.* **2020**, *11*, 1–8.

DOI: 10.1038/s41467-020-14656-8

„A Simply Synthesized, Tough Polyarylene with Transient Mechanochromic Response“

F. Kempe, O. Bruegner, H. Buchheit, S. N. Momm, F. Riehle, S. Hameury, M. Walter, **M. Sommer**, *Angew. Chem. Int. Ed.* **2018**, *57* (4), 997-1000.

DOI: 10.1002/anie.201709142

„Alkyl-substituted spiropyrans: electronic effects, model compounds and synthesis of aliphatic main-chain copolymers“

S. Schmidt, **F. Kempe**, O. Brügger, M. Walter, **M. Sommer**, *Polym. Chem.* **2017**, *8*, 5407-5414. DOI: 10.1039/C7PY00987A

„Novel Graphene UHMWPE Nanocomposites Prepared by Polymerization Filling Using Single-Site Catalysts Supported on Functionalized Graphene Nanosheet Dispersions“

M. Stuerzel, **F. Kempe**, Y. Thomann, S. Mark, M. Enders, R. Muelhaupt, *Macromolecules* **2012**, *45*, 6878–6887. DOI: 10.1021/ma301376q

Poster at Macromolecular Colloquium Freiburg (02/2016):

“Controlling Mechanochromic Behaviour of Spiropyran Main Chain Copolymers Using Substituent Effects”

Poster at Bayreuth Polymer Symposium (09/2017):

“A Tough Polyarylene by Rational Monomer Design and its Mechanochromic Copolymer with *para*-Spiropyran”

Talk at American Chemical Society National Meeting San Diego (08/2019):

“Transient Mechanochromic Response and Stereochemical Effects of Spiropyran Copolymers”

Acknowledgements

I would like to express my sincere gratitude to my supervisor Prof. Dr. Michael Sommer for his support throughout so many years, his patience and his tireless revisions of various publications. Thank you for improving my critical thinking and allowing me to teach so early in my career.

I am also thankful to Prof. Dr. Stefan Spange for the cordial welcome at TU Chemnitz, tremendous support during the lab transition and discussions about and beyond science. Additionally, I deeply appreciate you for agreeing to be reviewer of this thesis and your continued engagement even past retirement.

I would like to thank the Deutsche Forschungsgemeinschaft (DFG) and European Social Fund (ESF) for financial support.

I thank Felix Riehle, Hannah Buchheit and Sarah Momm for their help and for being excellent Bachelor students.

I thank all colleagues in both Freiburg and Chemnitz for their support, friendship and good memories: Dr. Fritz Nübling, Dr. Florian Lombeck, Dr. Daniel Schiefer, Dr. Sophie Hameury, Lukas Metzler, Dr. Simon Schmidt, Carolin Lienert, Dr. Yonghun Shin, Simone Kehr, Dr. Andreas Seifert, Maximilian Raisch, Desiree Adamczak, Dr. Rukiya Matsidik, Echo Wang, Dominik Stegerer, Andy Künzel-Tenner and Raphael Hertel. I enjoyed being in a research group with you and hope to meet again!

I am grateful to Dr. Hartmut Komber for NMR analysis. I thank Marina Hagios for SEC measurements.

I thank all of my family and friends for their continued support, not only during this thesis but all my studies beforehand.